RISK-BASED PERFORMANCE ASSESSMENT OF A SEISMIC RETROFIT TECHNIQUE FOR MEDIUM- AND HIGH-VOLTAGE TRANSFORMER BUSHING SYSTEMS

A Thesis

by

Andrew Leonard Brennan

Submitted to the Office of Graduate and Professional Studies of
Texas A&M University
in partial fulfillment of the requirements for the degree of

MASTER OF SCIENCE

Chair of Committee,	Maria Koliou
Committee Members,	Mary Beth Hueste
	Amir H. Behzadan
Head of Department,	Robin Autenrieth

August 2019

Major Subject: Civil Engineering

ABSTRACT

High voltage electrical transformers bushing systems have exhibited vulnerability during past earthquakes. The enhanced performance of bushings mounted on rigid base observed during shake table testing does not correlate well with their performance in the field. It is suspected that the seismic performance of high voltage bushings is improved when mounted on a rigid base as opposed to when mounted on more flexible cover plates of transformers. To aid in the protection of these bushing systems, different retrofitting techniques have been researched to protect vital equipment. In this study, the Performance-Based Earthquake Engineering (PBEE) framework developed by the Pacific Earthquake Engineering Research (PEER) center, combined with Monte Carlo Simulation is used to probabilistically evaluate the earthquake-induced economic losses for high and medium voltage transformer bushing systems under various mounting conditions (as-installed and retrofitted with flexural stiffeners) and evaluate the efficiency of the examined seismic retrofit technique in terms of direct and indirect (related to downtime) economic losses.

ACKNOWLEDGEMENTS

I would like to thank my committee chair, Dr. Maria Koliou, as well as my committee members, Dr. Hueste and Dr. Behzadan, for their guidance and patience with me as I conducted my research.

I thank my friends that I have made at Texas A&M University, as well as the Civil Engineering department who made my transition to campus smooth and very enjoyable during my time here.

I also thank my parents and siblings for their love and support during my journey even while away from home.

Lastly, I thank my girlfriend, Nicole Casamassina, for her affection and encouragement while we both completed our masters degrees and became stronger as a couple along the way.

CONTRIBUTORS AND FUNDING SOURCES

Contributors

This work was supervised by a thesis committee consisting of Dr. Maria Koliou [advisor and committee chair], and Dr. Mary Beth Hueste [committee member] of the Department of Civil and Environmental Engineering at Texas A&M University, and Dr. Amir Behzadan [committee member] of the Department of Construction Science at Texas A&M University.

The transformer numerical models used in this study were provided by Dr Koliou and further modified to address the needs of this project.

All other work conducted for the thesis was completed by the student independently under Dr. Koliou's supervision

Funding Sources

This work was made possible by the Texas A&M University Civil Engineering department, providing me with a Teaching Assistantship for my first year of studies allowing me to devote more time to my research.

In addition, this work was made possible by Professor Maria Koliou, providing me with an assistantship for a part of my second year of my M.S. towards the completion of this study.

NOMENCLATURE

CDF	Cumulative Distribution Function
C.O.V.	Coefficient of Variation
EDP	Engineering Demand Parameter
FEMA	Federal Emergency Management Agency (U.S. Government)
IEEE	Institute of Electrical and Electronics Engineers
POE	Probability of Exceedance
PBEE	Performance Based Earthquake Engineering
PEER	Pacific Earthquake Engineering Research
USGS	United States Geographical Survey

TABLE OF CONTENTS

Page

LIST OF FIGURES

Page

LIST OF TABLES

Page

1. INTRODUCTION AND LITERATURE REVIEW

1.1. Electrical Transformer Layout

In an electric power network system, one of the most important components to its successful operation is the substation, which is used to transfer direct electricity to lower voltage values to be supplied to communities. A typical substation setup can be seen in Figure 1.1. Electrical substation equipment is commonly used in the United States as a means of protecting components such as transmission lines, distribution lines, and other electrical equipment (Schiff 1999). An essential component to a functional substation is the power transformer, which is designed and used to transfer power between multiple circuits. Some points of interest include the high and low voltage bushings on the outside of the tank wall, and the core and coils which are kept on the inside of the steel tank to, "*protect them from the elements of nature, vandalism, and for safety purposes*" (Koliou et al. 2012). According to the HAZUS earthquake disaster technical manual (FEMA 2010), 115kV bushings are classified as "low-voltage", 230kV bushings are classified as "medium-voltage", and bushings of 500kV capacity and above are considered "high-voltage". A sample cross section of a typical high-voltage transformer is shown in Figure 1.2.

Of the components of an electrical transformer, the bushings are both crucial to its continued operation and functionality, as well as highly brittle and fragile under extreme ground shaking. These porcelain bushings provide an electrical connection between high-voltage lines and the transformer itself through insulated conductors.

They are often seen mounted at the top of the transformer tank (Gilani et al. 2004), similarly to Figure 1.1. To prevent the possibility of a flashover, a long distance is kept between the coils and the power cables used in a porcelain bushing. Because of this, a typical bushing contains multiple porcelain segments in a stack, which is then held together by condenser, gaskets, and the conductor itself (Reinhorn et al. 2011). Transformers are also known to normally be filled with oil which is used as an insulator for the connecting metal rod (Villaverde et al. 2001). Figure 1.2 presents a typical set-up of a porcelain bushing placed on transformer tank, while a typical cross section of a 230kV bushing is also shown in Figure 1.3.

Figure 1.1: Typical Substation Layout (OSHA)

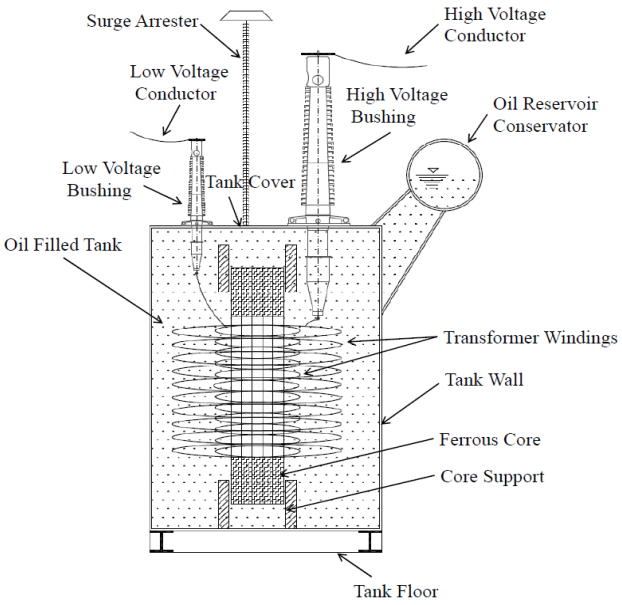

Figure 1.2: Cross Section of Typical High Voltage Transformer. Reprinted With Permission From (Koliou et al. 2012)

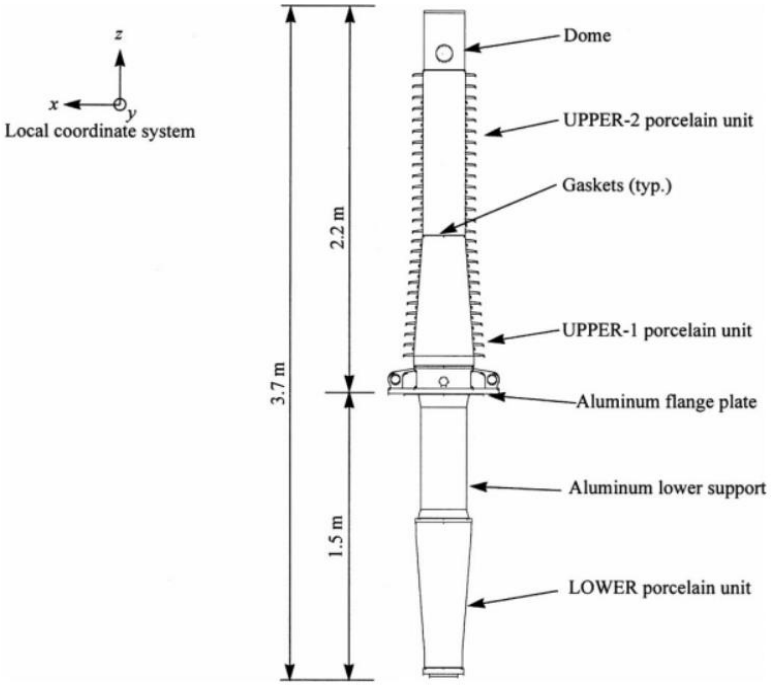

Figure 1.3: 230kV High Voltage Bushing Sample Cross-Section. Reprinted With Permission From (Gilani et al. 2001)

1.2. Seismic Performance on Past Earthquake Events and Associated Impact

High-voltage transformer-bushing systems have shown poor performance under extreme ground shaking in past earthquakes over the last 30 years including the 1989 Loma Prieta earthquake in the United States (Villaverde et al. 2001), the 2004 Bam-City earthquake in Iran (Fallahi 2004), the 1995 Kobe earthquake in Japan (Schiff 1998), and the 1999 Izmit earthquake based out of Turkey (Tang 2000). Each of these earthquakes had a lasting effect on their local areas, such as in Iran where approximately 70-90% of electrical infrastructure took significant damage (Fallahi 2004).

In particular, the porcelain bushings are known to be a key component of transformer failure caused by seismic activity. Strong earthquake shaking has been known to damage or even destroy/collapse porcelain bushings as shown in Figure 1.4, which was taken after the Bam-City earthquake. When damaged, porcelain bushings can be a major financial burden, both directly due to repair and removal cost for damaged material, and indirectly as the lack of power supply cripples local residents. Bushings have been known to fail most commonly in the form of either oil leakage, gasket extrusion, porcelain fracture, and or slippage of the porcelain units (Gilani et al. 2004). It should also be noted that the most vulnerable gasket is the one closest to the flange that connects the bushing to the transformer (Koliou et al. 2012).

Figure 1.4: Porcelain and Electrical Component Damage. Reprinted With Permission From (Fallahi 2004)

1.3. Literature Review – Past Studies

In this section a detailed literature review of past studies conducted on the seismic performance and enhancement of transformer bushing systems over the last two decades is summarized. These studies include a wide range of both analytical/numerical and experimental studies focusing either on understanding the seismic response of these systems or solutions to mitigate their seismic vulnerability.

Villaverde et al. (2001) studied the effects of ground motions on transformer bushings. It is reiterated in across that study that the bushings are susceptible to damage during heavy seismic activity. This is due to a wide variety of reasons, including (but not limited to) their low strength, non-homogeneous composition, and their tall yet slender design shape. The study by Villaverde et al (2001) focused on two different

formats of 500kV transformers, since they were most known at the time for having these issues. Numerical models of these transformers were generated in the SAP 2000 software and used to conduct time history analyses for a 2% damping ratio of the critical. The models were intended to be able to adequately represent the effect of ground motions on representative 500kV and 230kV transformer bushing systems. These analyses showed that a maximum ground motion amplification factor close to 2.0 was achieved for 500kV transformer bushings, and close to 4.0 for 230kV bushings. Because the bushings for the 500kV transformer was within the IEEE standard amplification factor, they were considered to be acceptable, however the 230kV transformer was outside of this acceptable range. It was concluded by Villaverde et al. (2001) that both analytical data could be an appropriate way to conduct seismic experimentation, as well as stating that future research should attempt to use higher levels of excitation to further investigate dynamic properties of transformers.

Gilani et al. (2001) performed a series of seismic evaluations of 230kV porcelain transformer bushings, as it was considered to be the more widely used form of transformer, and in some cases the more vulnerable setup that could be studied. Quasi-static tests were used to determine the responses of the bushing post-tensioning force, and doing so created a displacement history for the motion. In addition, three different support frame configurations were used to test the bushing structure namely, one for static testing, and two dynamic frames (one rigid and one flexible). Following this experimental study, it was observed that in certain cases, the 230kV bushing was unable to sustain a "*high-level qualification*" without some degree of damaging slippage or oil

leakage. In cases where it succeeded however, this study called into play the inaccuracy of testing methods due to the use of rigid frames in their testing. This study was one of the first to begin identifying the inaccuracy of qualification tests due to the use of rigid frames, which would be important in the future set-up to create seismic resistance methods.

Gilani et al. (2004) investigated the seismic impact on seven different bushing models used in either 196kV, 230kV, or 550kV transformers. The bushings were studied based on the 1997 version of the IEEE-693 standard for electrical transformers, which mandated three-component earthquake-simulator testing. Each bushing was mounted on a rigid frame, and Gilani et al (2004) also tested for fragility characteristics of the observed bushing, such as for example the relationship between peak ground acceleration resulting bushing conductivity after the ground motion had completed. In addition, the study incorporated two other variants of a 550kV transformer that was atypical to those in the field, attempting to see if either of them would perform better in testing. Upon running all scheduled ground motions, the 196kV and 230kV bushings had passed all tests with a high-level qualification. The 550kV bushings, however, all showed some form of damage at some point in the testing sequences, all leaking oil and slipping from their original position a considerable amount. Although the two proposed variants had showed improved resistivity to the ground motions, it was still not enough to reach a "*moderate*" qualification level.

Hatami et al. (2004) presented a study that focused on the seismic vulnerability of transformers, and did so in two major forms of tests. The first of these tests was done

in the laboratory on a flexible mounting frame, from which loads were imposed onto a rigid beam element representing the transformer. The second test was done analytically through a Finite Element Model as the entirety of the shape as a single entity. These were then compared to shake table tests of a full transformer model. This study was able to identify that the maximum tensile stress could be calculated from the bottom section of these transformers, and that the acceleration values were increased often due to most transformers commonly be placed on some form of base. This study also resulted in improved fragility models, identification of areas that could benefit from retrofitting, and validating the analytical methods used when compared to the shake table results.

Kong (2010) conducted research towards protecting electrical equipment against severe shocks and vibrations. This work primarily focused on any weak components that were identified through experimental and computational studies following the IEEE-693 2005 standard. However, rather than following the IEEE recommendation of testing a bushing mounted on a rigid frame, Kong et al. (2010) instead developed a model that would simulate a full transformer motion rather than just that of the bushing. In doing so, the motions that were applied appeared to have a greater degree of accuracy and realism, although a lack of prior testing using this method left a certain level of uncertainty. This style of testing also allowed Kong et al. (2010) to test factors such as bushing placement on the tested model, which was discovered to have a large impact on bushing performance. For example, bushings placed at the corner of the top plate seemed to have a limiting effect on the vertical motion of the transformer during activity, as well as closer to identical stiffness' in the principal x and y directions.

Reinhorn et al. (2011) devised a study to investigate the impact of seismic activity on electrical substations, paying particular attention to the transformer bushings. The focus of this research was to generate high fidelity models of high-voltage transformers in order to look at any structural modifications and changes that could be made to better protect fragile porcelain bushings, as well as assist in providing guidelines on modeling practices for transformers. The findings of this study proposed changes including redistribution of the weights of a typical electrical bushing and oil of each transformer, usage of a different meshing format for a typical transformer cover plate, and a reassembly of the core and coils used in the originally developed model. These changes were made individually and then analyzed on a case by case basis attempting to derive which models would give more realistic results. The proposed guidelines aid in understanding how these changes should be implemented, i.e., as how oil should be modeled as hitting one side at a time rather than both ends getting hit at half-force at once, as the former is more likely to occur in a common scenario.

Koliou et al. (2013a) and Koliou et al. (2013b) introduced the concept of flexural stiffeners added to the cover plates of transformers tanks close to the bushing base in order to lessen their susceptibility to seismic activity. The idea behind this method of using flexural stiffeners revolved around recreating rigid base testing scenarios that had caused the previously mentioned discrepancy between in-lab test results and real-world impact. Similar to Hatami et al. (2004), this study involved numerical and experimental analyses, using four different 3D finite element models of various geometric configurations as well as voltage ratings. The maximum bending moment at the base of

the high voltage bushing was considered to be the factor of interest, which was the reason for the use of flexural stiffeners as the design choice. Two different sets of ground motions were considered to conduct linear time history analyses on the four transformer-bushing models and develop cumulative distribution functions for the PoNE (probability of non-exceeding) the maximum allowable moment. These numerical studies had shown that the flexural stiffeners greatly benefiting the structures performance, reaching an effectiveness of 80%-97% when compared to a rigid plate. Proof of concept shake table experimental studies were conducted on a 230kV bushing system. These tests were conducted in three different formats: One containing a larger set of stiffeners, one with smaller set of stiffeners, and then one without any stiffening ("as-installed"). From these tests, it was found that the larger set of stiffeners (steel angle sections used) were the most effective at reducing the PoNE value, and the smaller stiffeners were able to reduce the values as well when compared to an unstiffened base. Reduction of moment amplification factor values was also achieved with the proposed stiffener configuration.

Probabilistic response in the form of fragility curves have been influential to the understanding of substation performance during seismic activity, including the work by Zareei et al. (2016) on the seismic failure probability of a 400 kV power transformer. The testing method considered in this study revolved around fragility curves which were used to estimate the level of exceedance in seismic activity, in the most common failure modes (i.e., from the porcelain bushing). This was performed in two ways, one scaling ground motions continuously until a collapse, and another at random different

intensities. The work revolved around the idea of a probability of exceedance of stress and displacement values, and was able to confirm that the vulnerable part of the observed power transformer was at the bottom of bushing, adjacent to the base similar to finding of previous studies (e.g., (Koliou et al. 2013a)).

In addition to flexural stiffeners, another method of protecting bushings has been explored by several studies available in the literature involving base isolation of a typical substation setup. Oikonomou et al. (2016) researched the impact of base isolation in the form of two different configurations. The first of those configurations was a stiffened and highly damped Lead-Rubber Bearing (LRB). The intention of the LRB was to provide high vertical stiffness, while still allowing for effective energy dissipation through plastic deformation in the lateral direction(s). The second configuration for base isolation was the use of Triple Friction Pendulum bearings. The "triple" aspect of its name is descendent of the Single Friction Pendulum, where this system contains four different sliding components (as opposed to two surfaces in a single friction pendulum system), allowing for a large capacity for displacement and, by definition of the system, damping potential. Both of these systems were investigated, both experimentally and analytically, on an ABB 196/230kV medium-voltage porcelain bushing. Both of these systems had achieved the goal of increasing the bushings ability to handle seismic interactions. It was found that the base shear forces were not as impactful on the transformers performance, and that the, "*achieved reduction in the average acceleration response was found to be on the order of 70%-80%*". The use of base isolation in this

system also reduced the horizontal acceleration demand at the base of the power transformer, as well as at the mounting interface of the bushing.

Gökçe et al. (2017) studied the seismic protection of high voltage bushings by considering the use of four polyurethane springs with steel plates which were used to generate a large rotational capacity with a low lateral displacement. To test the effectiveness of these polyurethane springs, three different tests were run on the sample layout. The use of these springs had shown success on multiple fronts, such as a less than 0.04in lateral displacement from an applied moment, and a much higher achieved damping ratio of 8.0% when compared to 0.2% of a typical rigid base. The spring system was also tested on a shake table representing seven earthquakes above a 6.0 magnitude, and displayed a substantial decrease in acceleration values across simulation in comparison to a fixed base. Finally, the proposed spring setup displayed an ability to self-center following extreme ground shaking, which could be seen as a great benefit in its ability to handle aftershocks as well as the initial ground motion.

Kitayama et al. (2017) proposed on another form of base isolation for medium- and high-voltage transformers. Their goal was to create a form of isolation that was three-dimensional in nature, but also practical for high-voltage transformers. The design requirements were based around the system being a modular extension of a horizontal isolation transformer system, where the horizontal and vertical systems were separate, and all components could be both passive and reliable. With this in mind, the developed system used triple friction pendulum isolators for horizontal restriction, and coil steel springs to aid in the vertical motions. This was investigated analytically with a

numerical model, before investigating the setup through shake table testing. The study used FEMA P695 far field ground motions, and also incorporated the vertical components of their study for the purpose of testing the vertical resistivity of their proposed system. Both sets of tests, one with horizontal isolation and the other with both horizontal and vertical isolation, resulted in a significant horizontal acceleration reduction at all times, and vertical acceleration reduction in most scenarios. The vertical direction outliers were considered to be an inevitability by Kitayama et al. (2017), as it would be impractical to further increase the high damping of the system.

Ma and Xie (2018) studied the dynamic interactions of high-voltage transformer components with the intent to measure the seismic response of the transformer components by mounting the tank, rather than mounting the turret as in other studies. In addition, the primary goal was to examine the relationship between the couplings of these two components, noting that past studies had not addressed this. Preliminary testing had shown that there was a relationship between the tank, turret, and bushing that positively impacted performance with the use of a more rigid mount as opposed to flexible mounts. This included both lower measured acceleration values and lower displacements at the top of the bushings. This study concluded that future seismic analysis should be primarily based on the structure of the transformer tank rather than just the turret and bushing to allow for better seismic design.

1.4. Problem Statement and Research Objectives

The purpose of this research was to evaluate the practicality and feasibility of the retrofit solution of flexural stiffeners at the transformer tank as proposed by Koliou et al. (2013a) for electrical transformer bushing systems in terms of decision variables associated with economic losses (dollars) and downtime related to the post-earthquake recovery of electrical substations. Although there has been extensive research conducted on evaluating the response of as-installed transformers as well as proposing seismic mitigation techniques, there is a gap in knowledge in quantifying the impact of the seismic vulnerability of such systems in terms of recovery attributes. The continued operation and functionality of electrical substation networks is of great significance to the rapid post-earthquake recovery of communities. The recovery of communities is a highly interdependent process where the restoration and functionality of lifeline networks (e.g., power, water) are the most critical and highly prioritized systems/components. Towards that direction, this study focused on risk-based performance assessment analyses of as-installed and retrofitted transformer systems following the PEER Performance-Based Earthquake Engineering Methodology (PBEE).

Four different numerical models of high-voltage electrical transformers of various voltage rating and geometries were used herein, each with one retrofitted version used for analysis. These models were subjected to selected types of seismic inputs including the FEMA P695 Far-Field and Near-Field ground motion ensembles (FEMA 2009). These motions were scaled according to the 5% damped IEEE-693 Response Spectrum (IEEE 2005). The results of the time history analyses and the associated

collapse fragility curves were then considered for conducting a set of probabilistic analyses to evaluate the downtime and economic losses (direct and non-direct) associated with each mounting condition (i.e., as-installed and retrofitted) under the considered seismic inputs. These metrics give a more comprehensive understanding of these forms of seismic protection which will lead to effective implementation of such techniques in order to mitigate the seismic vulnerability of these systems and their associated post-earthquake disruption and recovery trajectory.

1.5. Thesis Organization

Following this introductory section, the second chapter provides the structural details for all transformer model configurations used in this study, as well as the applied ground motions. This includes the base models, a description of the applied retrofitting technique, and the ground motions considered in this study for performing time history analyses. The chapter also encompasses the structural response of each transformer configuration when affected by each ground motion set considered. The third chapter then goes over the application of the Performance Based Earthquake Engineering (PBEE) framework and the components necessary for a performing a risk analysis of the transformer models both as-installed and retrofitted under various seismic inputs. The final sections of this chapter provide detailed descriptions of the sustained economic losses accounting for direct losses and downtime (indirect losses) in a side-by-side comparison of both individual expected transformer losses, as well as expected annual losses for the two chosen target locations within the state of California representing

distance to fault rupture lines. Finally, chapter four summarizes the components of this study, as well as the relevant conclusions and suggestions for future research pertaining to this topic.

2. NUMERICAL STUDIES ON STRUCTURAL PERFORMANCE OF TRANSFORMER BUSHING SYSTEMS UNDER SEISMIC EXCITATION

2.1. Introduction

In this chapter, the transformer bushing numerical models selected for this study will first be presented and their modifications to accommodate the retrofit scheme of flexural stiffeners, as well as the dynamic analyses of these models, providing the ground selected motions, their scaling procedure, the selection of the engineering demand parameter and the response analyses findings. The product of the time history analyses will be the development of fragility curves for each of the transformer bushing models for the mounting the two mounting conditions (as-installed and retrofitted) considered in this study.

2.2. Transformer Model Selection

For this study, four different transformer models of various voltage ratings and geometries were selected, namely the Siemens 230kV transformer, the Ferranti Packard 230kV transformer, the Siemens 500kV transformer, and the Westinghouse 525kV transformer. The 230kV transformer bushing structures are commonly used as "medium-voltage" transformers (FEMA 2010) and as such it was considered that by considering two different configurations in this study could produce more realistic results in terms of applicability. In addition to this, the 500kV and 525kV transformers represent a high voltage level (FEMA 2010), and therefore would be more crucial to the

areas in which they are present especially in case of the occurrence of strong seismic excitation resulting in damage to those transformer and disruption of the electrical power network. These four transformers therefore represent a good sample size of transformers to be used in the remainder of the project.

Based on the objectives of this study as presented in Chapter 1, the four transformer models were considered both as-installed and retrofitted with flexural stiffeners as proposed by (Koliou et al. 2013a) to be analyzed under seismic excitation inputs. All transformer bushing models, both as-installed and retrofitted versions, were modeled using the structural analysis program, SAP2000 (CSI 2018). The bushings were modeled as multiple beam elements in series with the appropriate geometry representative of their position; mounted to cover plate of each transformer model. Each bushing consisted of three parts: the medium- or high- voltage bushing itself; rigid elements representing the bushing flange, and the turret itself using a large number of surfaces to match with the rigid elements of the bushing (Koliou et al. 2012). The transformer frames were modeled as shell elements with a degree of thickness and mass that allowed for appropriate deformation and bending, while the stiffeners (used for the retrofit) were modeled with both beam and shell elements (Filiatrault and Matt 2006). The transformer tanks for each model were each made up of shell elements, and vertical loading was used to represent a scenario where the tanks were considered to be full of oil (Oikonomou 2010). This added weight of the oil is reflected in the transformer weight in Table 2.1.

The geometric and weight characteristics of the transformer models, as well as their fundamental frequencies for later uses in Chapter 3 are summarized in Table 2.1, while three dimensional view of all models is provided in Figure 2.1-Figure 2.4(Koliou et al. 2012).

Table 2.1: Basic Transformer Dimensions and Weight (Koliou et al. 2012)

Transformer Model	Length(ft)	Width(ft)	Height(ft)	Weight (kips)
Westinghouse 525kV	8.8	9.9	22.8	463
Siemens 230kV	10.0	24.2	14.4	478
Siemens 500kV	10.8	26.0	16.8	673
Ferranti Packard 230kV	8.3	26.0	13.0	266

Table 2.2: Transformer Resonant Frequencies (Koliou et al. 2012)

Transformer Model	First Mode Frequency (Hz) (As-Installed)	First Mode Frequency (Hz) (Retrofitted)
Westinghouse 525kV	8.8	9.9
Siemens 230kV	10.0	24.2
Siemens 500kV	10.8	26.0
Ferranti Packard 230kV	8.3	26.0

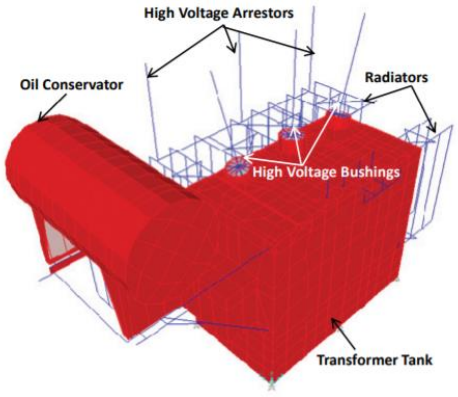

Figure 2.1 Ferranti Packard 230kV Transformer. Reprinted With Permission From (Koliou et al. 2012)

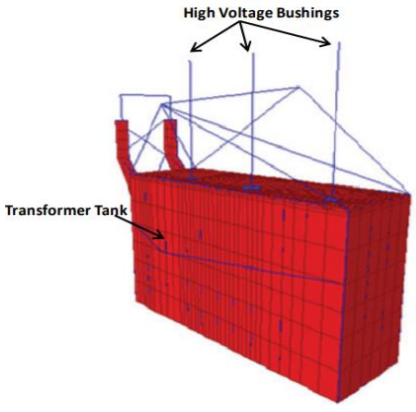

Figure 2.2: Siemens 230kV Transformer. Reprinted With Permission From (Koliou et al. 2012)

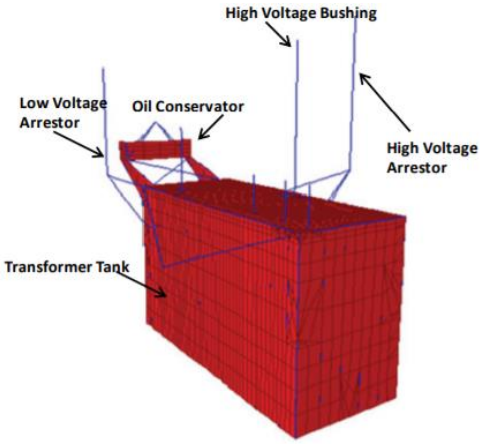

Figure 2.3: Siemens 500kV Transformer. Reprinted With Permission From (Koliou et al. 2012)

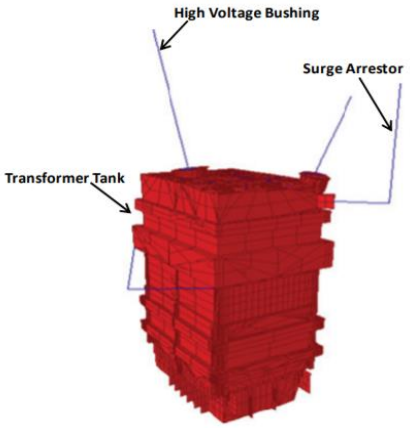

Figure 2.4: Westinghouse 525kV Transformer. Reprinted With Permission From (Koliou et al. 2012)

2.3. Dynamic Analyses of Transformer Bushing Models

2.3.1. Ground Motion Selection and Scaling Process

Ground motions from the FEMA P695 document were considered (FEMA 2009) in this project. The FEMA P695 study was published in 2009 and contained a methodology catered to quantify seismic based parameters into structural design. The purpose was to "*result in equivalent safety against collapse in an earthquake, comparable to the inherent safety against collapse intended by current seismic codes, for buildings with different seismic-force-resisting systems*" (FEMA 2009). In addition, this study would use two sets of ground motions, representing ground motions in both close and distant proximity to the ruptured faults. These sets are denoted as "*Far-Field*" for those in a proximity of 10km or greater, and "*Near-Field*" for recorded ground motions less than 10km from the fault. The near-field data set is also split up into two different sub-sets: "*Pulse*", referencing motions that contained strong pulses of motion; and "*Non-*

Pulse", those that were more uniform. All of the ground motions chosen have a magnitude of at least 6.5, and are detailed within the Pacific Earthquake Engineering Research Center (PEER) NGA database. Each ground motion set also contains multiple ground motions with a peak ground acceleration of at least 0.80. All motions have two components each and are selected to represent the seismicity of the Western United States. Table 2.3 summarizes the far-field data set considered for this study, while Table 2.4 and Table 2.5 summarized the sets of ground motions used in the near-field data set.

Guidelines on the design and testing of electrical substation equipment is included in the Institute of Electrical and Electronics Engineers (IEEE) standard 693, titled, "*IEEE Recommended Practice for Seismic Design of Substations*" (IEEE 2005). This standard goes into detail about the methods of obtaining the seismic capabilities of electrical substation equipment and provides guidelines for testing substation effectiveness with certain damping ratios based on the assumed characteristics of the object the motions are being applied to. For this study, the 5% damped IEEE high response spectrum will be considered. Figure 2.5 shows the IEEE high response spectra for various damping ratios (2%, 5% and 10%).

Before the dynamic analyses were performed, the spectral values of all ground motion ensembles were scaled to match the IEEE – 693, 5% damped, high required response spectrum in a range of frequencies between 2.0 and 30.0 Hz. This range was selected based on the reported frequencies of the high voltage bushings for all four transformer models varying from 2.5 Hz (as-installed) to 25 Hz (rigid base) (Koliou et

al. 2012) and was identified as the range of interest to scale the ground motions for this study.

Table 2.3: FEMA P695 Far-Field Ground Motion Set

EQ Index	EQ ID	NGA Number	EQ Name	Year	Magnitude	PGA_{max}(g)
1	12011	953	Northridge	1994	6.7	0.52
2	12012	960	Northridge	1994	6.7	0.48
3	12041	1602	Duzce, Turkey	1999	7.1	0.82
4	12052	1787	Hector Mine	1999	7.1	0.34
5	12061	169	Imperial Valley	1979	6.5	0.35
6	12062	174	Imperial Valley	1979	6.5	0.38
7	12071	1111	Kobe, Japan	1995	6.9	0.51
8	12072	1116	Kobe, Japan	1995	6.9	0.24
9	12081	1158	Kocaeli, Turkey	1999	7.5	0.36
10	12082	1148	Kocaeli, Turkey	1999	7.5	0.22
11	12091	900	Landers	1992	7.3	0.24
12	12092	848	Landers	1992	7.3	0.42
13	12101	752	Loma Prieta	1989	6.9	0.53
14	12102	767	Loma Prieta	1989	6.9	0.56
15	12111	1633	Manjil, Iran	1990	7.4	0.51
16	12121	721	Superstation Hills	1987	6.5	0.36
17	12122	725	Superstation Hills	1987	6.5	0.45
18	12132	829	Cape Mendocino	1992	7	0.55
19	12141	1244	Chi-Chi, Taiwan	1999	7.6	0.44
20	12142	1485	Chi-Chi, Taiwan	1999	7.6	0.51
21	12151	68	San Fernando	1971	6.6	0.21
22	12171	125	Friuli, Italy	1976	6.5	0.35

Table 2.4: FEMA P695 Near-Field Ground Motion Set, Pulse

EQ Index	EQ ID	NGA Number	EQ Name	Year	Magnitude	PGA_{max}(g)
PULSE						
1	820181	181	Imperial Valley-06	1979	6.5	0.44
2	820182	182	Imperial Valley-06	1979	6.5	0.46
3	820292	292	Irpinia, Italy-01	1980	6.9	0.31
4	820723	723	Superstation Hills-02	1987	6.5	0.42
5	820802	802	Loma Prieta	1989	6.9	0.38
6	820821	821	Erzican, Turkey	1992	6.7	0.49
7	820828	828	Cape Mendocino	1992	7	0.63
8	820879	879	Landers	1992	7.3	0.79
9	821063	1063	Northridge-01	1994	6.7	0.87
10	821086	1086	Northridge-01	1994	6.7	0.73
11	821165	1165	Kocaeli, Turkey	1999	7.5	0.22
12	821503	1503	Chi-Chi, Taiwan	1999	7.6	0.82
13	821529	1529	Chi-Chi, Taiwan	1999	7.6	0.29
14	821605	1605	Duzce, Turkey	1999	7.1	0.52

Table 2.5: FEMA P695 Near-Field Ground Motion Set, Non-Pulse

EQ Index	EQ ID	NGA Number	EQ Name	Year	Magnitude	PGA_{max}(g)
NON-PULSE						
15	820126	126	Gazli, USSR	1976	6.8	0.71
16	820160	160	Imperial Valley-06	1979	6.5	0.76
17	820165	165	Imperial Valley-06	1979	6.5	0.28
18	820495	495	Nahanni, Canada	1985	6.8	1.18
19	820496	496	Nahanni, Canada	1985	6.8	0.45
20	820741	741	Loma Prieta	1989	6.9	0.64
21	820753	753	Loma Prieta	1989	6.9	0.51
22	820825	825	Cape Mendocino	1992	7	1.43
23	821004	1004	Northridge-01	1994	6.7	0.73
24	821048	1048	Northridge-01	1994	6.7	0.42
25	821176	1176	Kocaeli, Turkey	1999	7.5	0.31
26	821504	1504	Chi-Chi, Taiwan	1999	7.6	0.56
27	821517	1517	Chi-Chi, Taiwan	1999	7.6	1.16
28	822114	2114	Denali, Alaska	202	7.9	0.33

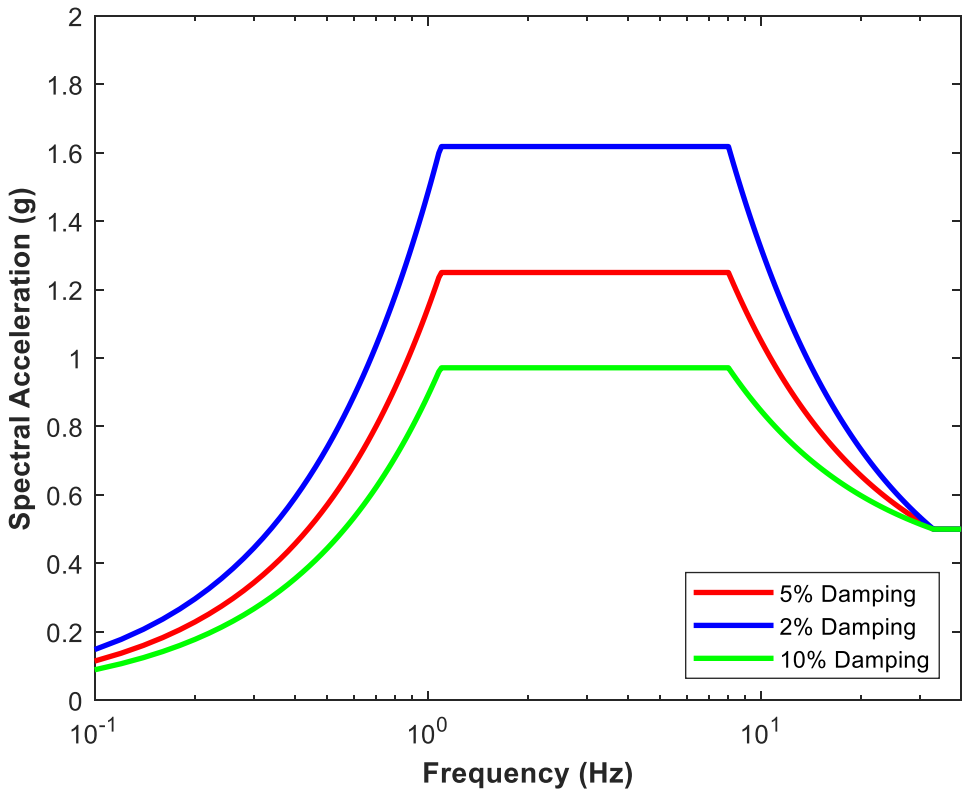

Figure 2.5: IEEE High Required Response Spectra (IEEE 2005)

The goal is to have the selected ground motions reflect a similar structure and values by multiplying their spectral accelerations by a provided scale factor. Although typically the median is used to attempt to calculate such scaling factors, the geometric mean of the respective ground motion sets would instead be selected for this study. This is primarily due to the fact that the geometric mean is a calculatable value, where errors can be minimized through checking its calculated variance, whereas the median scale factor's effectiveness can be different depending entirely on the skewness of the ground motion sets. Furthermore, the geometric mean is an orientation independent measure for all ground motions selected (Fahad and Roh 2013; Fahad and Oikonomou 2010;

Filiatrault and Matt 2006). Once a preliminary scale factor was chosen from the use of the geometric mean, they were then confirmed based on the IEEE spectra that was previously referenced in Figure 2.5. Following the procedure outlined by (Koliou et al. 2012), the geometric mean values taken from the ground motions were then used in tandem with the IEEE spectrum in order to obtain the estimated scale factor. The formula used to achieve this can be seen below in equation 2.1:

$$F_j = \frac{\sum w_k S_{IEEE}(f_k) S_{ageomean}(f_k)}{\sum w_k S_{ageomean}(f_k)^2} \qquad \textbf{EQ 2.1}$$

where F_j represents the scale factor used for our ground motions, w_k is the weight factor considered at prescribed frequencies, $S_{IEEE}(f_k)$ is the IEEE-693 spectrum value at frequency f_k, and $S_{ageomean}(f_k)$ is the geometric mean of the spectral acceleration at frequency f_k. Summing these values up and calculating F_j provides the scale factors listed in Table 2.6. The graphical representations of these spectra (IEEE spectrum and scaled ground motion set spectrum) can be seen in Figure 2.6 and Figure 2.7 below:

Table 2.6: FEMA P695 Far-Field Ground Motion Set

Ground Motion Set	Number of Motions	Applied IEEE Scale Factor	IEEE Damping Ratio Used
P695 Far-Field	22	1.90	5%
P695 Near-Field (Pulse)	14	1.297	5%
P695 Near-Field (Non-Pulse)	14	1.565	5%

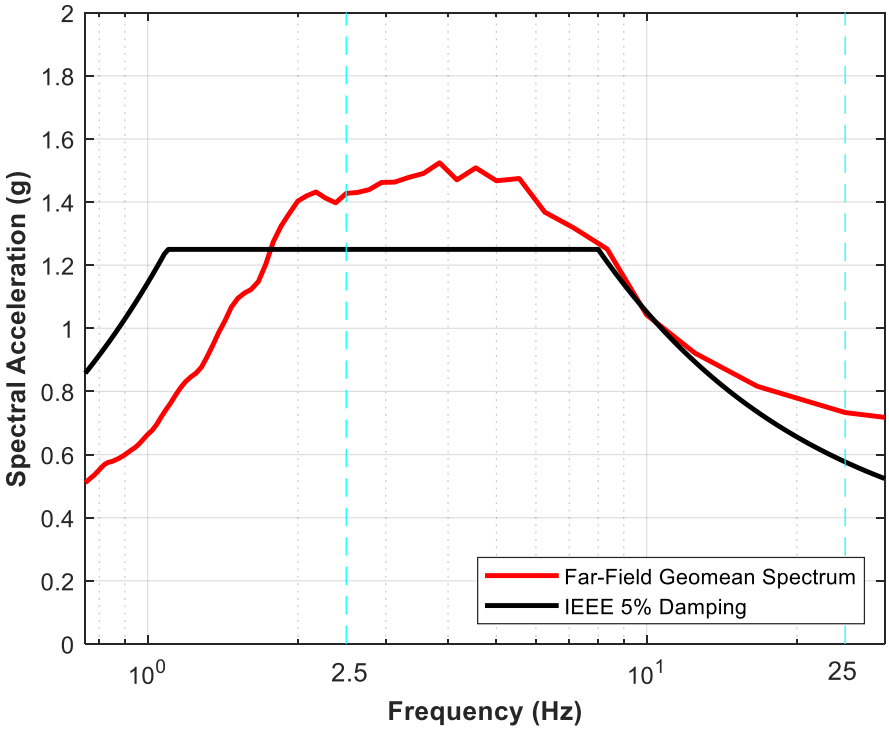

Figure 2.6: Far-Field Ground Motion Set Scaling to Match the IEEE Spectra

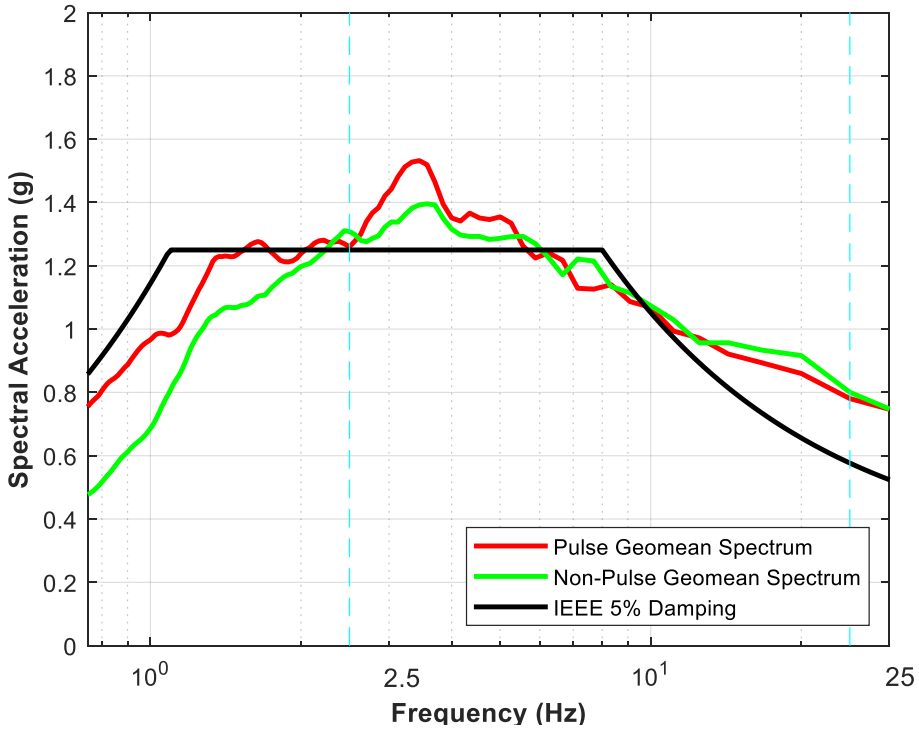

Figure 2.7: Near-Field Ground Motion Sets Scaling to Match the IEEE Spectra

2.3.2. Selection of Engineering Demand Parameter

When looking at the remaining scope of this study, it was important to establish early on how the damage of each transformer structure caused by the selected ground motions will be quantified and select the appropriate engineering demand parameter (EDP) of interest. Based on previous studies on the seismic performance of high voltage bushing structures (Villaverde, 2001; Gilani, 2004; Reinhorn, 2011; Koliou, 2012; Zareei, 2016), the parameter of choice is the maximum bending moment at the base of the observed bushing(s). Since all motions were applied in both a longitudinal and transverse direction, the motions were calculated by taking the maximum observed resultant moment at a given time period *t*. These values were taken from the SAP2000 frames representing transformer bushings, as can be seen from Figure 2.1- Figure 2.4. Once those points were selected, their resulting moment values were put into the following equation to account for the response of both the longitudinal and transverse moment response as stated in equation 2.2:

$$\boldsymbol{M_R(t) = \mathbf{Max_t}(\sqrt{M_T(t)^2 + M_L(t)^2})} \qquad \textbf{EQ 2.2}$$

Where $M_T(t)$ and $M_L(t)$ represent the moments of the bushing base at a provided time *t* in the transverse and longitudinal axis' respectively, and $M_R(t)$ represents the resultant moment value. The $\mathrm{Max_t}$ is representative of the process of applying our ground motions, where the resultant force chosen will be the maximum observed value across all ground motions in a given set. This ensures that across the multiple chosen scale factors, the most impactful ground motion in terms of damage is chosen for each scale factor.

2.3.3. Dynamic Analysis Results

After obtaining the scale factors for the data based off of the IEEE-693 Spectrum, linear time history analyses were performed on the previously described transformer models in SAP 2000 (Computers and Structures, 2009). To simulate our transformer models, each model was run through all P695 Far-Field and Near-Field ground motion ensembles at varying degrees of seismic intensity (incremental dynamic analyses were performed). These ranges were augmented by the scale factor determined for each ground motion ensemble, with every used acceleration also being multiplied by said scale factor. The intent was for the ground motions to run at a prescribed level of increasing intensity, thereby creating an incremental dynamic analysis (IDA) based approach (Vamvatsikos and Cornell 2002). After running fourteen different variations of acceleration for each ground motion ensemble, the resulting maximum observed moment values were taken from the joints and frames at the bushings base by using equation 2.2. Each of these maximum values were then fit by means of a lognormal cumulative distribution function, thereby creating fragility curves. Fragility curves are crucial to the dynamic analysis in that their purpose is to represent the probability of exceeding a damage state based on a provided demand parameter, which at the moment is proposed to be the maximum observed bushing moment values. This parameter has been previously found to be a good indication of the vulnerability of transformer bushings (Koliou et al. 2012). Using these, we can have a clear representation of values that would cause significant damage to our transformers.

The retrofitted models were designed based on the addition of flexural stiffeners to the transformers. As was detailed by Koliou et al. (2013a), stiffeners were added to various transformer models either between the tank surface and bushing, or between the tank surface and the bushing turret. After further analysis, stiffeners were also applied to the top plate of the transformer tank in both the longitudinal and transverse direction to assist with the effectiveness of the former ones. The stiffeners appeared to increase the degree of stiffening of the transformer bushings to be closer to the fixed-base conditions mentioned previously in Chapter 1. Each retrofitted transformer was run through the same format of ground motions as the as-installed models. The results of the analysis of these models can be seen in Figure 2.8-Figure 2.19 in the form of lognormal cumulative probability distribution curves for exceeding a prescribed maximum bending moment at the bushing's base (fragility curves generated). Table 2.8 can be used to see a direct percentage difference between the median observed values of the retrofitted transformers and as-installed models. The fragility curves presented in this chapter correspond to collapse fragility curves. For the purpose of the risk-based assessment as introduced and discussed in the next chapter (Chapter 3), based on the analysis results from the SAP2000 models, fragility curves for the various damage states considered were developed.

After the fragility curves were created (Figure 2.8-Figure 2.19), a Kolmogorov-Smirnov (KS) Test was computed for each individual curve to ensure that they are appropriately shaped and the lognormal distribution was the appropriate distribution selected for the particular set of the data from the analyses. The Kolmogorov Smirnov

test is designed to analyze a cumulative distribution function and provide approximate values of the curve at designated intervals provided by the data. The test then examines the differences between observed data and the approximations to determine if the difference passes a critical value, D_n which would equate to an improper data point (Ang and Tang 1984). For these tests a 95% level of confidence was used, and having 14 distinct data points per ground motion set would equate to a critical D_n of 0.34890. After testing each data set through a KS Test, each as-installed data set observed a maximum difference below D_n, with all values being below 0.15, thereby passing the KS test. As for the retrofitted models, all of the fragility curves also passed the KS test reaching maximum values below 0.16. This would indicate that each fragility curve adequately fits the data and is representative of its nature. The results of all KS tests can be seen in Table 2.9 following the fragility curve figures.

Table 2.7: Transformer Fragility Curve Log Medians & Standard Deviations

Transformer Model	As-Installed or Retrofitted	Ground-Motion Ensemble	Lognormal Median θ	Lognormal Standard Deviation β
230kV Packard	As-Installed	Far-Field	1.346	0.672
230kV Packard	As-Installed	Near-Field (Pulse)	1.513	0.672
230kV Packard	As-Installed	Near-Field (Non-Pulse)	1.463	0.672
230kV Packard	Retrofitted	Far-Field	0.888	0.672
230kV Packard	Retrofitted	Near-Field (Pulse)	0.884	0.672
230kV Packard	Retrofitted	Near-Field (Non-Pulse)	1.093	0.672
230kV Siemens	As-Installed	Far-Field	2.256	0.672
230kV Siemens	As-Installed	Near-Field (Pulse)	2.360	0.672
230kV Siemens	As-Installed	Near-Field (Non-Pulse)	2.382	0.672
230kV Siemens	Retrofitted	Far-Field	1.832	0.672
230kV Siemens	Retrofitted	Near-Field (Pulse)	2.025	0.672
230kV Siemens	Retrofitted	Near-Field (Non-Pulse)	2.050	0.672
500kV	As-Installed	Far-Field	1.739	0.672
500kV	As-Installed	Near-Field (Pulse)	1.710	0.672
500kV	As-Installed	Near-Field (Non-Pulse)	1.817	0.672
500kV	Retrofitted	Far-Field	1.274	0.672
500kV	Retrofitted	Near-Field (Pulse)	1.239	0.672
500kV	Retrofitted	Near-Field (Non-Pulse)	1.326	0.672
525kV	As-Installed	Far-Field	2.097	0.672
525kV	As-Installed	Near-Field (Pulse)	2.052	0.672
525kV	As-Installed	Near-Field (Non-Pulse)	1.976	0.672
525kV	Retrofitted	Far-Field	1.810	0.672
525kV	Retrofitted	Near-Field (Pulse)	1.775	0.672
525kV	Retrofitted	Near-Field (Non-Pulse)	1.724	0.672

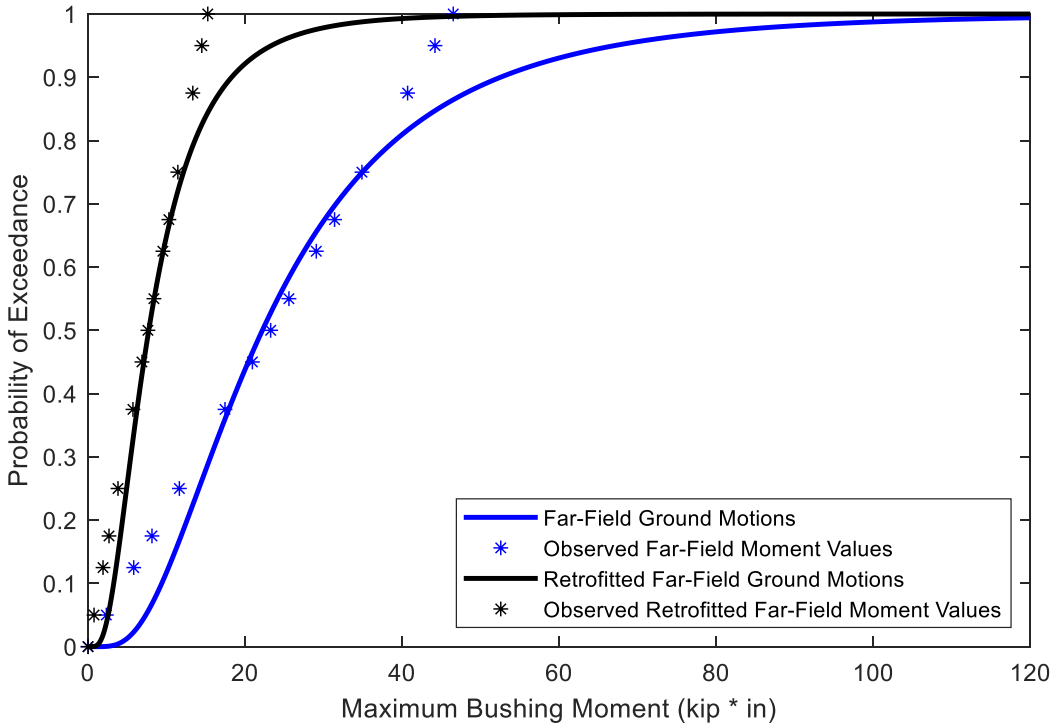

Figure 2.8: 230kV Packard Far-Field Fragility Curves

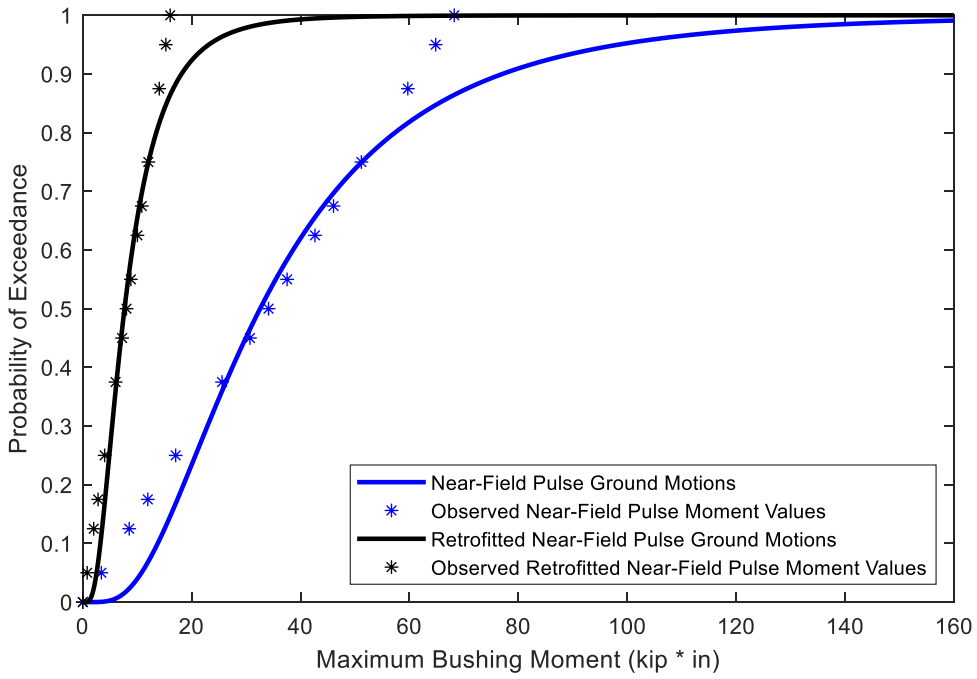

Figure 2.9: 230kV Packard Near-Field Pulse Fragility Curves

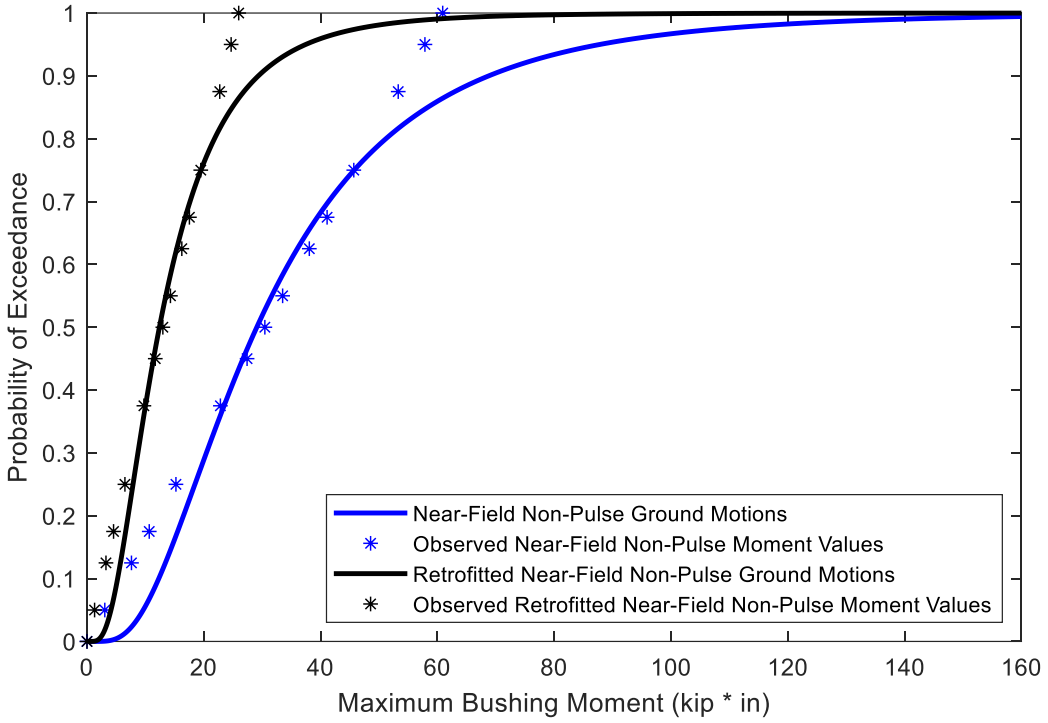

Figure 2.10: 230kV Packard Near-Field Non-Pulse Fragility Curves

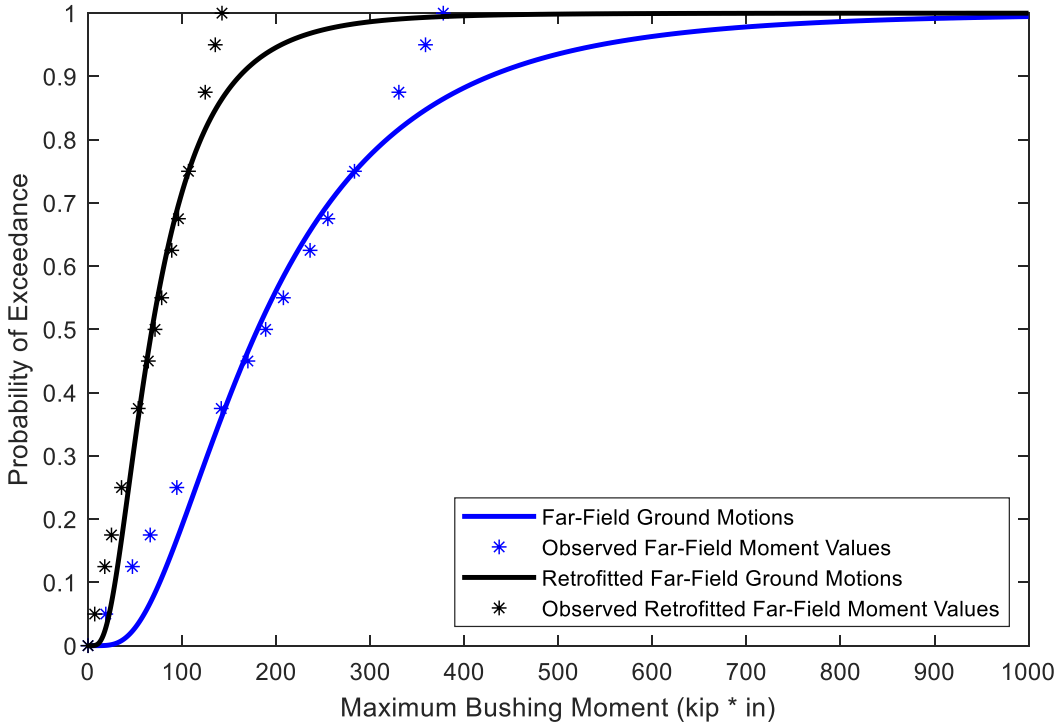

Figure 2.11: 230kV Siemens Far-Field Fragility Curves

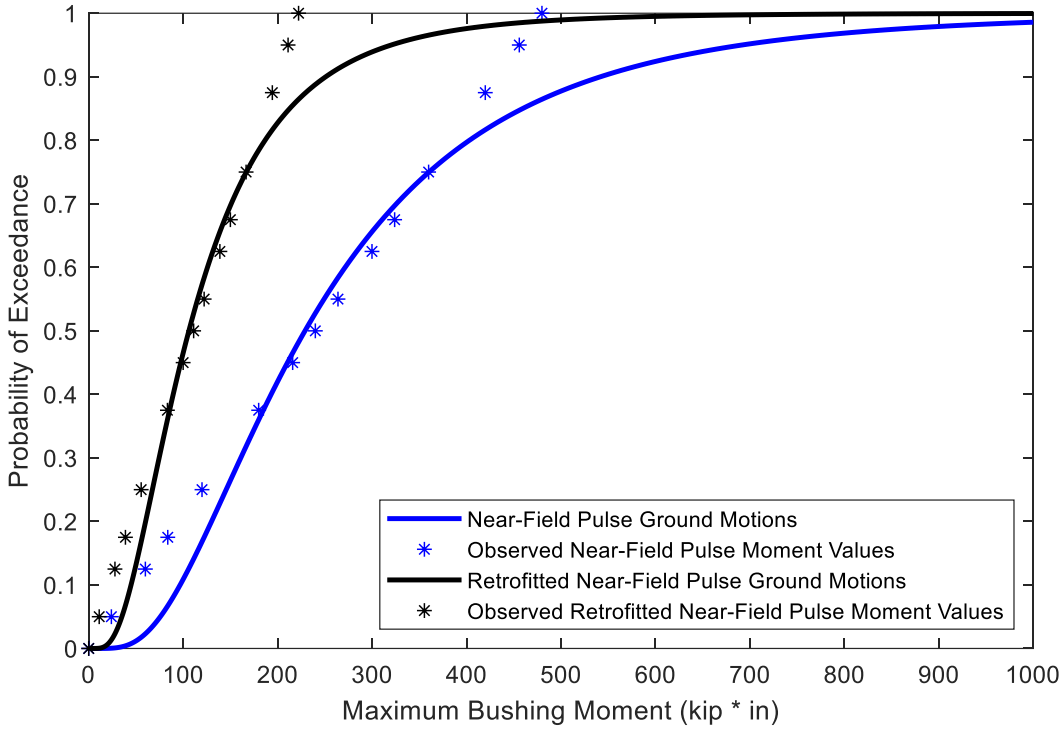

Figure 2.12: 230kV Siemens Near-Field Pulse Fragility Curves

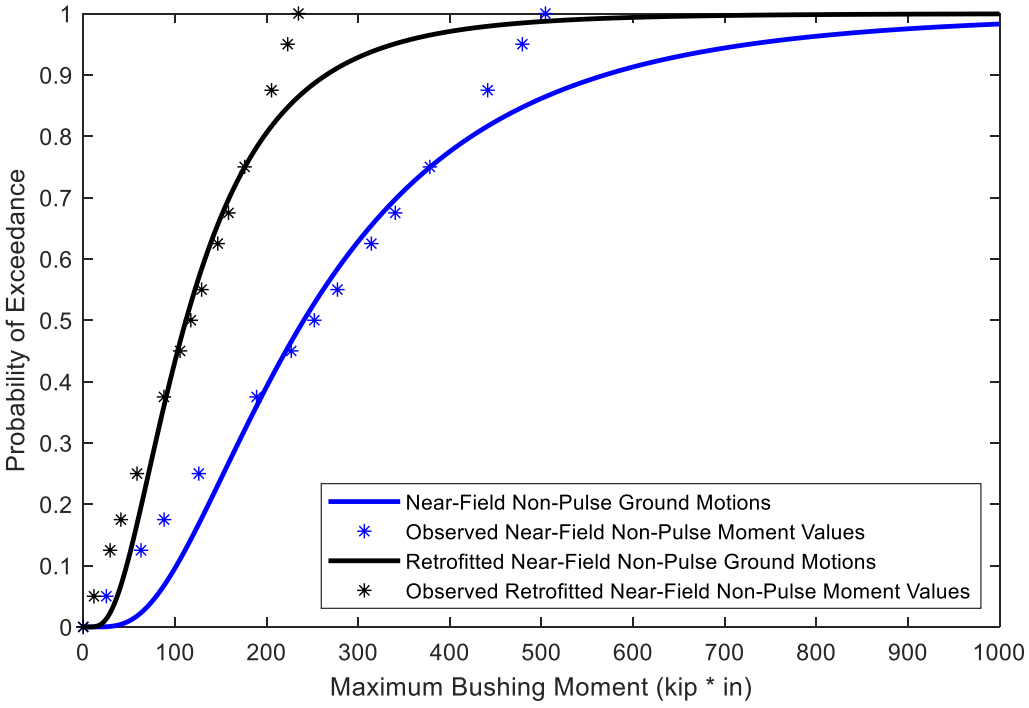

Figure 2.13: 230kV Siemens Near-Field Non-Pulse Fragility Curves

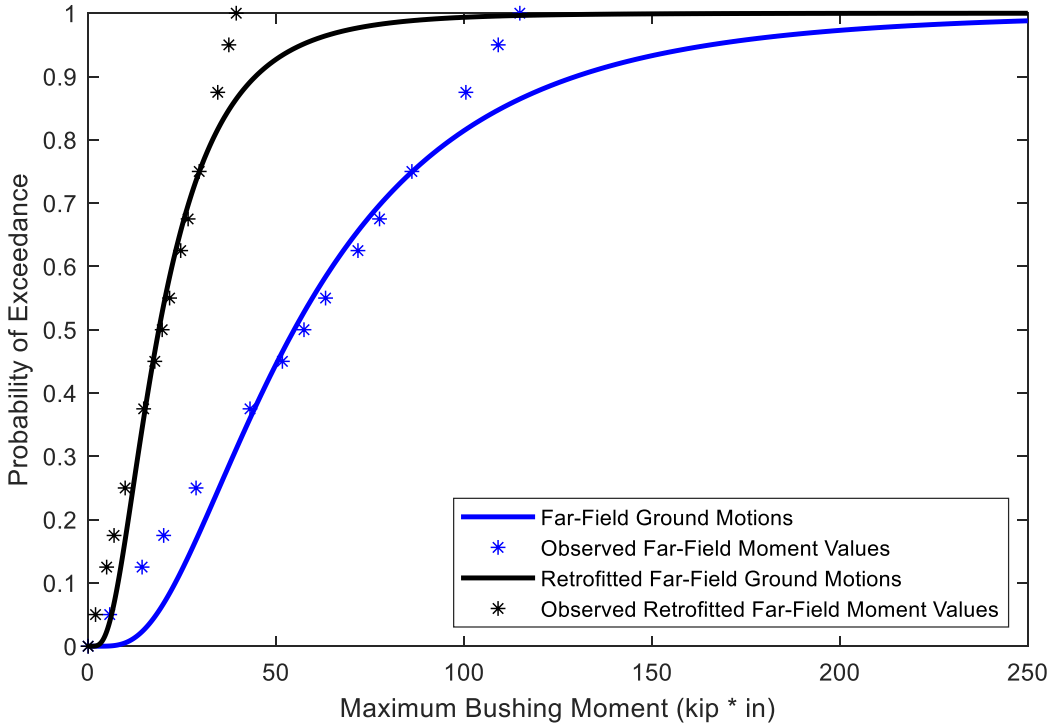

Figure 2.14: 500kV Far-Field Fragility Curves

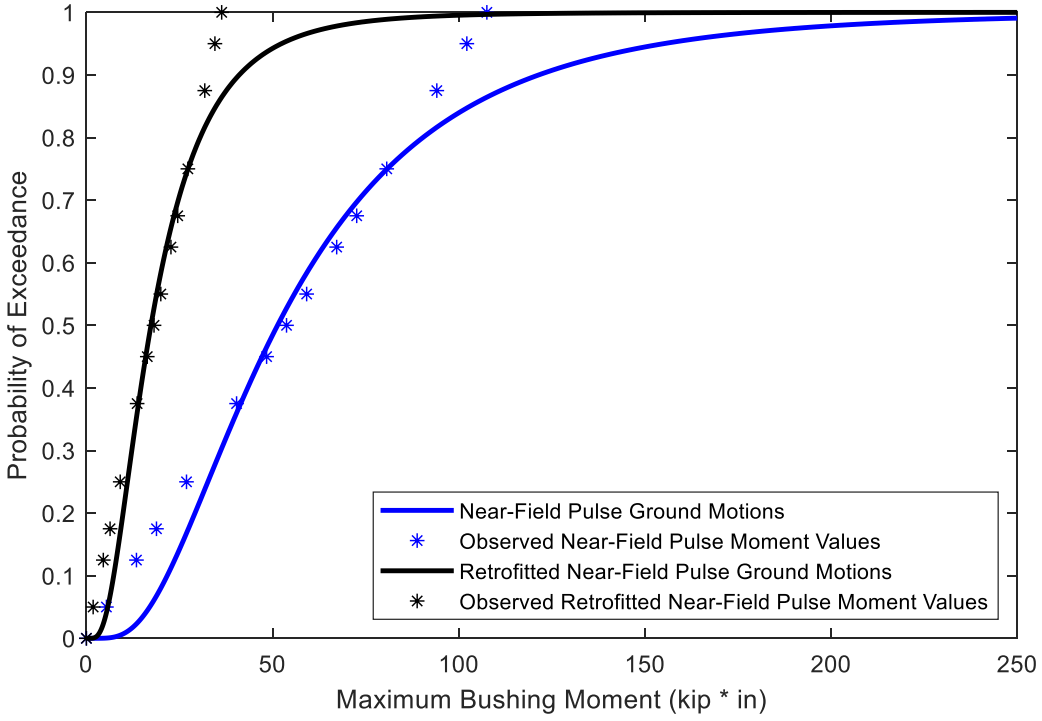

Figure 2.15: 500kV Near-Field Pulse Fragility Curves

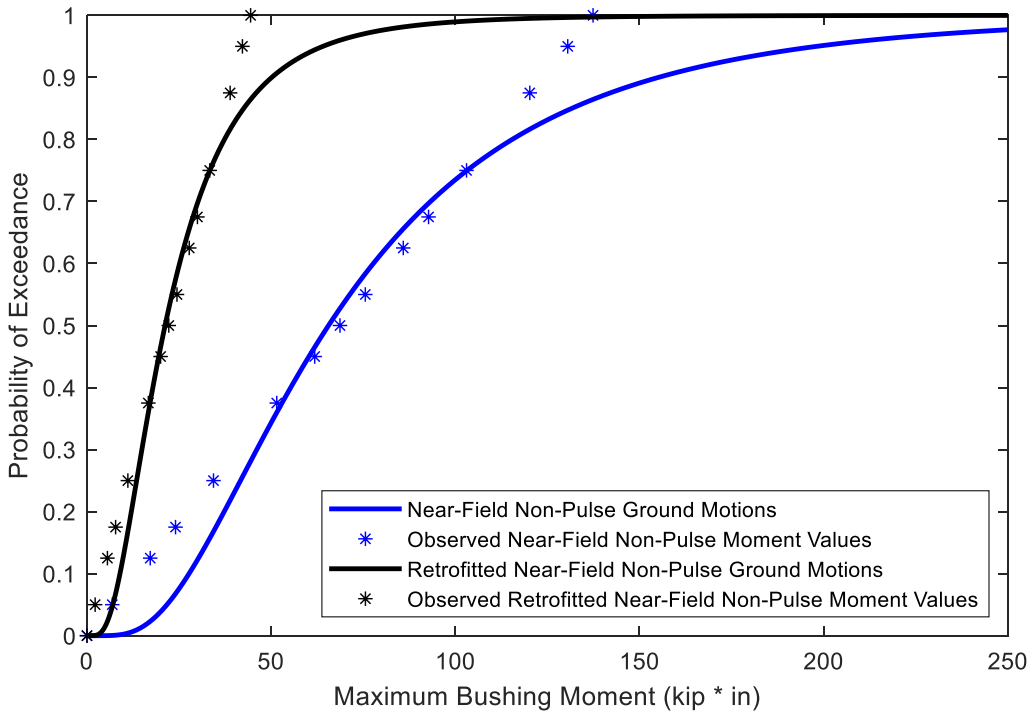

Figure 2.16: 500kV Near-Field Non-Pulse Fragility Curves

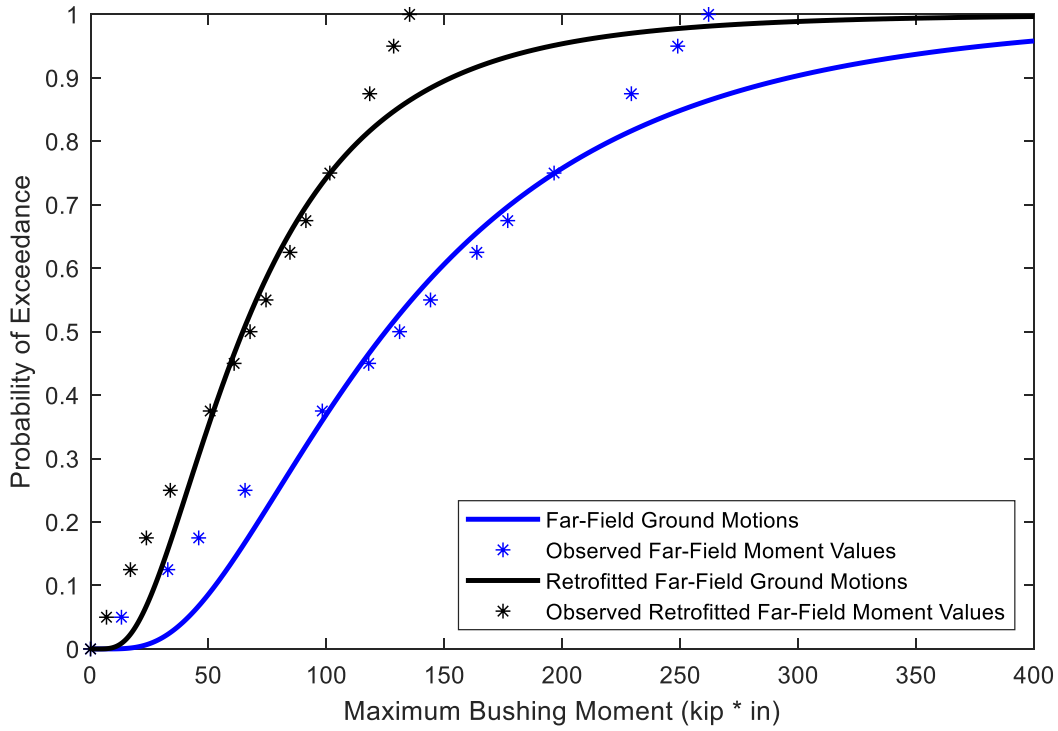

Figure 2.17: 525kV Far-Field Fragility Curves

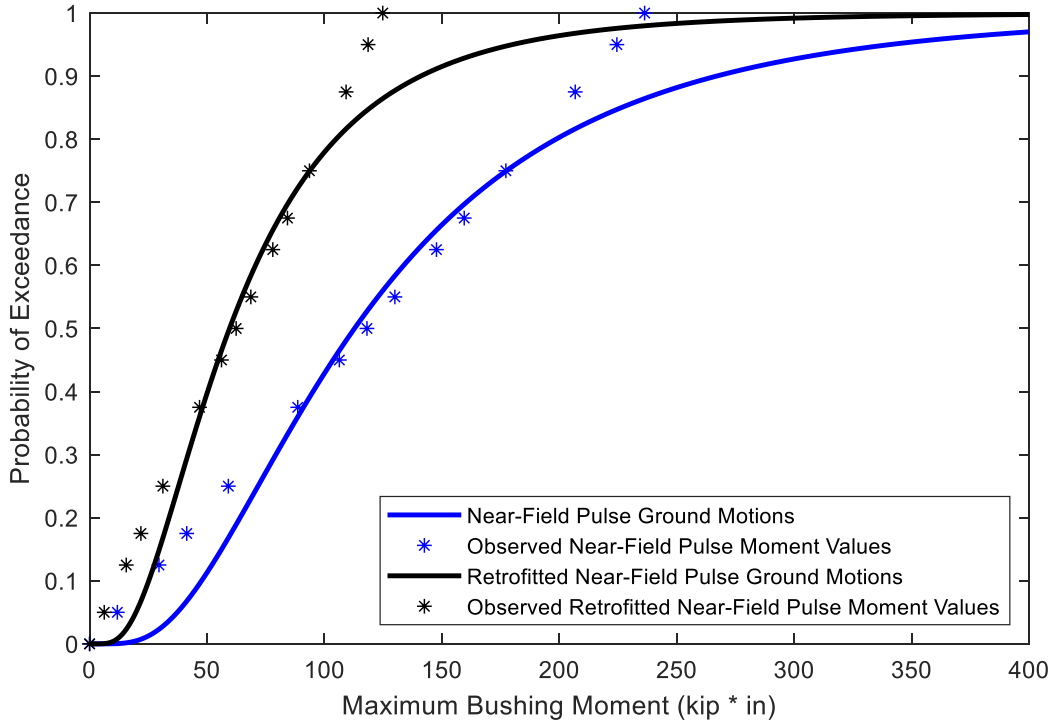

Figure 2.18: 525kV Near-Field Pulse Fragility Curves

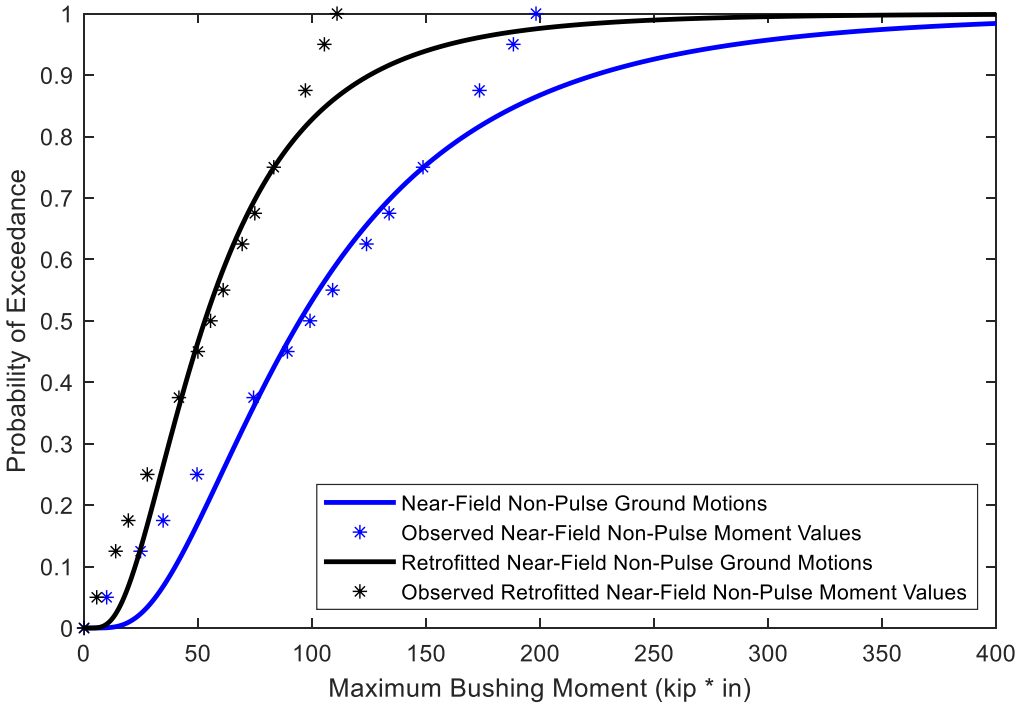

Figure 2.19: 525kV Near-Field Non-Pulse Fragility Curves

Table 2.8: Transformer Percentage Difference in Medians between Retrofitted and As-Installed Models

Ground Motion Ensemble	230kV Packard	230kV Siemens	500kV	525kV
Far-Field	34.81%	37.71%	34.31%	51.62%
Near-Field (Pulse)	23.53%	46.31%	33.76%	52.82%
Near-Field (Non-Pulse)	42.65%	46.57%	32.33%	55.97%

Table 2.9: Transformer Fragility Curve KS Test Results

Transformer Model	Condition	Ground-Motion Ensemble	KS 95% Critical Value	Max Observed KS Value
230kV Packard	As-Installed	Far-Field	0.3489	0.1466
230kV Packard	As-Installed	Near-Field (Pulse)	0.3489	0.1466
230kV Packard	As-Installed	Near-Field (Non-Pulse)	0.3489	0.1466
230kV Packard	Retrofitted	Far-Field	0.3489	0.1575
230kV Packard	Retrofitted	Near-Field (Pulse)	0.3489	0.1465
230kV Packard	Retrofitted	Near-Field (Non-Pulse)	0.3489	0.1466
230kV Siemens	As-Installed	Far-Field	0.3489	0.1466
230kV Siemens	As-Installed	Near-Field (Pulse)	0.3489	0.1472
230kV Siemens	As-Installed	Near-Field (Non-Pulse)	0.3489	0.1465
230kV Siemens	Retrofitted	Far-Field	0.3489	0.1466
230kV Siemens	Retrofitted	Near-Field (Pulse)	0.3489	0.1466
230kV Siemens	Retrofitted	Near-Field (Non-Pulse)	0.3489	0.1466
500kV	As-Installed	Far-Field	0.3489	0.1466
500kV	As-Installed	Near-Field (Pulse)	0.3489	0.1466
500kV	As-Installed	Near-Field (Non-Pulse)	0.3489	0.1466
500kV	Retrofitted	Far-Field	0.3489	0.1465
500kV	Retrofitted	Near-Field (Pulse)	0.3489	0.1465
500kV	Retrofitted	Near-Field (Non-Pulse)	0.3489	0.1466
525kV	As-Installed	Far-Field	0.3489	0.1466
525kV	As-Installed	Near-Field (Pulse)	0.3489	0.1466
525kV	As-Installed	Near-Field (Non-Pulse)	0.3489	0.1466
525kV	Retrofitted	Far-Field	0.3489	0.1466
525kV	Retrofitted	Near-Field (Pulse)	0.3489	0.1466
525kV	Retrofitted	Near-Field (Non-Pulse)	0.3489	0.1466

3. RISK AND PERFORMANCE BASED EARTHQUAKE ENGINEERING ANALYSES

3.1. Introduction

With the structural analysis results now presented in Chapter 2, this chapter will now go into the details regarding the risk analysis methodology as well as the results of such applied for the various transformer bushing cases (including variation of mounting conditions and loading). First, this chapter will discuss in detail the Performance Based Earthquake Engineering (PBEE) framework as developed by the Pacific Earthquake Engineering Research Center (PEER). Then, the various steps of the PEER PBEE framework as applied in this study will be discussed including a detailed explanation of the hazard analysis, and decision variable analysis given that the damage and structural analyses/steps of the PBEE framework were performed in Chapter 2 of this thesis.

3.2. Introduction into the PEER PBEE Framework

The PBEE framework includes four major steps that make up the methodology used to perform a risk-based analysis, including Hazard Analysis, Structural Analysis, Damage Analysis (also written as "Final Analysis"), and Loss Analysis (also identified as "Consequence Analysis") (Günay 2013). Each of the analyses goes through a different component of how a hazard can impact an area, incorporating differing probability distributions based on the hazard type being applied to a given geographic location. This provides a clear representation of whether or not the asset (e.g., structure,

design, location, mitigation action) in question is likely to be affected by the metric of choice in a multitude of different scenarios. A visual representation of the format of the PBEE framework can be seen in Figure 3.1.

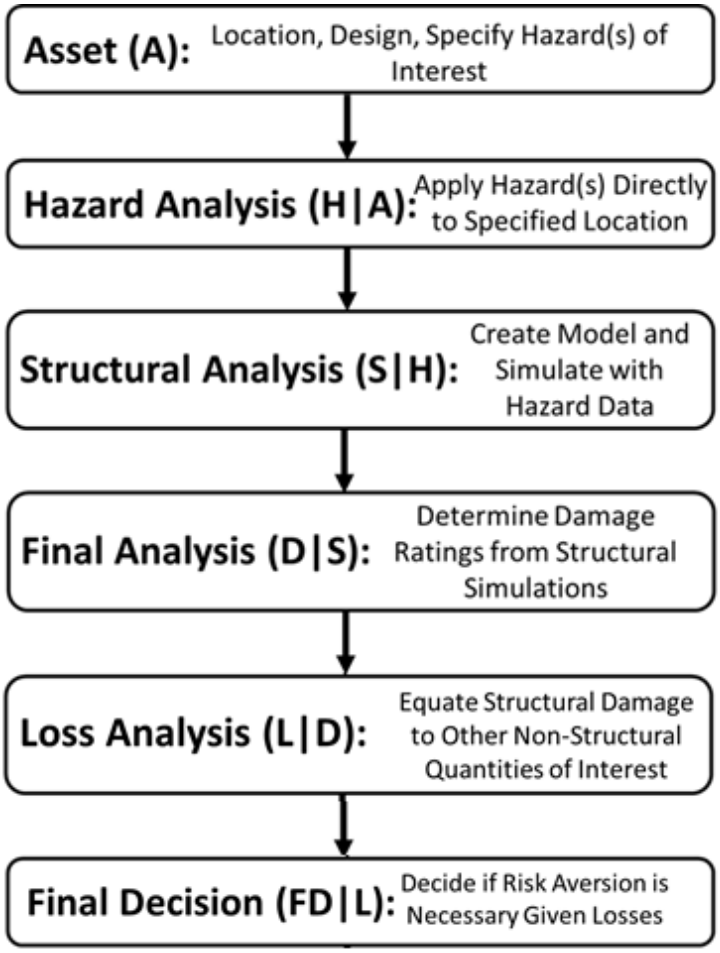

Figure 3.1: PBEE Framework Flow Chart

Hazard analysis is where the hazard in question (e.g., earthquake, wind, or tsunami) is analyzed based on factors such as fault locations and levels of attenuation (for earthquake hazard). The impact of the hazard analysis is dependent on the location where the asset resides, as the location of hazard inducing components (e.g., fault lines

in the case of earthquake hazard) alters the levels of risk associated with a given asset. Depending on the chosen parameters of interest in reference to the asset location, such as peak ground acceleration or a period based spectral acceleration, this analysis creates what is known as a hazard curve. The purpose of a hazard curve is to relate the frequency of exceedance of the specified intensity measure (i.e., ground motion level) based on the requested time horizon. In the case of seismic hazard analysis, this relationship is based on the assumption that earthquake occurrence follows a Poisson distribution (Günay 2013), leading to the relationship seen in equation 3.1, where λ represents the mean annual frequency of exceedance, *IM* represents the intensity measure, and *t* represents the amount of time passed in years. More details about the hazard analysis applied in this study will be discussed in section 3.3.

$$\boldsymbol{P(IM) = 1 - e^{-\lambda(IM)t}} \qquad \textbf{EQ 3.1}$$

Structural analysis consists of the creation of a model representative of the characteristics of the asset in question. This structural model is then run through where the structure in mind is made to shape, and then tested to determine structural capabilities under the allocated hazard. This includes adding *any* and *all* elements that have any form of specified mass, volume etc. for *any* and *all* components that may be impacted (included structural and nonstructural components). In addition, any unknown quantities or dimensions that may impact results are given varying properties so that the analysis can be as realistic as possible accounting for various degrees of uncertainties. This stage of the risk analysis framework is also crucial towards establishing the Engineering Demand Parameter (EDP), which dictates the component of interest for the

analysis. This is often determined by what factor in the created structural model would be impacted the greatest by the applied hazard based on the created figure. This component is then monitored throughout the analysis to determine its reactions to the remaining portions of the risk analysis.

The ***final analysis*** then coordinates the EDP related values taken from the structural analysis and relates them to a general measure denoted as "*Probability of Exceedance*". This measurement, as defined previously in section 2.3.3, gives an indication of the probability that the response parameter of interest (i.e., EDP) will exceed a certain measurement in a given state based on the sampled analyses. These values can also be used to incorporate the idea of a "*Damage State*", in which levels of operations of the asset are defined based on degrees of deterioration (Günay 2013). There damage states and analyses are represented in the form of fragility curves, where the peak values of the individual ground motions are represented by a lognormal Cumulative Distribution Function (CDF) curve that represents the probability of exceeding the values of interest (as discussed in Chapter 2). With damage states, a final analysis for a single asset can contain multiple curves based on the states defined by the analysis. Often times these states will be compared with a limit state, which would provide a physical description of the model to match what deficiencies would be the result of being in the specified damage state.

The final section of the PBEE framework is the ***loss (or consequence) analysis***, where the previously derived fragility curve results are redefined to relate directly to the situation at hand. Depending on the desired analysis, this can be in the format of direct

(economic losses) and indirect (fatalities, injuries, downtime) losses, based on both the severity of the hazard specified in the first step of this framework, as well the damage state provided by the final analysis (conditioned on the hazard severity). This analysis can then produce a summarized probability of damage at given instances based on specified factors, such as asset model, asset location (e.g., different hazard analyses), and or community reliance on said asset. The end result is a mean annual frequency at which the decided decision variable would be exceeded in the provided circumstances. This can allow owners and stakeholders the opportunity to decide based on the provided probability on their choice of action to change/alter the asset in question.

In essence, equation 3.2 summarizes the entirety of the PBEE framework as a single instance as was provided by (Mitrani-Reiser 2007). In this case, any instance of P[X|Y] indicates the probability of X, given the component(s) provided of Y, and λ[X|Y] indicated the mean of all occurring instances of X given Y over the course of the simulation. The nomenclature for the variables used in this equation can be seen in Figure 3.1. In verbal representation, the formula takes the components of each analysis and takes the mean result of the individual PBEE components depending on the chosen risk aversion option (or lack thereof). This calculated loss value can then be used to determine the appropriate decision for the asset depending on the calculated losses.

$$\boldsymbol{\lambda[L|FD]} = \int\int\int \boldsymbol{P[L|D,FD]} * \boldsymbol{P[D|S,FD]} * \boldsymbol{P[S|H,FD]} * \boldsymbol{\lambda[H|FD]dHdSdD} \qquad \textbf{EQ 3.2}$$

3.3. Application of the PEER PBEE Framework to Evaluate the Efficiency of Mitigation Actions on Medium- and High-Voltage Bushing Systems

3.3.1. Hazard Curve Generation

As mentioned in the previous section, hazard analysis is the first step that is undergone in the current iteration of PBEE analysis. Hazard analysis is used to get a proper relationship between our asset (in this case the various electrical transformers mounting conditions – as-installed and retrofitted) and the seismic presence of a specific area. This relationship is typically based on the location of the asset, and its proximity to major fault lines. For this reason, the first decision that was made related to this study was the locations of interest to be accounted for in the analyses. To best approximate the transformers durability under seismic activity, four locations across California (region of highest seismic activity in the United States) were chosen: two in the northern part of the state near San Francisco and Alameda counties, and another two in the Los Angeles county representing the southern area. Those locations were selected based on their proximity to the Hayward and San Andreas faults for Northern and Southern California, respectively. To select appropriate locations, the Esri map titled, "*California Operational Power Plant (Base Map)*" was used (Thong 2018). This map, as can be seen in Figure 3.2, details the locations, and well as voltage transmission line ratings, of all transformer locations across the state of California, where seismic activity are of great concern and can disrupt the electric network operations.

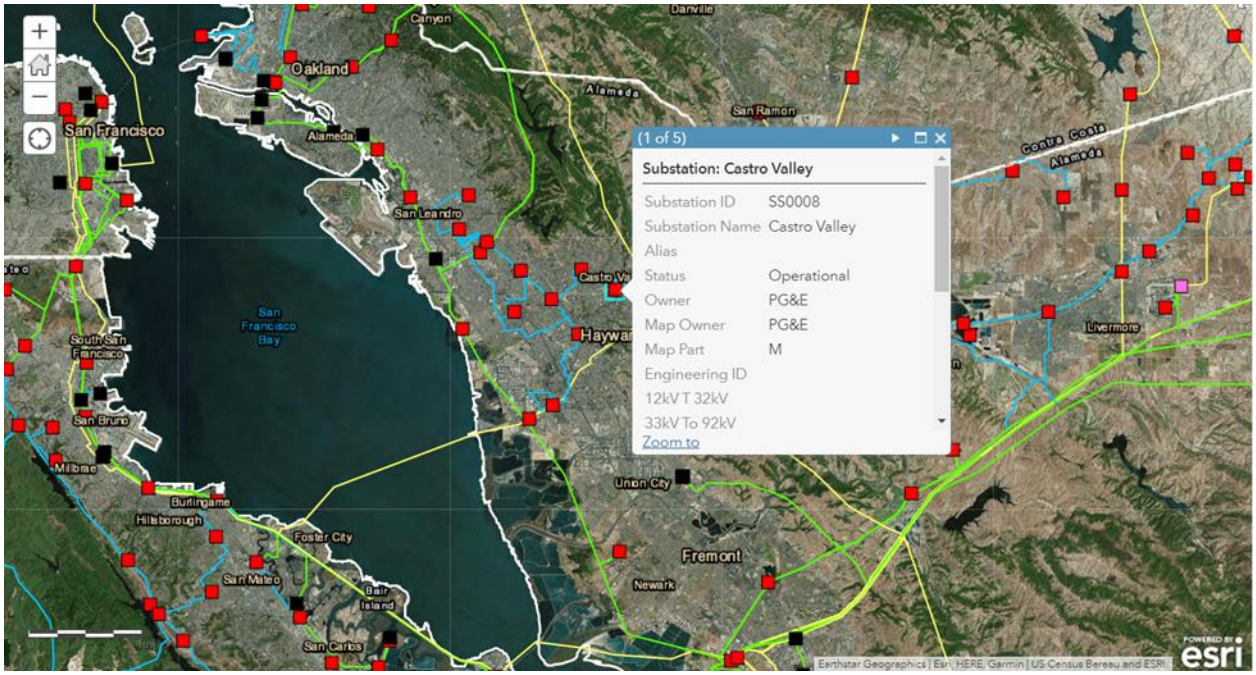

Figure 3.2: California Transformer Location Map (Thong 2018)

This map was then cross referenced with a fault map of California as seen in Figure 3.3, which would be used to detail the distance between the transformer and the nearest fault. By using these two resources, an area in both Southern and Northern California was found, each with one area representative of Far-Field ground motions and another location indicative of Near-Field ground motions. Each chosen location was verified to have medium-voltage transformers in its immediate area of 230kV-345kV as well as high-voltage transformers (500kV+), making it a good representation of potential damage for the analyzed transformer models (described in Chapter 2). The coordinate positions used for the hazard analysis can be seen in Table 3.1.

Table 3.1: Transformer Locations

Geographic Location Represented	Far/Near-Field Location	Latitude	Longitude
Southern California	Far-Field	34.85977	-118.436647
Southern California	Near-Field	34.48657	-118.11863
Northern California	Far-Field	37.69129	-122.061211
Northern California	Near-Field	36.80614	-121.775744

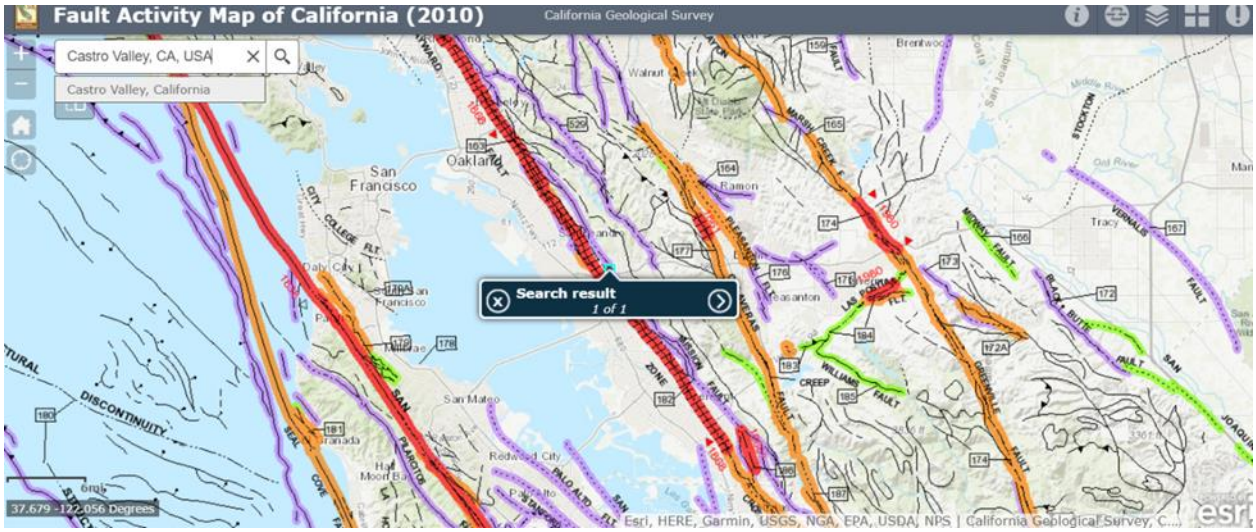

Figure 3.3: California Fault Map (Jennings and Bryant 2010)

In order to create the curves that are representative of the hazard analyses results, the United States Geographical Survey (USGS) provides a tool on their website that can be seen in Figure 3.4. This tool allows the user to input the latitude and longitude of a specific location within the United States, as well as the site class (representing the condition of the soil and foundation of the area) and the return period of the ground motion. The end result is the data representing the annual probability of exceedance of a certain degree of ground motions (USGS 2018). For California, the site class is pre-defined with only one option available for use (760 m/s shear wave velocity

(B/C Boundary)). As for the ground motion acceleration, this value is determined by the resonant frequencies of our transformer configurations provided previously in section 2.1. With that in mind, it should be noted that the USGS hazard tool only provides the hazard curves for a spectral period of 0.2s and 1.0s (USGS 2018). Therefore, the values of the ground motion acceleration, as well as the annual frequency of exceedance, were linearly interpolated between the two known curves. This was performed for all relevant points of the hazard curve (those with a range from 0g that includes 2.5g) for all of the four locations in Table 3.1. The obtained data sets were then used to produce the hazard curves that can be seen in Figure 3.5 to Figure 3.8 for the Southern and Northern California selected sites, respectively.

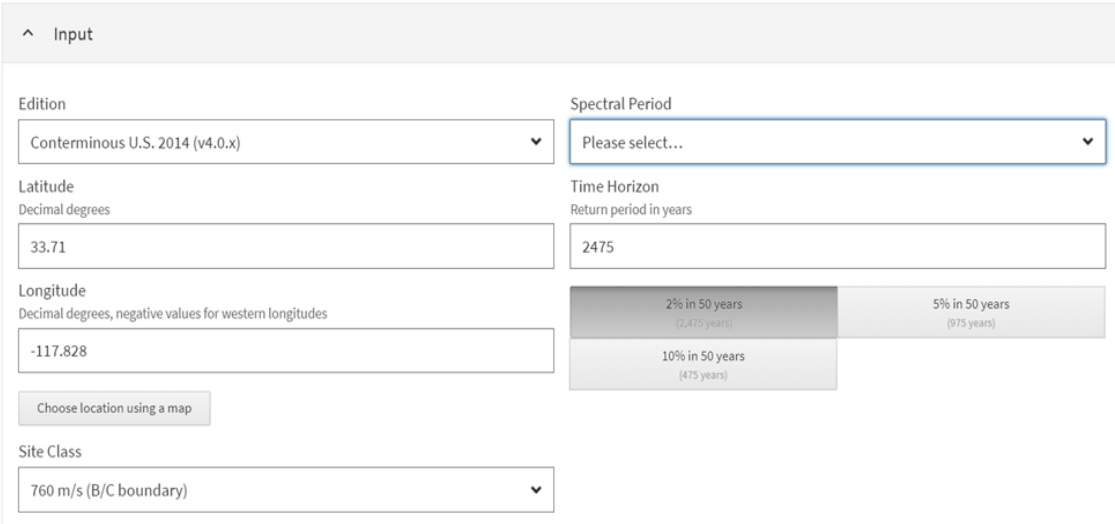

Figure 3.4: Screen Capture of the USGS Hazard Tool Input (USGS 2018)

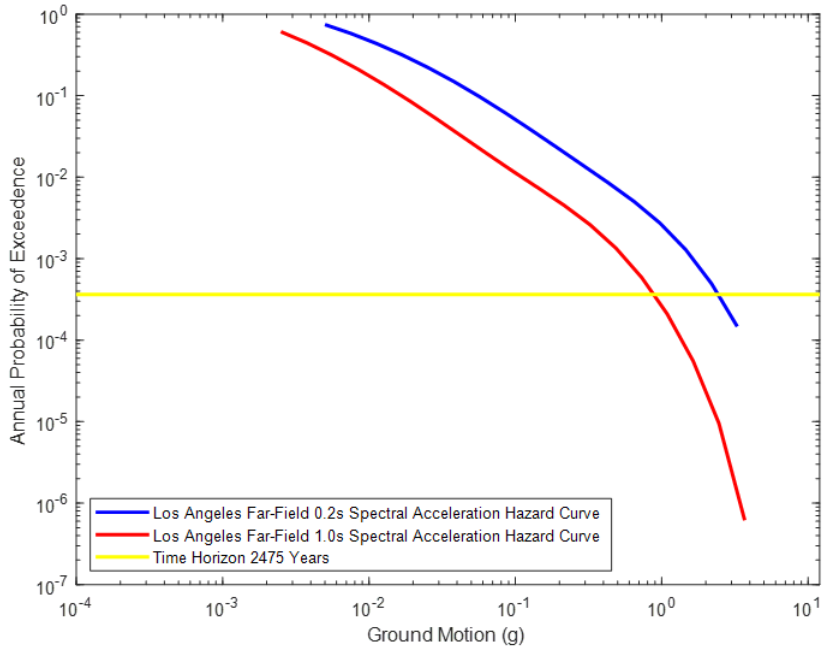

Figure 3.5: Los Angeles Far-Field Hazard Curve

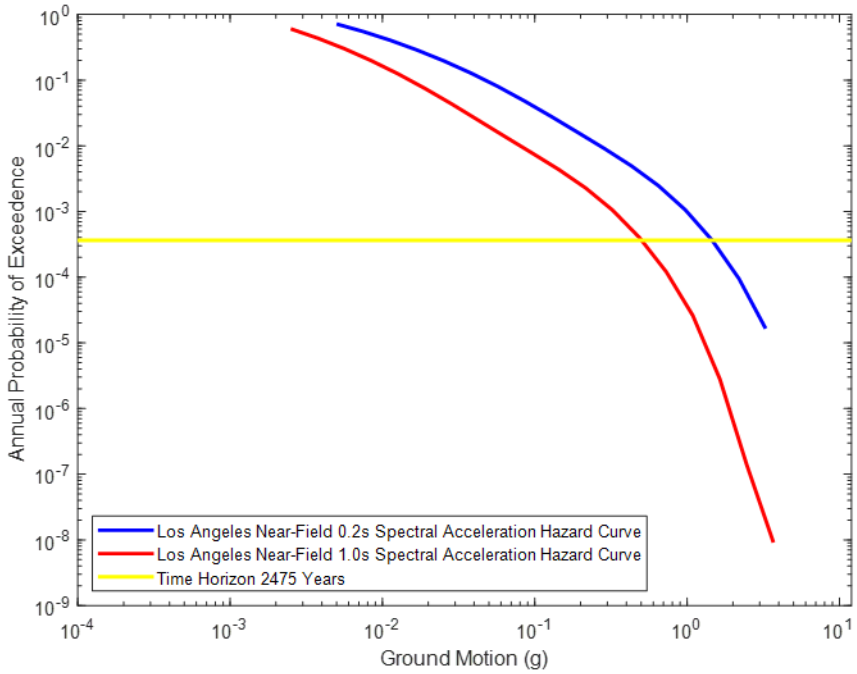

Figure 3.6: Los Angeles Near-Field Hazard Curve

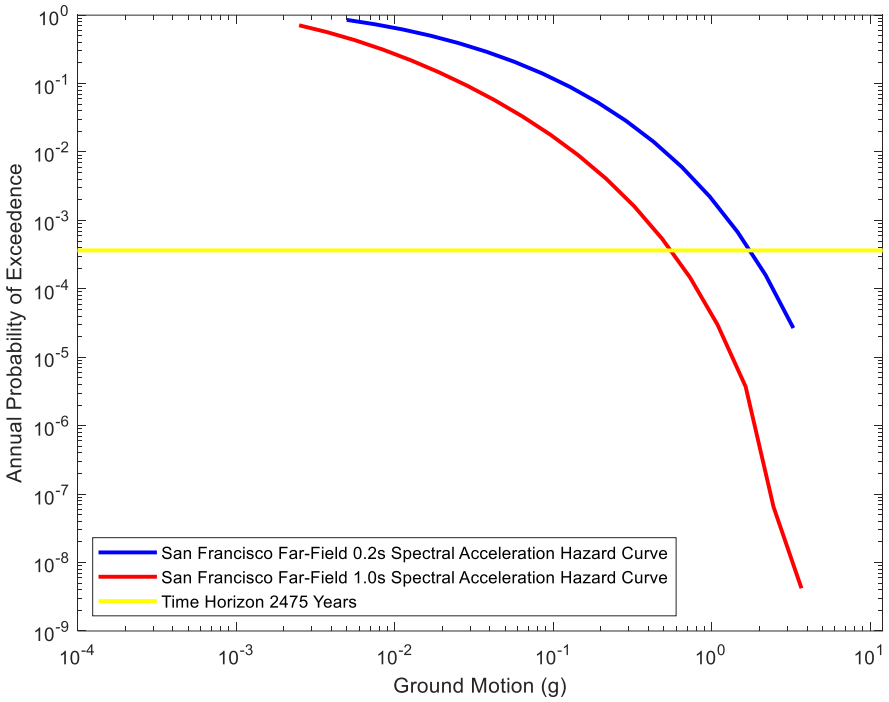

Figure 3.7: San Francisco Far-Field Hazard Curve

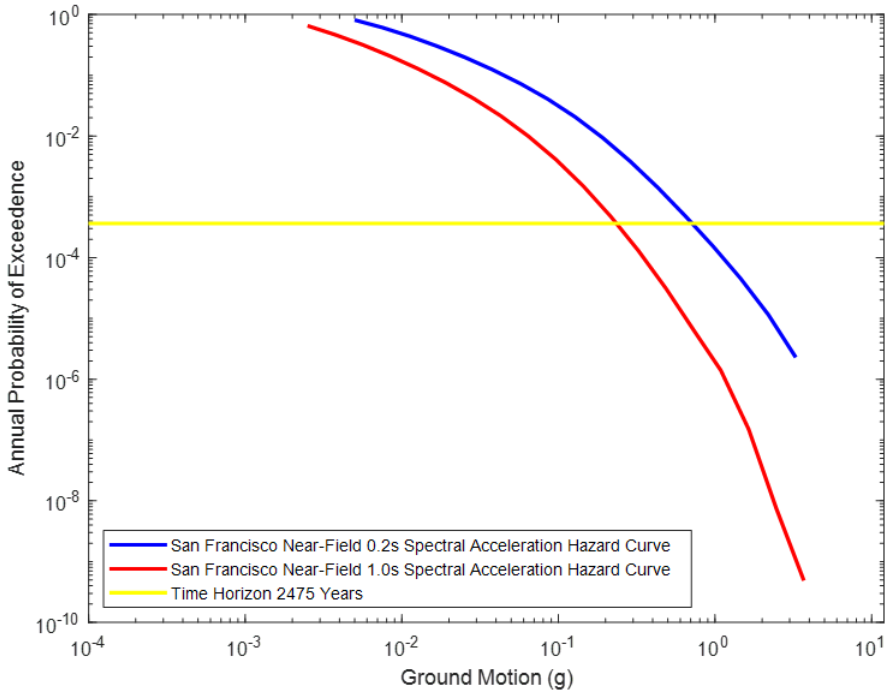

Figure 3.8: San Francisco Near-Field Hazard Curve

3.3.2. Structural & Damage Analysis

The details for the structural and damage analyses are primarily comprised of the details provided in Chapter 2. Figure 2.1-Figure 2.4 represent the structural models that were considered in this study, and since they were based on real transformer models, there were no components of uncertainty that required any kind of variation. The retrofitting technique of the added flexural stiffeners on the transformer top plate also were based on components with known weights and dimensions, and no variation was required there either as a result. With the ground motions having been scaled to meet the IEEE 5% damping requirements mentioned in section 2.3.1, those ground motions were applied to each structural model as a representation of the ground motions affecting the structure at different scale factors (incremental dynamic analyses preformed as described in Chapter 2). From this, each transformer variation obtained 42 different structural analysis' for as-installed and retrofitted variations, 14 for each ground motion ensemble applied, based on the determined EDP of the moment at the base of the transformer bushing.

In a typical PBEE framework as described in section 3.2, the fragility curves from Chapter 2 would be created for the purpose of structural analysis, and then the structural response would be used to determine the components of the damage analysis. However, based on the SAP 2000 models as presented in Chapter 2, the outputs of the structural analysis were obtained in the form of the previously defined EDP of interest (being the moment value at the base of the bushing) conditioned on the hazard (seismic) intensity (i.e., intensity measure). Therefore, the two different components of the typical

PBEE framework are herein combined into a single step. In terms of the previous equation 3.2, the probabilities P[D|S, FD] and P[S|H, FD] are herein put into a single factor of P[D|H, FD]. Equation 3.2 was updated to equation 3.3 to better reflect the adaptation of the PBEE framework used in this project. The fragility curves provided in section 2.3.3 of the format P(D > d | SA) is representative of the results of the damage analysis, where the individual ground motion components have been combined to generate fragility curves, which are then used to specify the damage states.

$$\boldsymbol{\lambda[L|FD] = \int\int P[L|D,FD] * P[D|H,FD] * \lambda[H|FD] dH dD} \qquad \textbf{EQ 3.3}$$

With the information previously provided from Chapter 2, we will use such to coordinate what the appropriate damage states are for this study. The data from the fragility curves can be used to get an adequate idea of the structural performance of the transformer. The HAZUS earthquake model technical manual (FEMA 2010) provides detailed descriptions of substation equipment in various damage states. The five listed damage states are *none, minor, moderate, severe, and collapse*. For this study, those damage states were adopted for the transformer models, and with the HAZUS descriptions, as well as information from (Fallahi 2004), (Gilani et al. 2004), and (Koliou et al. 2013a), these damage states were given proper descriptions in terms of their physical damage to accurately represent the individual transformer. These are dependent on how much damage is sustained by the given hazard based on what was detailed in the previous subsection. The damage states physical description is presented in Table 3.2 and Table 3.3.

While the moment at the base of the bushing was previously known to be the EDP of interest, there was not a previously defined method of knowing the potential damage states of such. The work performed by (Zareei et al. 2016) was adapted herein, where they related the bushing damage states by the percentage of the ultimate stress of the bushing. Their work consisted of using a three-dimensional stress time history analysis to determine the maximum moment observed by their transformer bushing. This was used as their maximum limit state in this regard, having a "*minor*" damage state be represented by 5% of their ultimate stress values, and 25% and 50% ultimate stress representing a "*moderate*" and "*severe*" damage state, respectively. For this study however, since having four different kinds of transformers would lead to completely different limit state representations, it was decided that the value for the "*ultimate stress*" of each bushing would be that of the stress observed at the maximum applied ground motion of 2.0g at the base of the bushing. This value could then be taken and put as the approximate mean values for the three non-collapse damage states by taking 5, 25, and 50% of this value. As for the collapse damage state, both to be conservative and to account for a more realistic provocation of the damage state, this iteration of the framework will consider that damage state to achieve at approximately 75% of this value. For each of these approximated mean values, a C.O.V. of 0.4 was deemed appropriate for the sake our distributions (FEMA 2012).

To test the work done by (Zareei et al. 2016) and be sure that it would be applicable to the obtained results, the stress value was taken from the as-installed model of the 230kV Packard transformer using the same frame and joint the moment values for

the fragility curves were based on. Upon examining the stress value, and then using the bushing dimensions provided by the model, equation 3.4 was used to determine an approximate maximum moment of the transformer model, where M_u represents the ultimate moment of the bushing, y represents the height from the base of the bushing to its center of gravity, I is the moment of inertia of the bushing, and σ_u represents the ultimate observed stress value:

$$\boldsymbol{\sigma_U = \frac{M_U * y}{I}} \qquad \textbf{EQ 3.4}$$

For the 230kV Packard model this method was tested first, and the value obtained appeared to be indicative of what could be a representative ultimate moment value. For this reason, as well as the understanding that the relationship between ultimate stress and ultimate moment is linear, it was concluded that the measure of moment at an acceleration of 2.0g for the as-installed model would be a sufficient measurement of "ultimate moment" of our transformer bushings. These values were then used to determine the approximate damage state for the transformer based on the sustained hazard. The physical description of each damage state and associated limit states are presented in Table 3.2 and Table 3.3.

3.3.3. Loss Analysis

The final step of the PBEE methodology involves the loss (consequence) analysis for the transformer model variations (i.e., as-installed and retrofitted). The ultimate goal is to evaluate the efficiency of the proposed retrofit technique not only in terms of structural performance but also economic decision variables (direct and indirect losses). This is performed by considering the damage analysis results from the previous

subsection and relating them fiscally to the particular scenario laid out by this study. In this case, the two represented areas of Northern and Southern California will be fiscally analyzed based on the impact a seismic hazard would have on medium- and high-voltage transformers in the area. Table 3.2 and Table 3.3 provide information that would be used for this section with regards to determining the distributions of direct and indirect losses considered in this study associated with prescribed damage states.

3.3.3.1. Direct Losses

For direct economic losses, the transformer replacement cost percentages used in each damage state is adopted from the HAZUS technical manual (FEMA 2010), which provides an approximate substation value of $20 million and $50 million for medium-voltage and high-voltage substations, respectively. However, since this study is focused at the single transformer-level and not at the substation-level, the descriptions provided by (Salman and Li 2018) were adapted, stating that medium-voltage substations typically contain two transformers, and high-voltage substations typically contain four transformers. Therefore, this study will use the mean replacement cost value of $10 million and $12.5 million, respectively for medium- and high-voltage transformers. These values, as well as any other baseline monetary values for loss calculations can be found in Table 3.4. With that in mind, the losses will be expressed in a normalized format in our results, meaning that the representation of direct costs will be more subjective towards the state of the transformer rather than solely the monetary value of damage.

For any non-collapse damage states, the mean values of cost distributions for each of the prescribed damage states are associated with a certain percentage of the total transformer replacement cost. HAZUS describes the approximate percentage of transformer components damaged during a seismic event for minor, moderate, severe, and collapse damage states to be 5%, 40%, 70%, and 100%, respectively. This percentage is clearly defined below (e.g., the moderate damage state, 'ds3', representing 40% direct damage):

> *"For substations, ds3 is defined as the failure of 40% of disconnect switches (e.g., misalignment), or 40% of circuit breakers…or failure of 40% of current transformers (e.g., oil leaking from transformers, porcelain cracked), or by the building being in moderate damage state."*

While not definite for any case, these descriptions should provide a proper representation of how the different proposed damage state would appear in the field. The coefficient of variation (C.O.V.) of these components was determined through a sensitivity study discussed in detail in section 3.4. These components as they relate to their individual damage states are summarized in Table 3.2 and Table 3.3.

3.3.3.2. Indirect Losses

For indirect losses, Table 3.2 and Table 3.3 detail the downtime associated for each damage state as provided by HAZUS (FEMA 2010). These downtimes are representative of the amount of time necessary for the repair (or replacement in the collapse damage state) based on the amount of damage sustained by the transformer. These values were supplied with the C.O.V. for each damage state, making it easy to

randomly simulate the downtime of simulated models once the damage state is determined. This downtime could then be multiplied by the cost relationship analyses in Table 3.4 to obtain a monetary representation of the indirect losses.

It should be noted that for this study in particular, indirect losses were taken as a function of a single application of residential, industrial, and commercial losses using the relationships from Table 3.4. However, for the sake of analyzing a single instance of transformer damage, these found monetary values will then be normalized to the transformer in question, allowing for a uniform representation of damage.

Table 3.2: Damage State Description Table.

Damage State (D.S.):	**None**	**Minor**	**Moderate**
D.S. #	1	2	3
D.S. Details:	•No Oil Leakage •Bushing Maintains Shape •No Visible Strain or Warping at Gasket •No damaged circuit breakers/disconnect switches	•No Oil Leakage •Bushing Maintains Shape •No Visible Strain or Warping at Gasket •Approximately 5% of circuit breakers and disconnect switches damaged	•Minor Oil Leakage •Bushing is misshapen but still intact •Warped Gasket, not fractured •Approximately 40% of circuit breakers and disconnect switches damaged
Limit State Value:	<5% Transformer Ultimate Stress	5% Transformer Ultimate Stress	25% Transformer Ultimate Stress
Limit State C.O.V.	0.40	0.40	0.40
Representative % of Transformer Replacement Cost	0	5%	40%
Replacement Cost C.O.V.	0.30	0.30	0.30
Days Out-of-Commission	0	1	3
Days Out-of-Commission C.O.V.	N/A	0.50	0.50

Table 3.3: Damage State Description Table CTND.

Damage State (D.S.):	Severe	Collapse
D.S. #	4	5
D.S. Details:	•Major Oil Leakage •Bushing Porcelain is Fractured/Broken •Gasket Failure or Bushing Separation •Approximately 70% of circuit breakers and disconnect switches damaged	•Complete Oil Leakage •Broken Porcelain Bushing •Gasket Failure or Bushing Separation •All circuit breakers and disconnect switches damaged
Limit State Value:	50% Transformer Ultimate Stress	75% Transformer Ultimate Stress
Limit State C.O.V.	0.40	0.40
Representative % of Transformer Replacement Cost	70%	100%
Replacement Cost C.O.V.	0.30	0.30
Days Out-of-Commission	7	30
Days Out-of-Commission C.O.V.	0.50	0.50

Table 3.4: Loss Analysis Monetary Considerations

230kV Individual Transformer Replacement Value	$100,000,000
500/525kV Individual Transformer Replacement Value	$125,000,000
Losses Per Hour of Downtime (Residential)	$2.70
Losses Per Hour of Downtime (Commercial)	$886.00
Losses Per Hour of Downtime (Industrial)	$3,253.00

3.4. Multilayer Monte Carlo Simulation

With the methodology explained and planned with the obtained data, the next step was to perform simulations of ground motions to determine the loss analysis results of our models. In order to properly simulate a variety of scenarios, a series of Monte Carlo simulations were implemented. The primary purpose of Monte Carlo simulations is to be able to simulate a large multitude of random outcomes and determine the results

based on the generated variables. The end result, as mentioned in section 3.3.3, is a final loss curve which would be representative of the amount of damage sustained by the transformer in question based on the probability of the ground motion occurring. These curves were expressed in the format of normalized losses vs. applied spectral acceleration. The way in which these simulations were handled are explained in the remainder of this section.

3.4.1. Outline of the Implemented Monte Carlo Simulation

The first component of each individual simulation was to determine the spectral acceleration that would be used on the transformer in question. The values of spectral acceleration examined were taken between 0.1g and 2.5g with increments of 0.1g. This would lead to a pool of 25 different ground motion accelerations that could be examined per transformer case, with some going past the 2.0g that would represent the ultimate stress value discussed in section 3.3.2. Using values past that 2.0g measurement allows for a clearer indication of damage that can be achieved by the retrofit, while also allowing for a more conservative maximum loss to be accrued by the as-installed models.

After this is completed and the maximum observed moment of the simulation is known, the second layer of Monte Carlo simulation begins. In this second loop, the sustained damage state is randomly generated based on the probability of each damage state. To do so, the determined simulation maximum moment is cross referenced with the probability distribution of each damage state of the transformer to determine its likelihood of being present in each. These distribution values are provided in Table 3.2

and Table 3.3, and equation 3.5 provides the method for determining their individual probabilities of being within the damage state in question. In this equation, *M* represents the current iteration moment value, $P(d > ds_n)$ represents the probability of the damage sustained by moment m being greater than the moment value representing damage state *n*, μ_{dsn} represents the mean moment value for damage state *n*, and σ_{dsn} represents the lognormal standard deviation of damage state *n*. It should be noted that $P(d \geq ds_5) = 0$. The second layer of simulation then randomly generates a probability value, which is then used to determine the damage state that will be used in that instance based on the damage state that would collectively exceed the generated probability value. This damage state is then stored so that the last remaining Monte Carlo layer can adequately distinguish between collapse (ds_5) and non-collapse based results.

$$\boldsymbol{P(d \geq ds_n) = \Phi\left(\frac{\ln(M) - \ln(\mu_{dsn})}{\sigma_{dsn}}\right) - \sum_{i=1}^{5-n} P(d \geq ds_{(n-i+1)})} \qquad \textbf{EQ 3.5}$$

Once the damage state is determined from the randomly generated probability in the second later of simulations, the losses of the transformer can then be calculated as well. This is performed in the third and final layer of Monte Carlo simulations, where the transformer replacement values and downtime per provided damage state are randomly determined based on the provided median and C.O.V. values from Table 3.2 and Table 3.3. For direct losses, the losses for each transformer model are determined by multiplying the replacement value of a given damage state (e.g., 5%, 40%, etc.) with the transformer replacement value of the transformer model in question. This then gives a median value for the direct losses, and with the C.O.V. provides an approximate loss

distribution. A random number is then generated to determine the replacement value taken from that distribution, and this value is stored as the direct losses for that simulation. The indirect losses are then calculated in a similar fashion, where the replacement value percentage is instead replaced with the provided downtime median per damage state. Once the downtime is determined however, it can be multiplied by the financial cost relationships provided in Table 3.4 to approximate the financial losses due to the indirect relationships.

Once the loss analysis section is completed in each simulation, the values are stored of the direct and indirect losses for each of the two major areas. The third loop then repeats a set number of times, to generate multiple potential values of losses. The second loop also iterates the same amount, leading to *n* different damage states being simulated, and a total of *n***n* losses simulated. Once the second and third loops finish running, two additional measurements are calculated in the form of the total direct-based losses (EQ. 3.6) and the total indirect-based losses for the simulation (EQ. 3.7). These are then stored with the spectral acceleration value that resulted in said losses, so that it can be known what value of spectral acceleration resulted in the provided losses. Once *n* runs of the first loop are completed, the individual loss values at each spectral acceleration are averaged out and used to plot the figures found in section 3.4.4.

$$\boldsymbol{Total\ Direct\ Losses} = \sum_{i=1}^{n*n} \boldsymbol{Direct\ Collapse\ Losses_i} + \boldsymbol{Direct\ Non-Collapse\ Losses_i} \qquad \textbf{EQ 3.6}$$

$$\boldsymbol{Total\ Indirect\ Losses} = \sum_{i=1}^{n*n} \boldsymbol{Indirect\ Collapse\ Losses_i} + \boldsymbol{Indirect\ Non-Collapse\ Losses_i} \qquad \textbf{EQ 3.7}$$

3.4.2. C.O.V. Sensitivity Study

Although the information of Table 3.4 provided by the HAZUS Manual provides the replacement values for the two transformer types, there is no listed C.O.V. value that can be used for damage simulation for non-collapse cases. Unlike the components of downtime, there isn't meant to be a varying value for those components, or at least not to a considerable degree. However considering that non-collapse damage states are intended to have a varying potential for damage, one of the challenges of the created simulations was to determine what this C.O.V. should be. As such, the value for this C.O.V. was simulated for five different values, ranging between 0.2 and 0.4, with a difference of 0.05 between simulated values. Each run was conducted with a run through of 400 iterations, which while not as accurate as the final iteration number which will be discussed in the next section, was more than enough to provide accurate results.

Figure 3.9 provides the results of that C.O.V. based run. Other than the peak value at 0.9g, which is zoomed in to see more clearly with Figure 3.10, there does not seem to be any severe difference in the resulting loss value across the different C.O.V. options. With that being said, in this instance it was decided that being conservative would be the best option in order to have the greatest impact on the results of the full simulation run. Therefore, the C.O.V. used for the remainder of this study with regards to the direct losses was denoted to be 0.3.

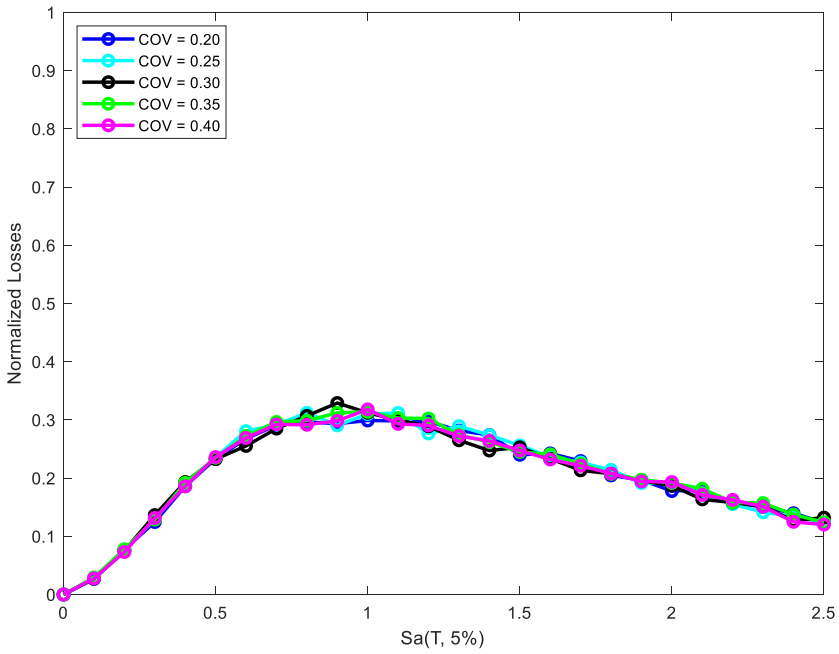

Figure 3.9: Direct Non-Collapse C.O.V. Test Graph

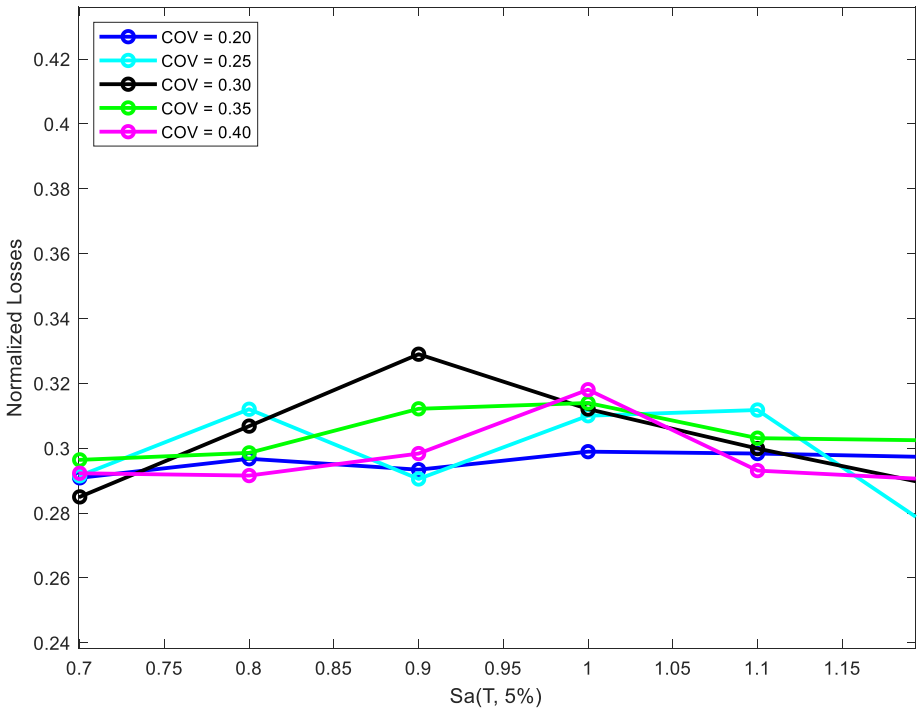

Figure 3.10: C.O.V. Test Graph Peak Value

3.4.3. Multi-Layer Monte Carlo Simulation Iteration Convergence Analysis

After confirming the C.O.V. analysis results discussed in the previous subsection, the next component to handle is the number of iterations for each layer of Monte-Carlo simulation to achieve convergence and computation efficiency simultaneously. Because of the amount of cases and requirements present in this code, as well as the nature of multi-layer Monte Carlo simulation, the amount of processing time per single case goes up exponentially as iterations are added. For example, if a typical three-layer simulation such as the one used in this study typically takes t time per layer, then the total time would be equivalent to $t*t*t$. In addition, running double the amount of iterations per layer (resulting in $2t$) would then increase the total time to $2t*2t*2t = 8t^3$ and so on. Therefore, to be as efficient as possible while still retaining accurate values, a convergence analysis was performed. To do so, the simulation for computing economic losses was conducted for the 230kV Packard transformer model Far-Field case, with a steadily increasing number of iterations: starting at 200, then going to 250, per layer and steadily increasing from there. Figure 3.11 and Figure 3.12 show the results of this testing for the non-collapse direct damage state and total losses, respectively for this sensitivity study.

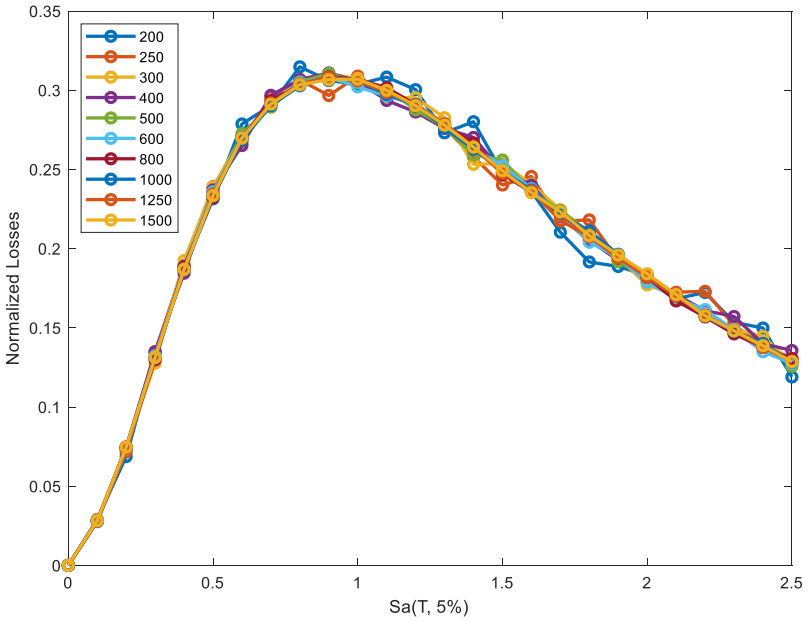

Figure 3.11: Direct Non-Collapse Damage Full Convergence Analyses

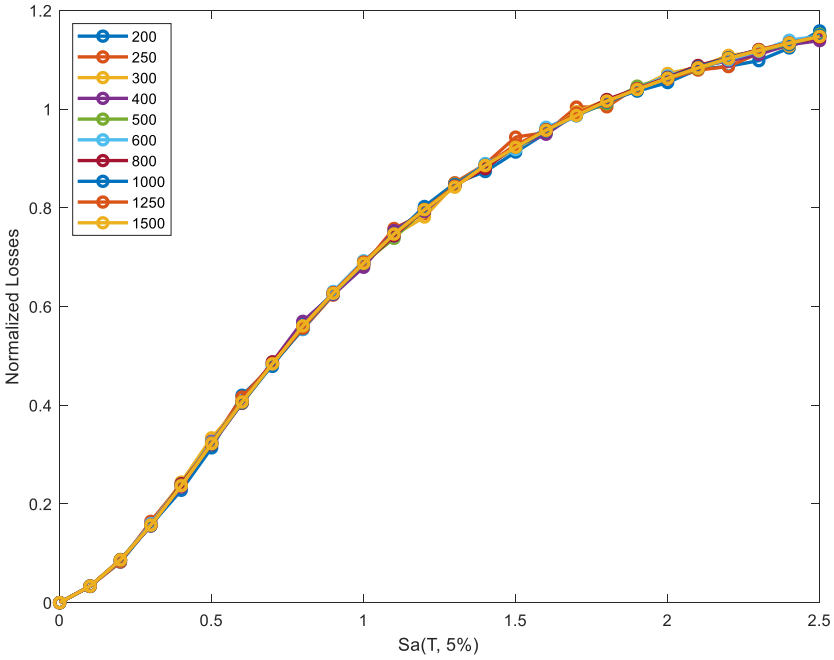

Figure 3.12: Total Damage Full Convergence Analyses

Although there are some views of cohesion across the plots, especially at lower values of spectral acceleration, there is also a clear sense of convergence among all values as they have been plotted. To get a clearer view of the cohesion as large numbers of iterations were implemented, refer to Figure 3.13, which shows almost no visible deviations from a full view of the analysis. Figure 3.14 and Figure 3.15 are used to view magnified points of Figure 3.13. Viewing them further reinforces the visible cohesion, with most points being safely within a range of a 0.01 normalized loss of each other. These two figures also show why the value of 1500 iterations per loop was decided to be the stopping point in that at multiple instances the line was a median value between the other degrees of iteration. This was representative that it was reaching a well enough convergence value, and as such this was the number of iterations used for the remaining untested transformer configurations.

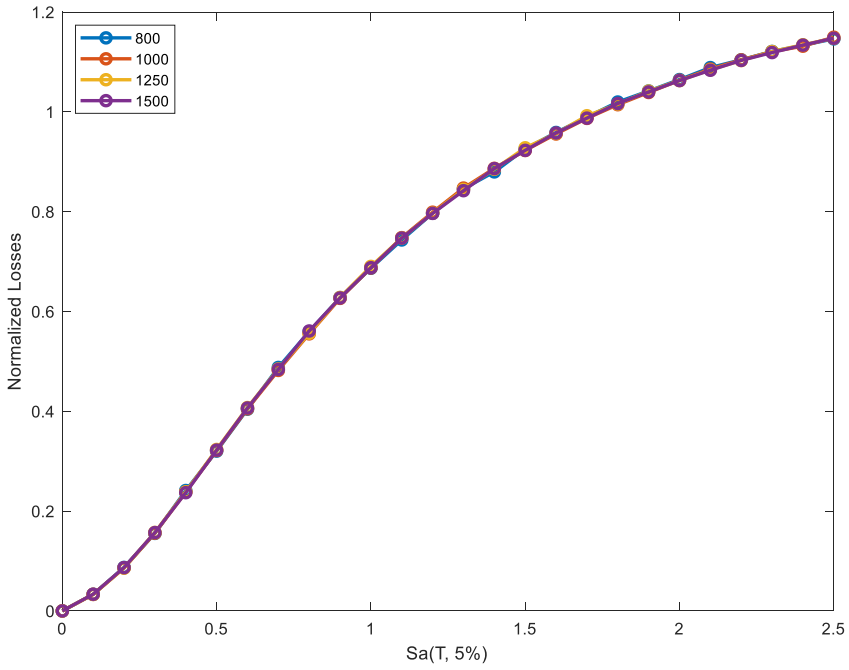

Figure 3.13: Total Damage Convergence Test (High-Iteration Numbers)

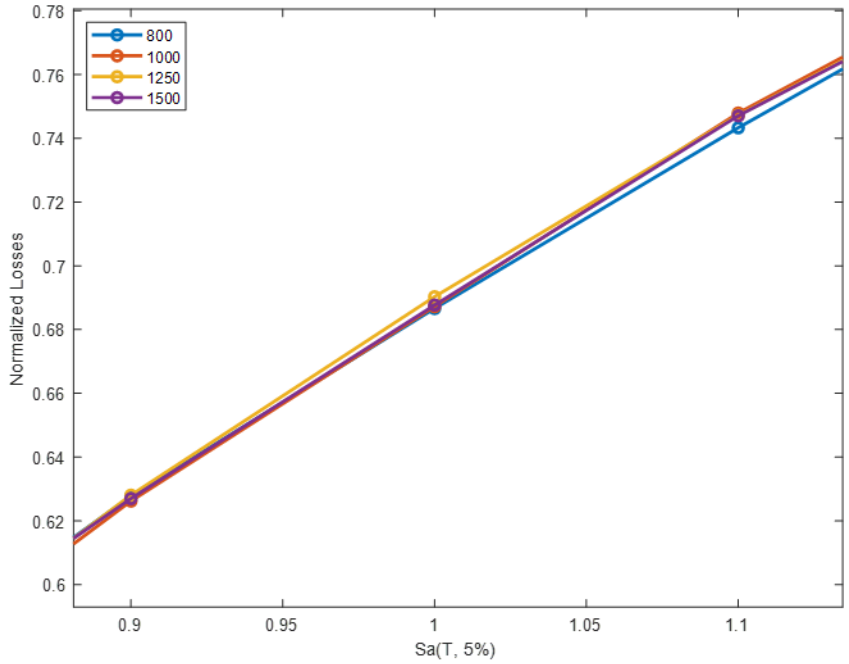

Figure 3.14: Proof of Convergence for 1500 Iteration Test

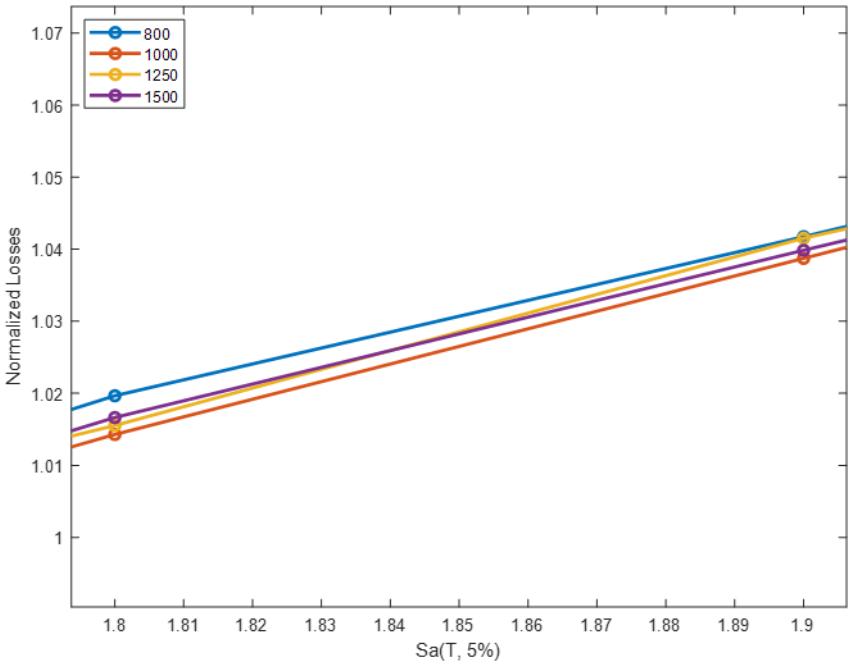

Figure 3.15: Proof of Convergence for 1500 Iteration Test CTND

3.4.4. Final Analyses and Results

3.4.4.1. Expected Losses Conditioned on Seismic Activity

After determining the direct damage C.O.V. and the number of iterations per Monte Carlo simulation loop that would result in convergence, the remaining cases were simulated with those assumptions. Each case followed the format described in section 3.4.1, and the loss curves of such can be seen in Figure 3.16 to Figure 3.39. The discussion of the results is presented in section 3.5.

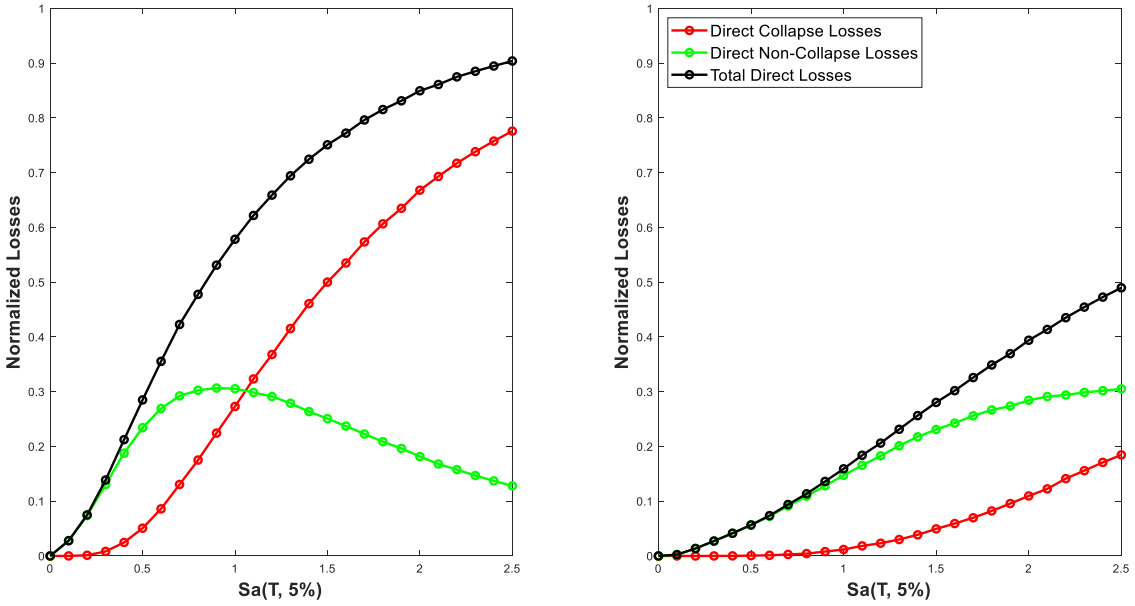

Figure 3.16: 230kV Packard As-Installed (Left) and Retrofitted (Right) Direct Far-Field Ground Motion Comparison

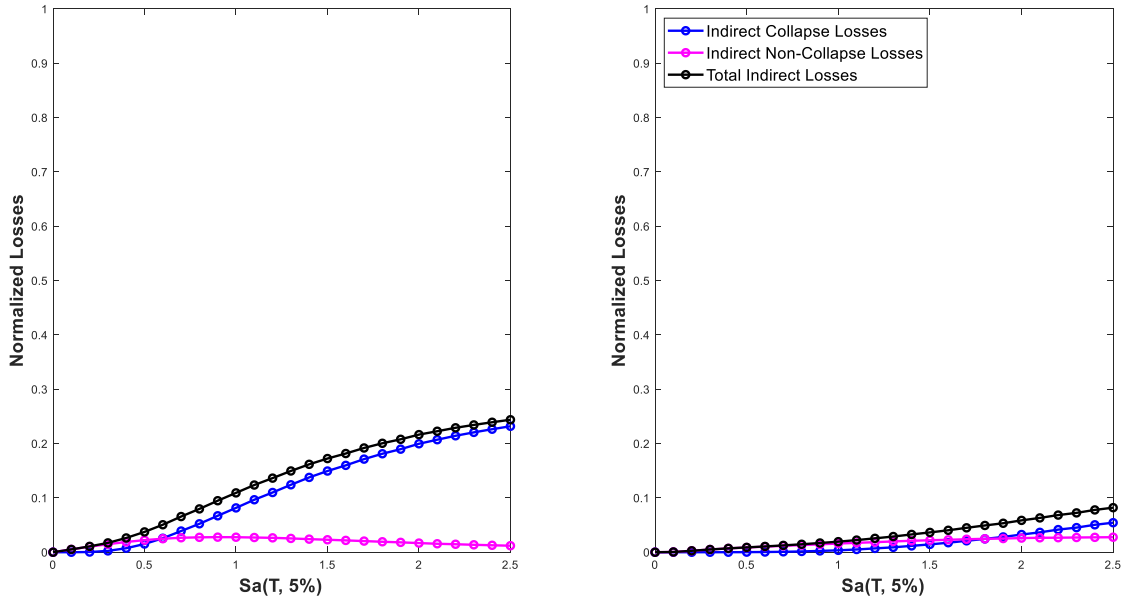

Figure 3.17: 230kV Packard As-Installed (Left) and Retrofitted (Right) Indirect Far-Field Ground Motion Comparison

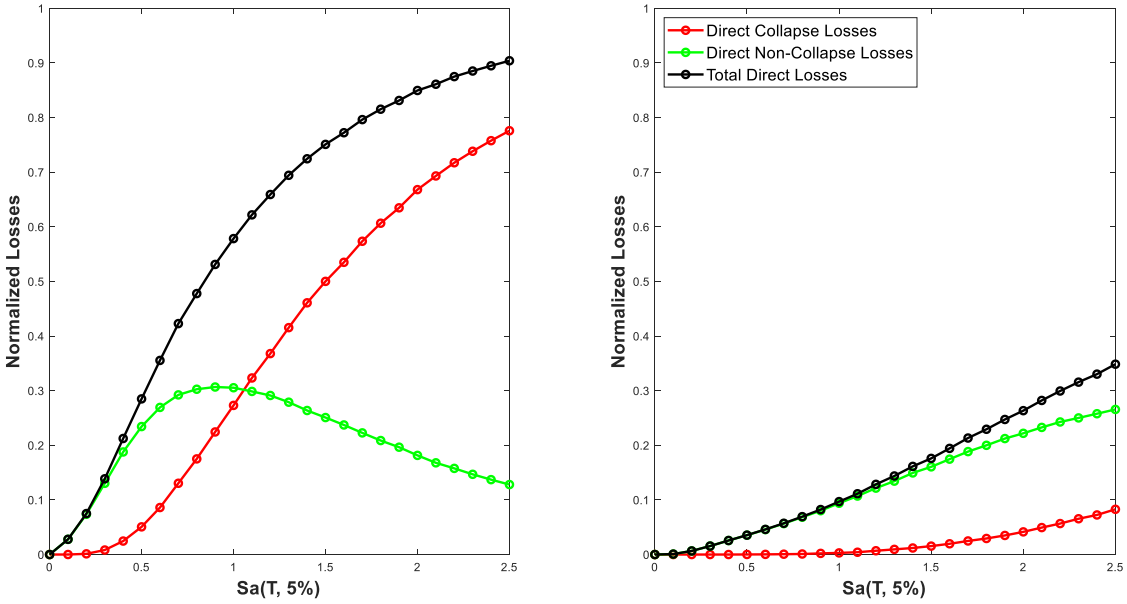

Figure 3.18: 230kV Packard As-Installed (Left) and Retrofitted (Right) Direct Near-Field Pulse Ground Motion Comparison

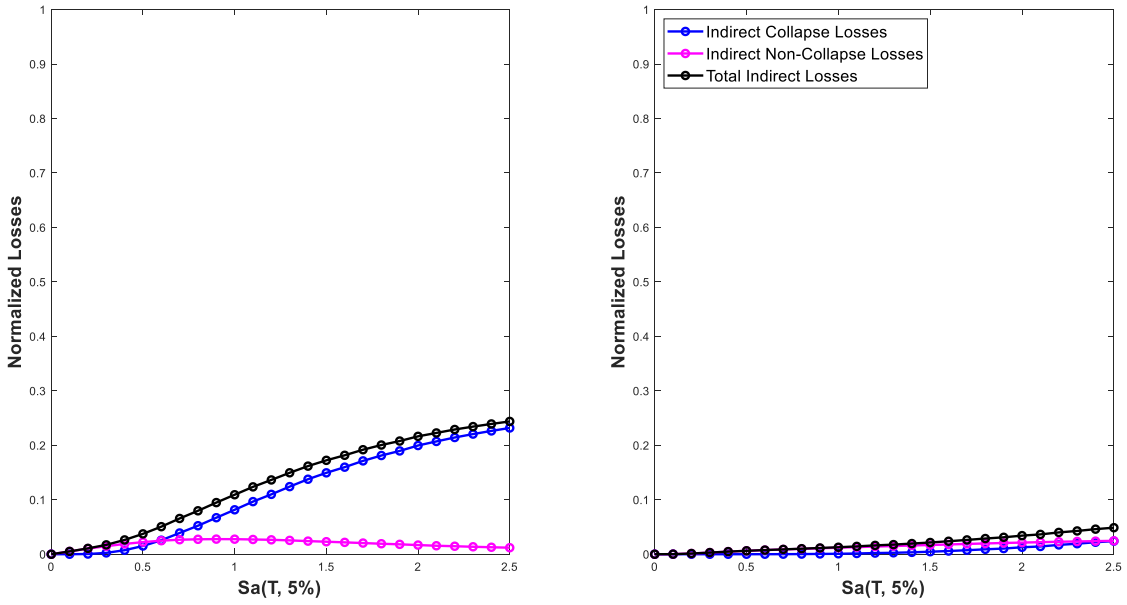

Figure 3.19: 230kV Packard As-Installed (Left) and Retrofitted (Right) Indirect Near-Field Pulse Ground Motion Comparison

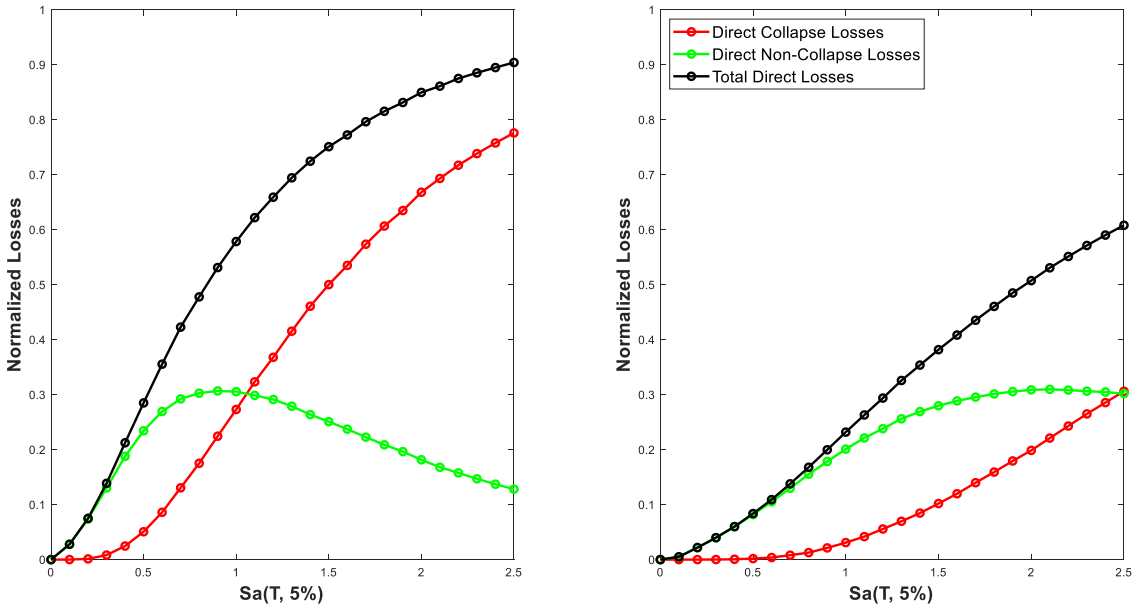

Figure 3.20: 230kV Packard As-Installed (Left) and Retrofitted (Right) Direct Near-Field Non-Pulse Ground Motion Comparison

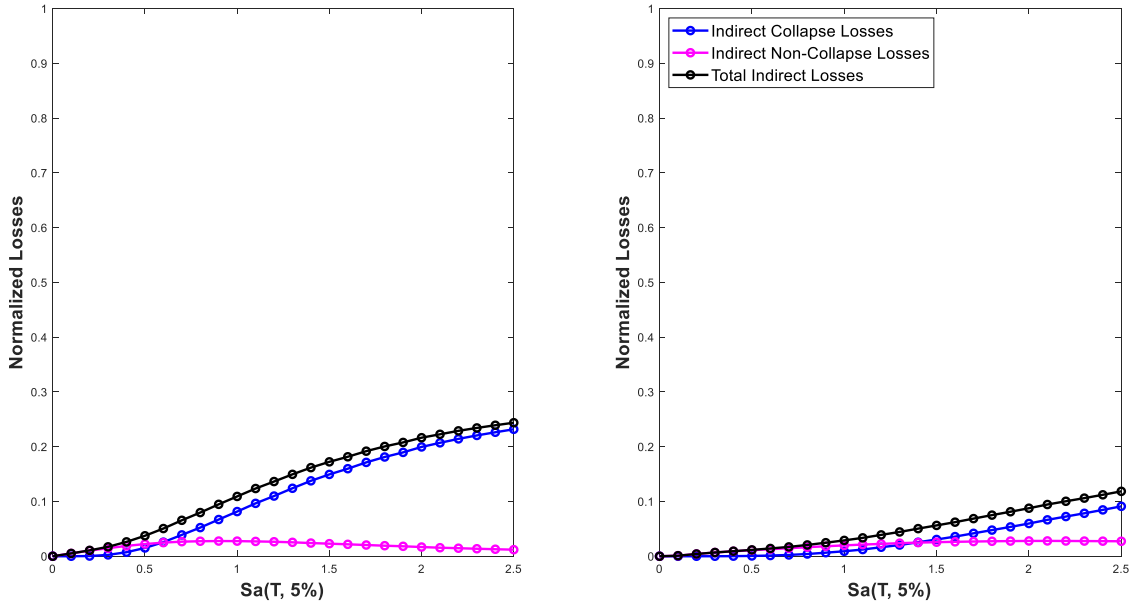

Figure 3.21: 230kV Packard As-Installed (Left) and Retrofitted (Right) Indirect Near-Field Non-Pulse Ground Motion Comparison

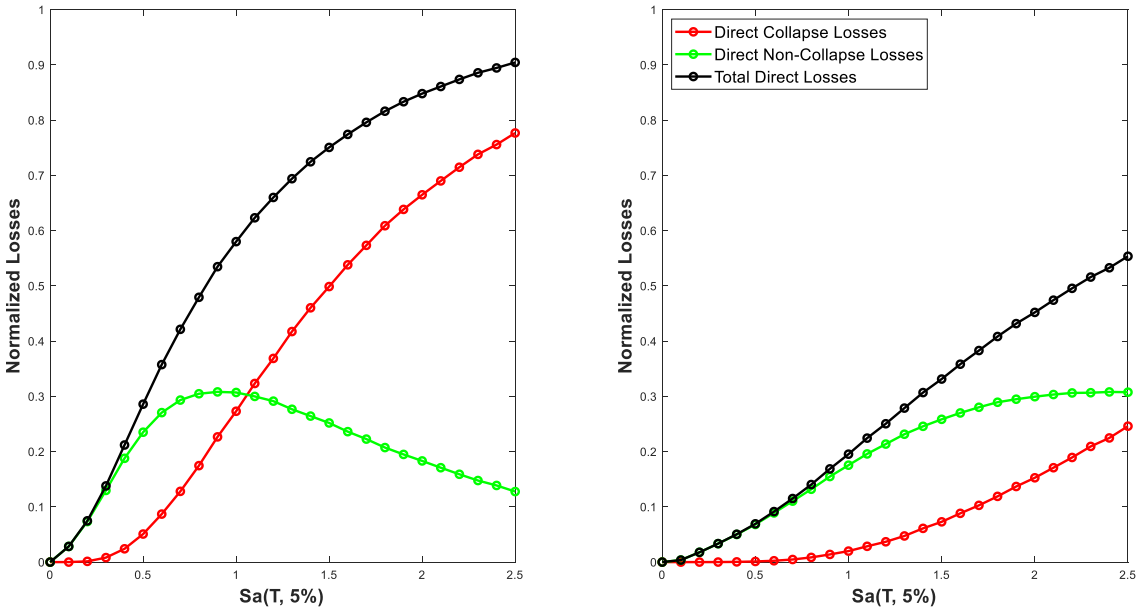

Figure 3.22: 230kV Siemens As-Installed (Left) and Retrofitted (Right) Direct Far-Field Ground Motion Comparison

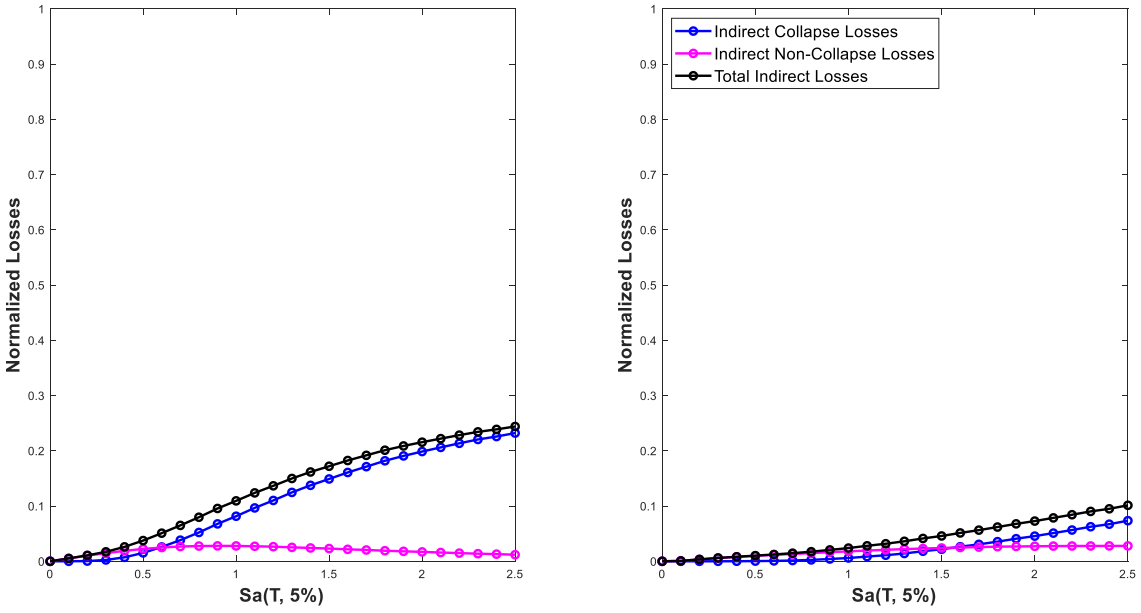

Figure 3.23: 230kV Siemens As-Installed (Left) and Retrofitted (Right) Indirect Far-Field Ground Motion Comparison

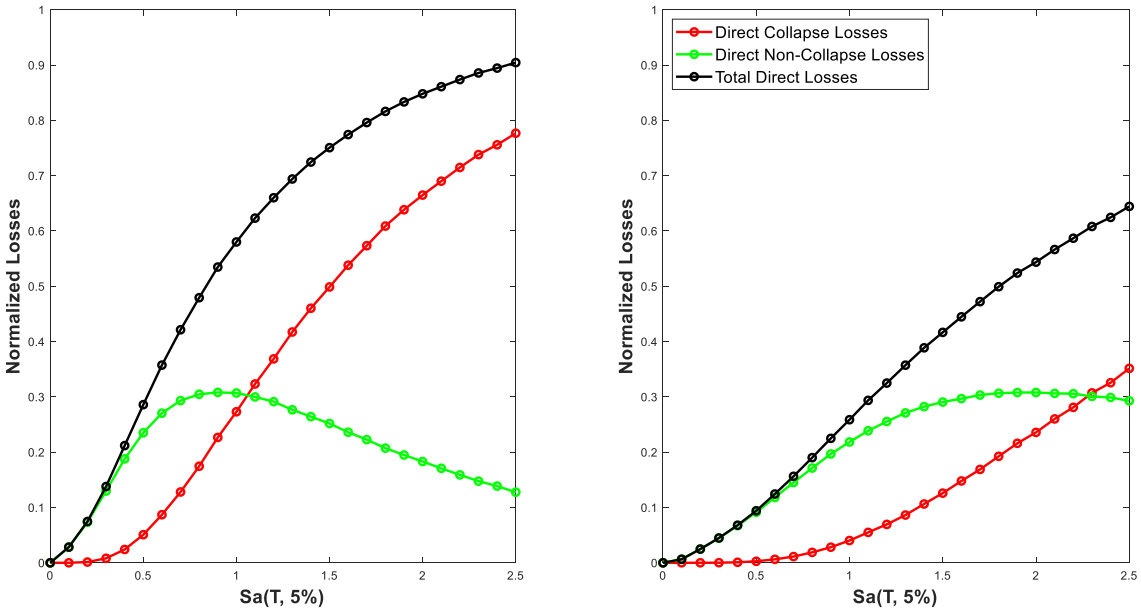

Figure 3.24: 230kV Siemens As-Installed (Left) and Retrofitted (Right) Direct Near-Field Pulse Ground Motion Comparison

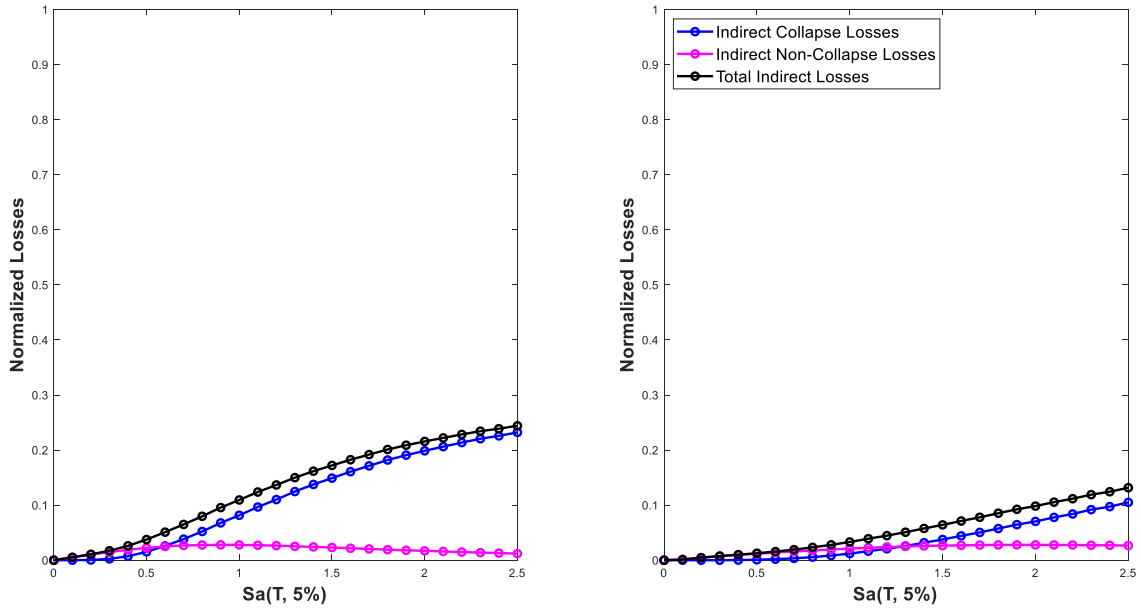

Figure 3.25: 230kV Siemens As-Installed (Left) and Retrofitted (Right) Indirect Near-Field Pulse Ground Motion Comparison

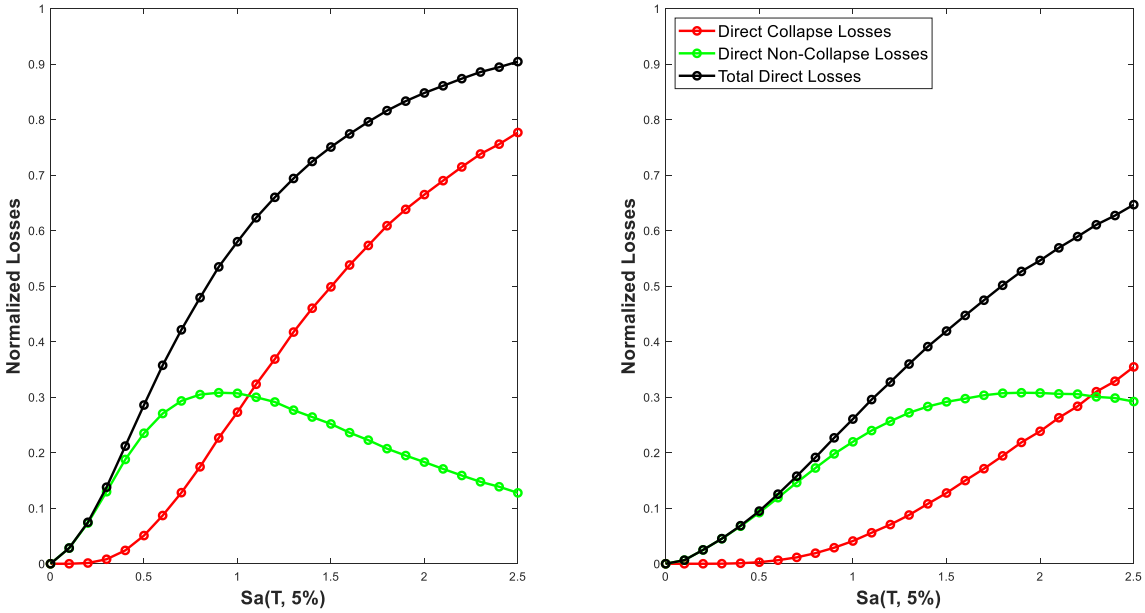

Figure 3.26: 230kV Siemens As-Installed (Left) and Retrofitted (Right) Direct Near-Field Non-Pulse Ground Motion Comparison

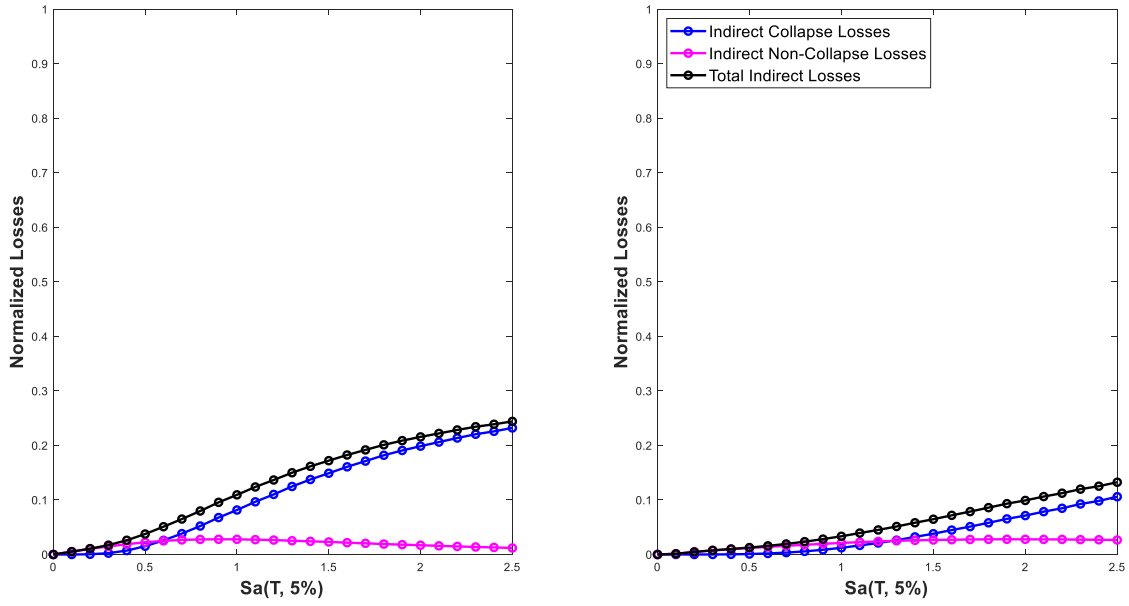

Figure 3.27: 230kV Siemens As-Installed (Left) and Retrofitted (Right) Indirect Near-Field Non-Pulse Ground Motion Comparison

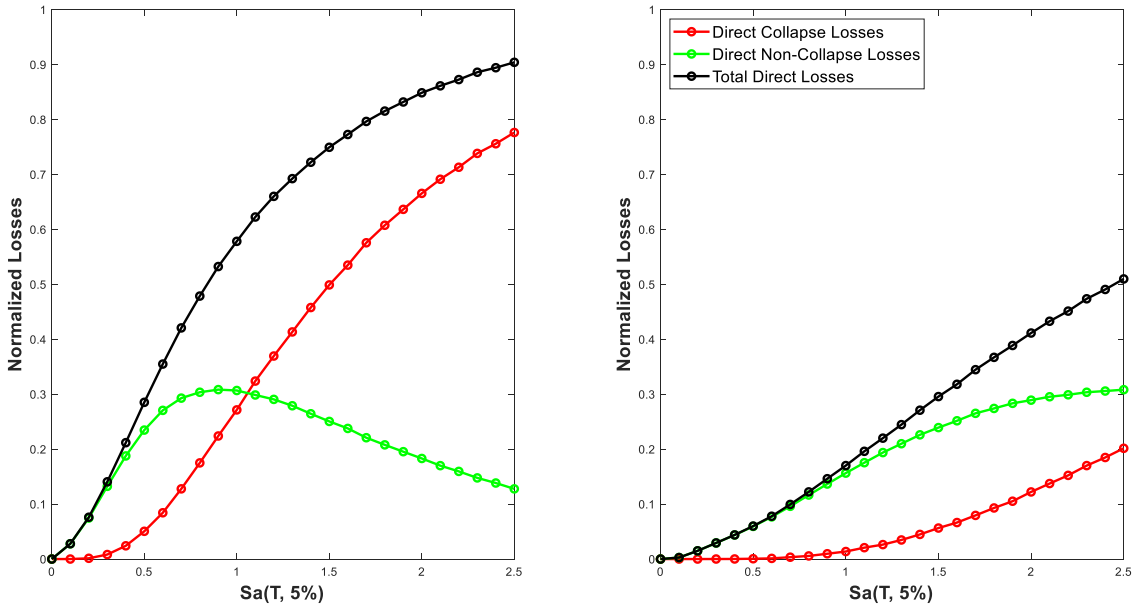

Figure 3.28: 500kV As-Installed (Left) and Retrofitted (Right) Direct Far-Field Ground Motion Comparison

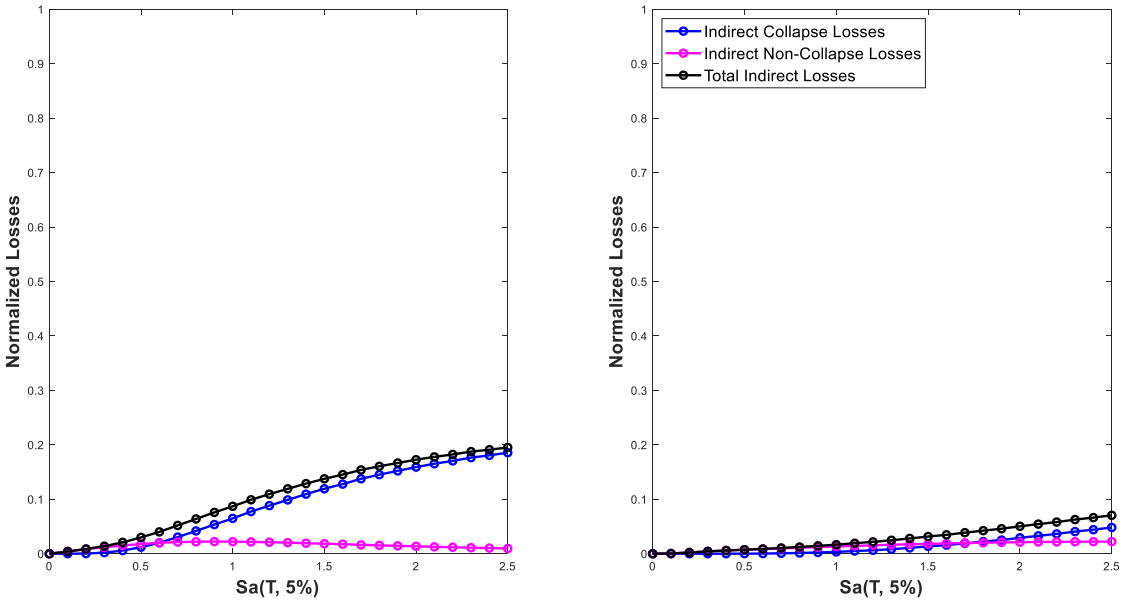

Figure 3.29: 500kV As-Installed (Left) and Retrofitted (Right) Indirect Far-Field Ground Motion Comparison

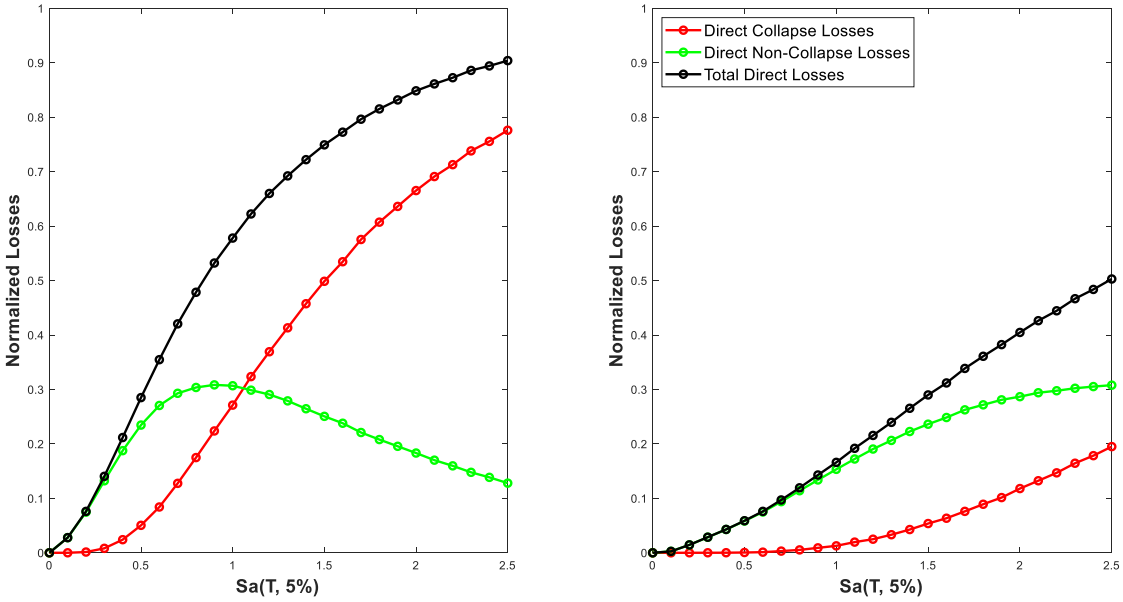

Figure 3.30: 500kV As-Installed (Left) and Retrofitted (Right) Direct Near-Field Pulse Ground Motion Comparison

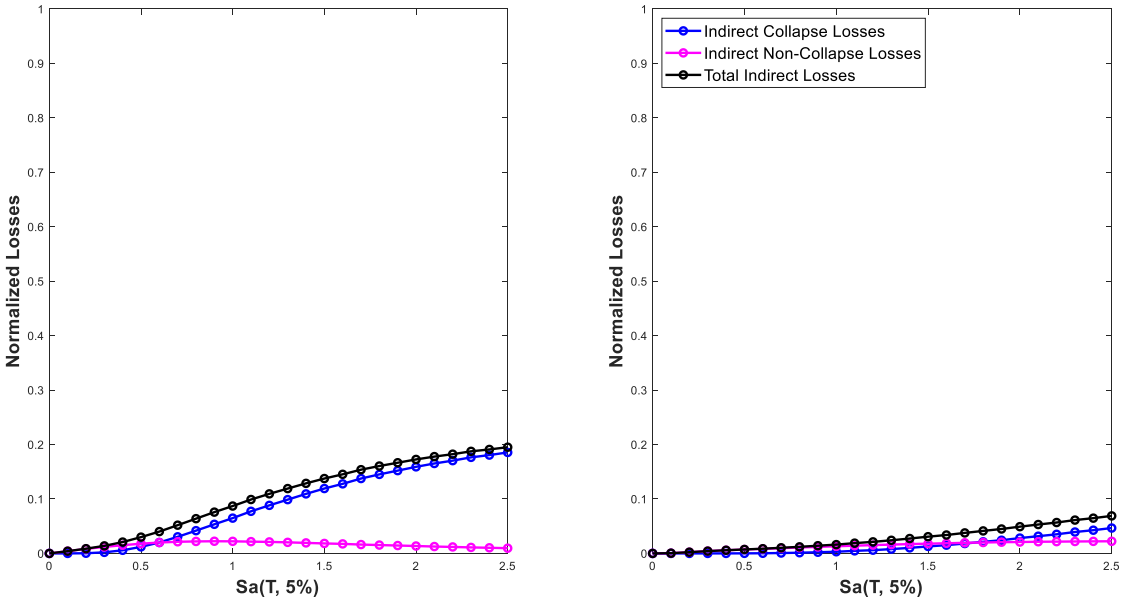

Figure 3.31: 500kV As-Installed (Left) and Retrofitted (Right) Indirect Near-Field Pulse Ground Motion Comparison

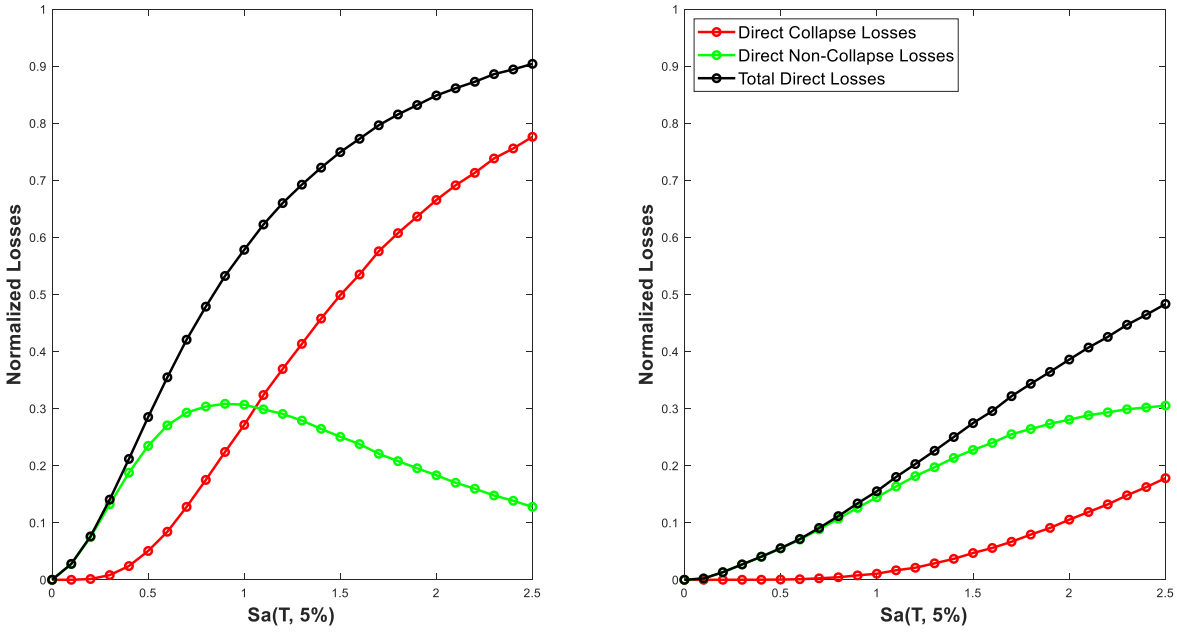

Figure 3.32: 500kV As-Installed (Left) and Retrofitted (Right) Direct Near-Field Non-Pulse Ground Motion Comparison

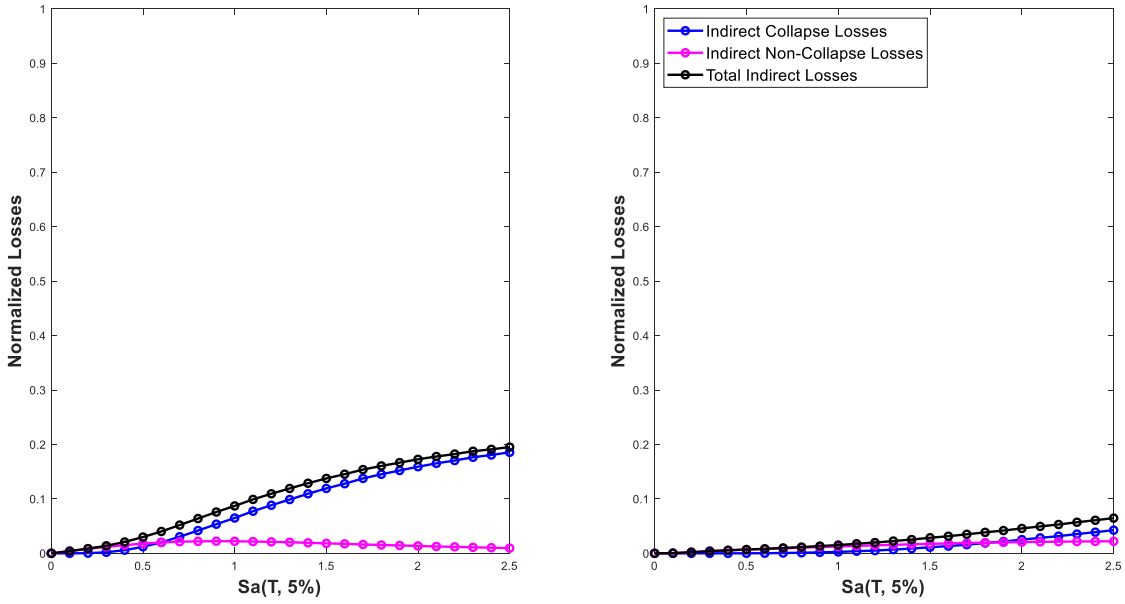

Figure 3.33: 500kV As-Installed (Left) and Retrofitted (Right) Indirect Near-Field Non-Pulse Ground Motion Comparison

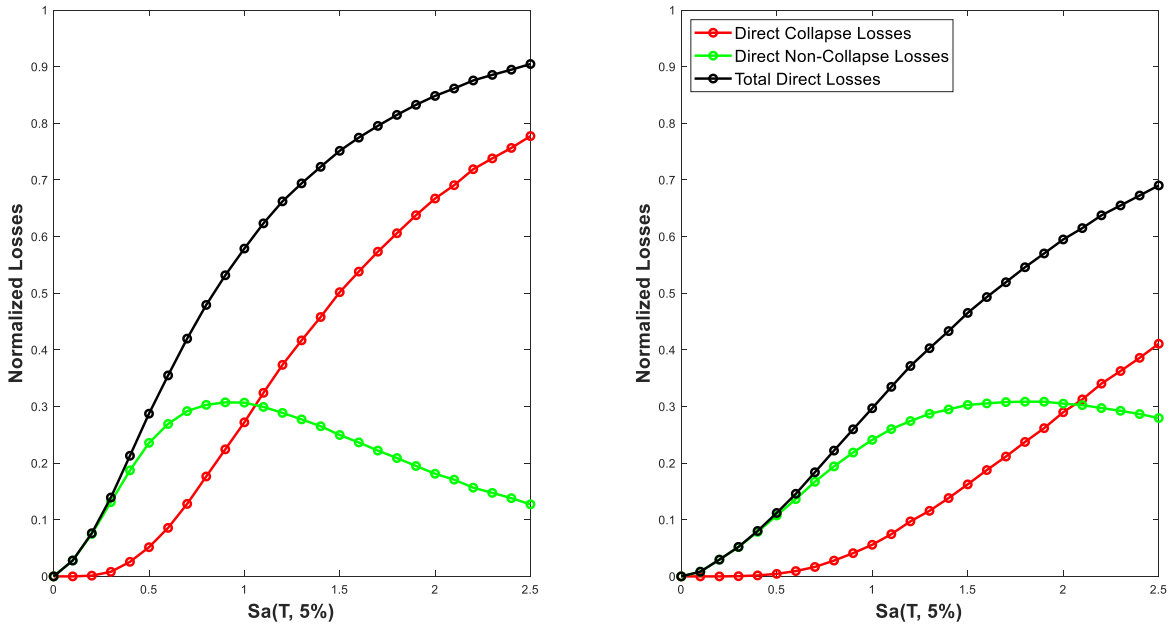

Figure 3.34: 525kV As-Installed (Left) and Retrofitted (Right) Direct Far-Field Ground Motion Comparison

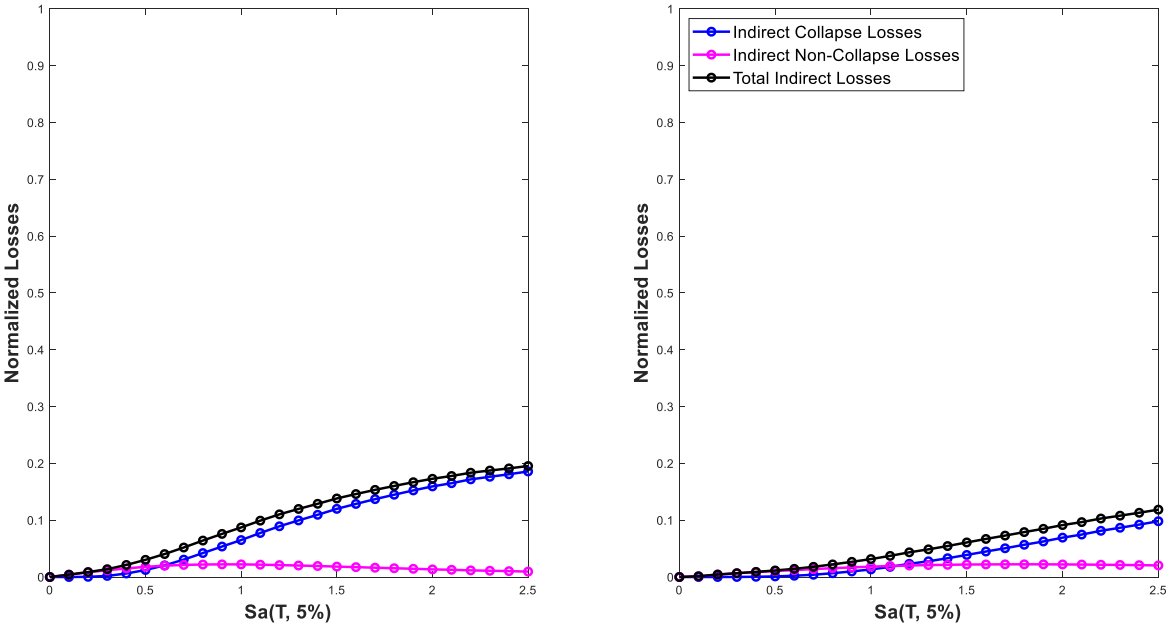

Figure 3.35: 525kV As-Installed (Left) and Retrofitted (Right) Indirect Far-Field Ground Motion Comparison

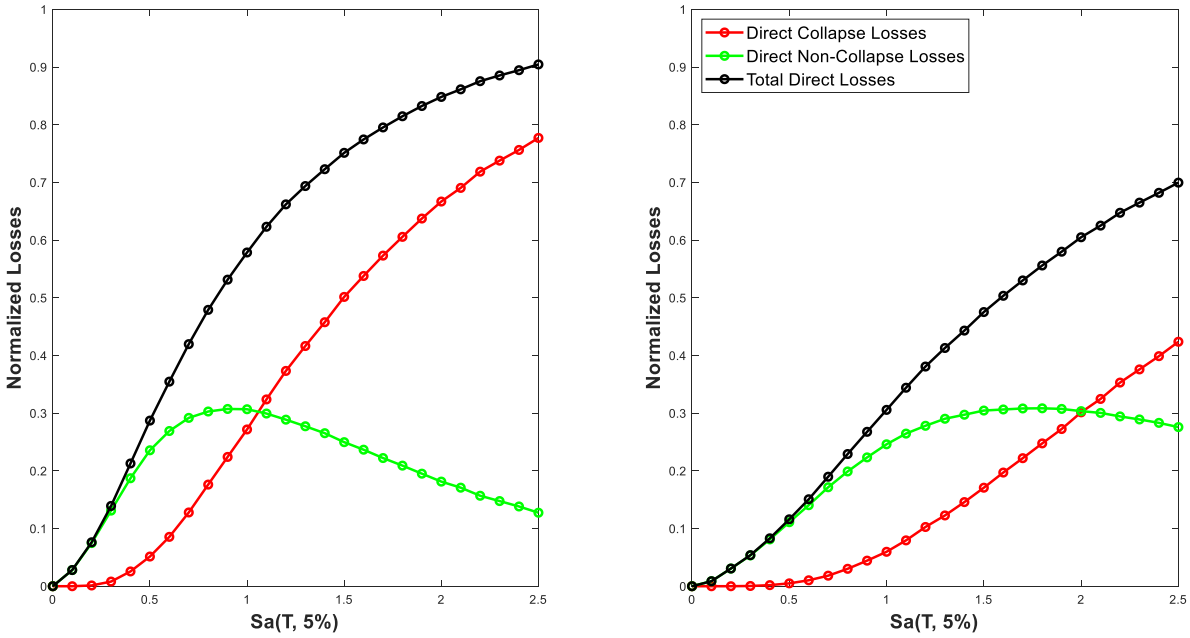

Figure 3.36: 525kV As-Installed (Left) and Retrofitted (Right) Direct Near-Field Pulse Ground Motion Comparison

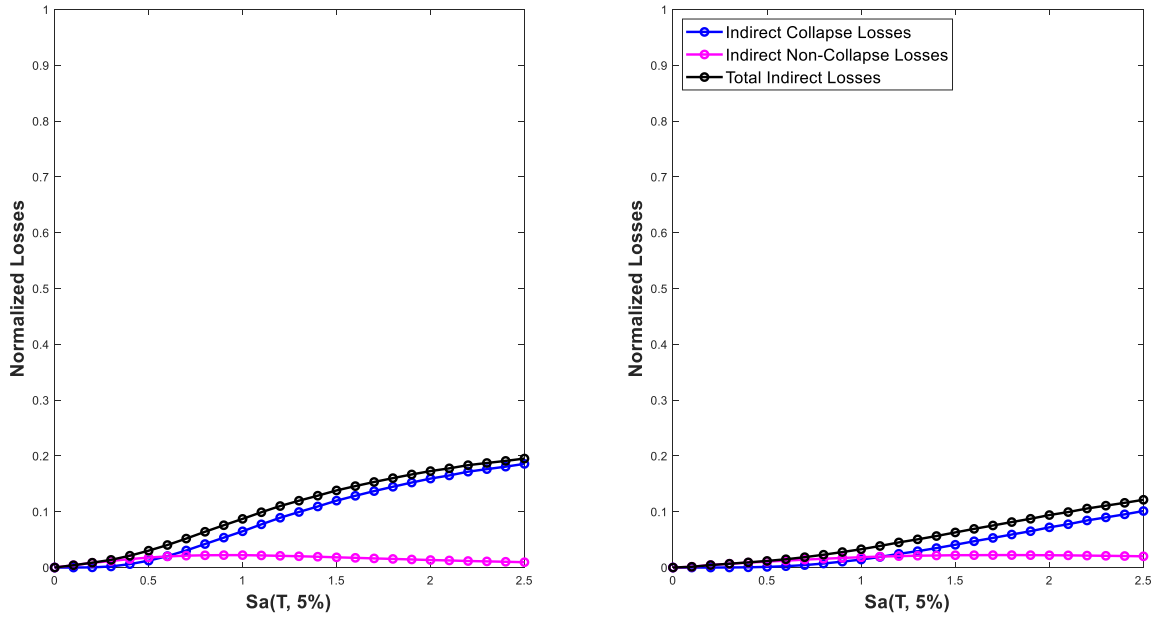

Figure 3.37: 525kV As-Installed (Left) and Retrofitted (Right) Indirect Near-Field Pulse Ground Motion Comparison

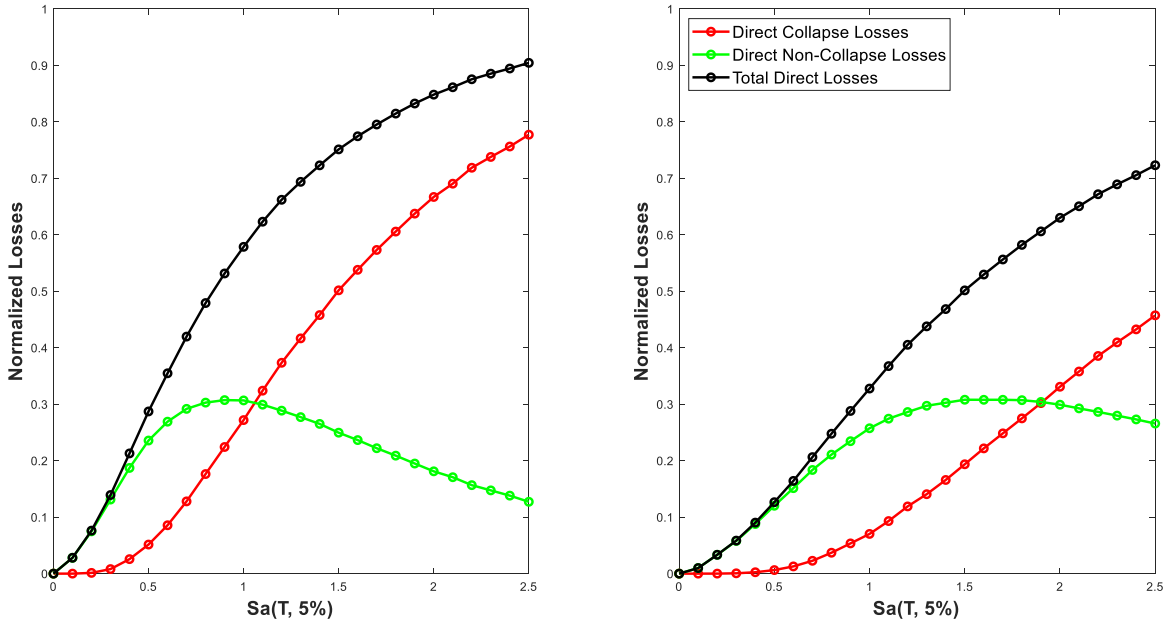

Figure 3.38: 525kV As-Installed (Left) and Retrofitted (Right) Direct Near-Field Non-Pulse Ground Motion Comparison

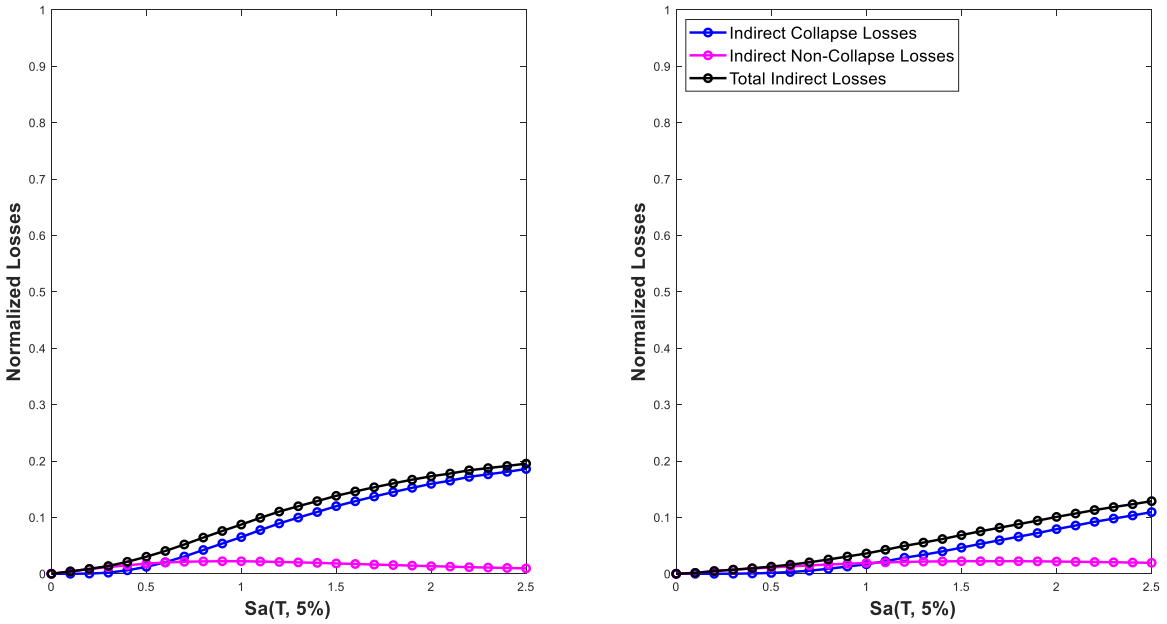

Figure 3.39: 525kV As-Installed (Left) and Retrofitted (Right) Indirect Near-Field Non-Pulse Ground Motion Comparison

3.4.4.2. Annual Expected Losses

With the curves produced in section 3.4.4.1 detailing the final results for the normalized expected losses conditioned on seismic intensity, the next step is to determine the values of the Expected Annual Losses (EAL) for each case of transformer bushing system (with varying mounting condition and seismic intensity). To achieve this, the hazard curves provided in section 3.3.1 are cross referenced with the spectral acceleration values from our curves in the previous section, to determine the annual probability of each of the ground accelerations in each of the 4 respective target areas. Once that is completed, the loss curves from section 3.4.4.1 are integrated in order to compute the EAL of each target area based on their individual hazard curve for each transformer configuration, based on its fundamental period value. The equation for this was taken from (Huang and Lignos 2017), and can be seen in equation 3.8, where $E[L_T|IM]$ represents the expected (total) losses at a given intensity measure value, and $\lambda_{Sa}(IM)$ represents the mean annual frequency of a particular intensity measure occurring.

$$\boldsymbol{EAL = E[L_T] = \int_0^\infty E[L_T|IM][\frac{d\lambda_{Sa}(IM)}{dIM}]dIM} \qquad \textbf{EQ 3.8}$$

Once each EAL value was found for each case, they were plotted on the histograms seen in Figure 3.40 to Figure 3.63. The implications of such will be discussed further in section 3.5.

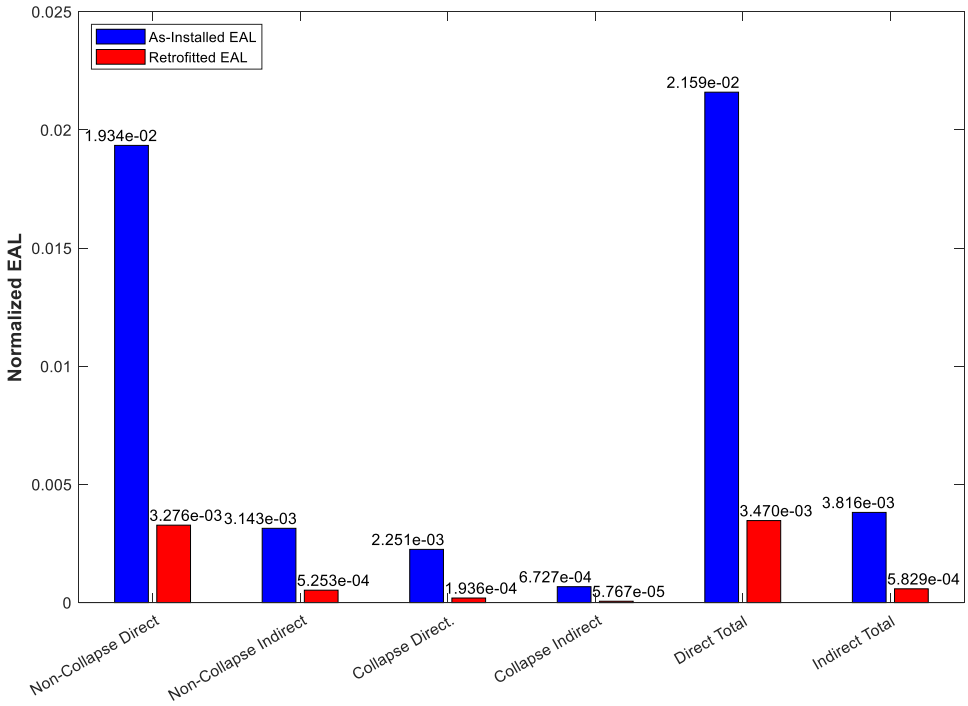

Figure 3.40: 230kV Packard EAL Far-Field Analysis Results for Southern California

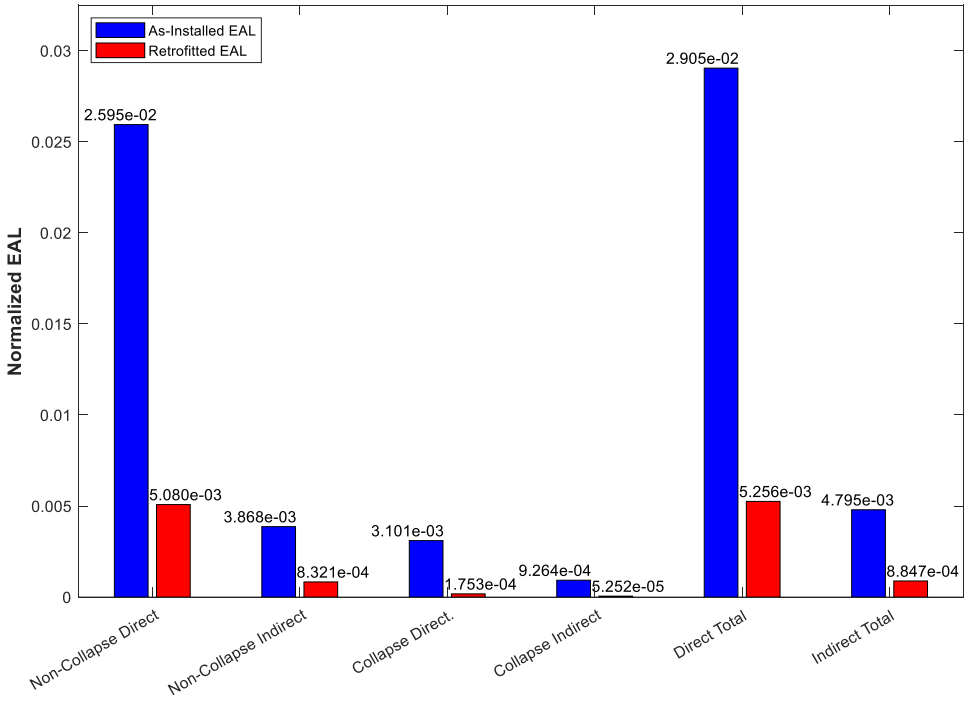

Figure 3.41: 230kV Packard EAL Far-Field Analysis Results for Northern California

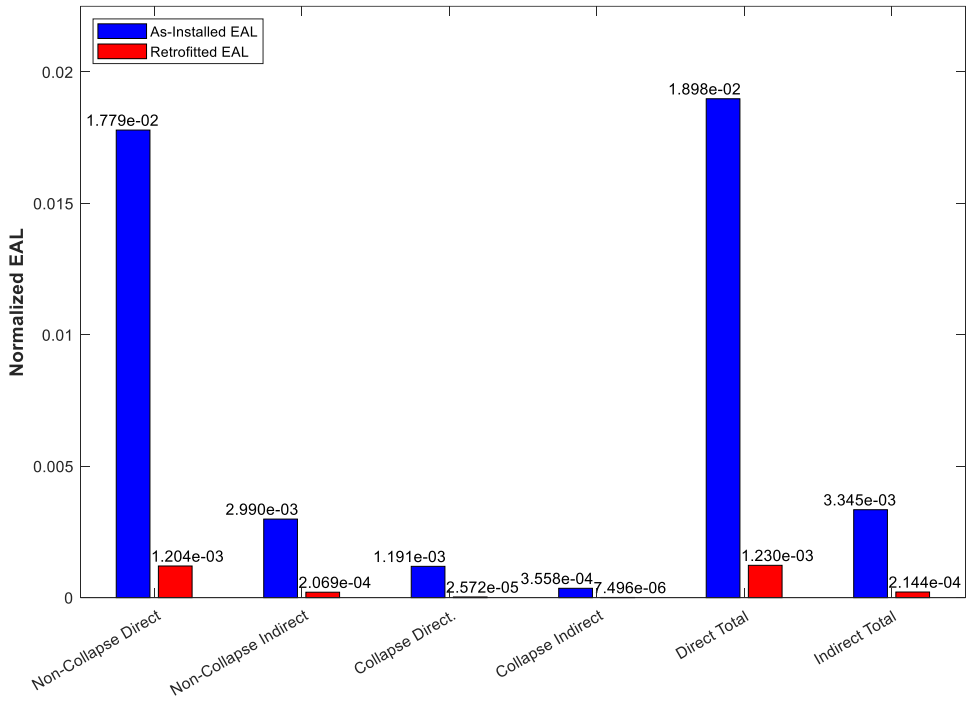

Figure 3.42: 230kV Packard EAL Near-Field Pulse Analysis Results for Southern California

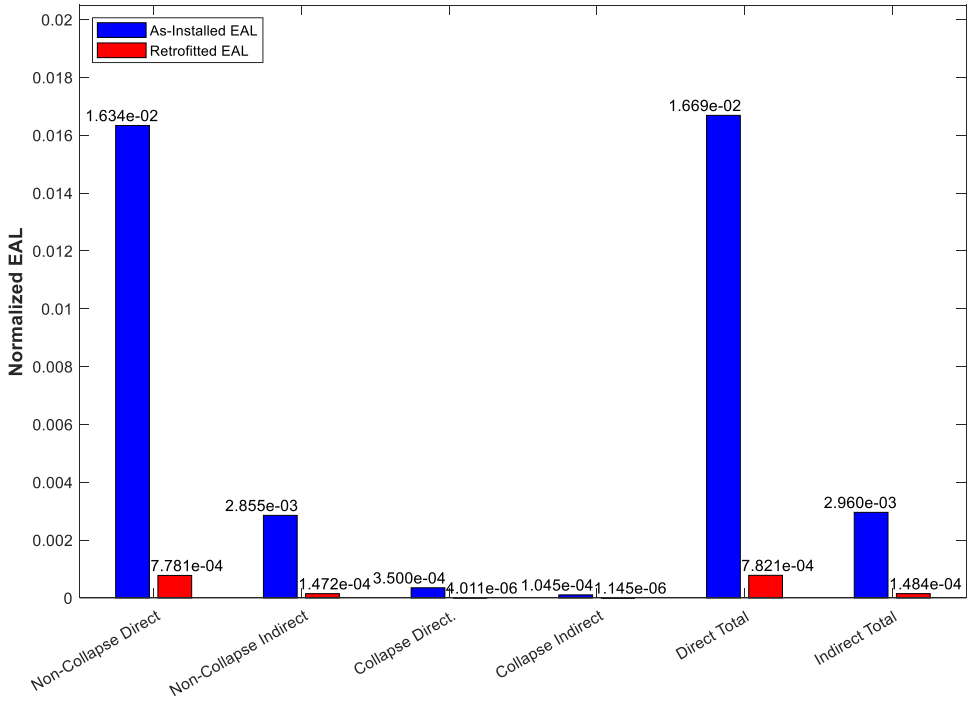

Figure 3.43: 230kV Packard EAL Near-Field Pulse Analysis Results for Northern California

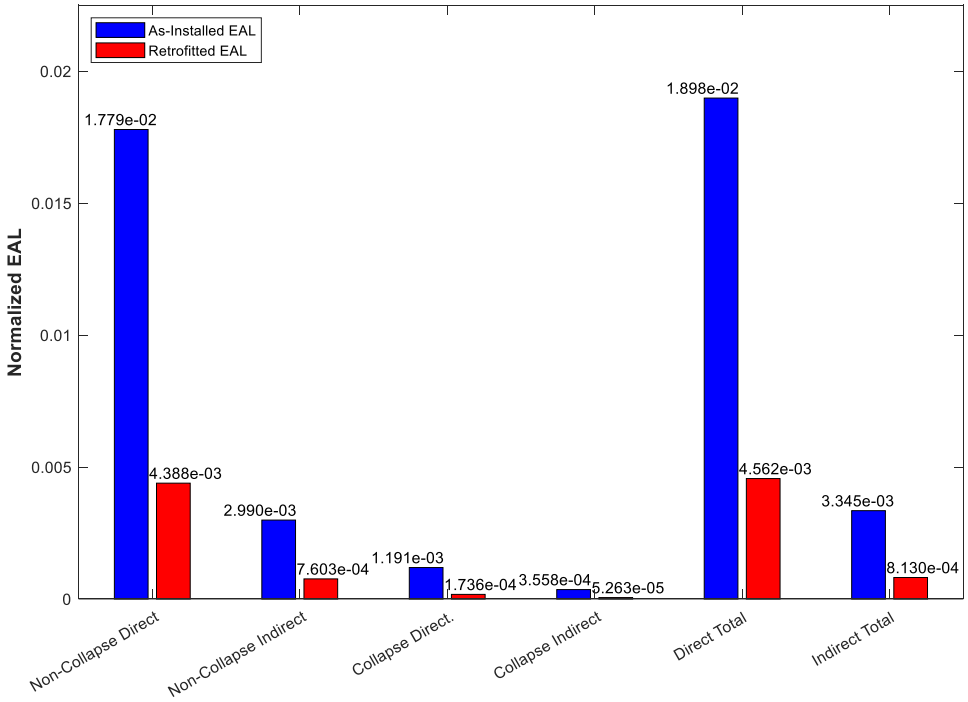

Figure 3.44: 230kV Packard EAL Near-Field Non-Pulse Analysis Results for Southern California

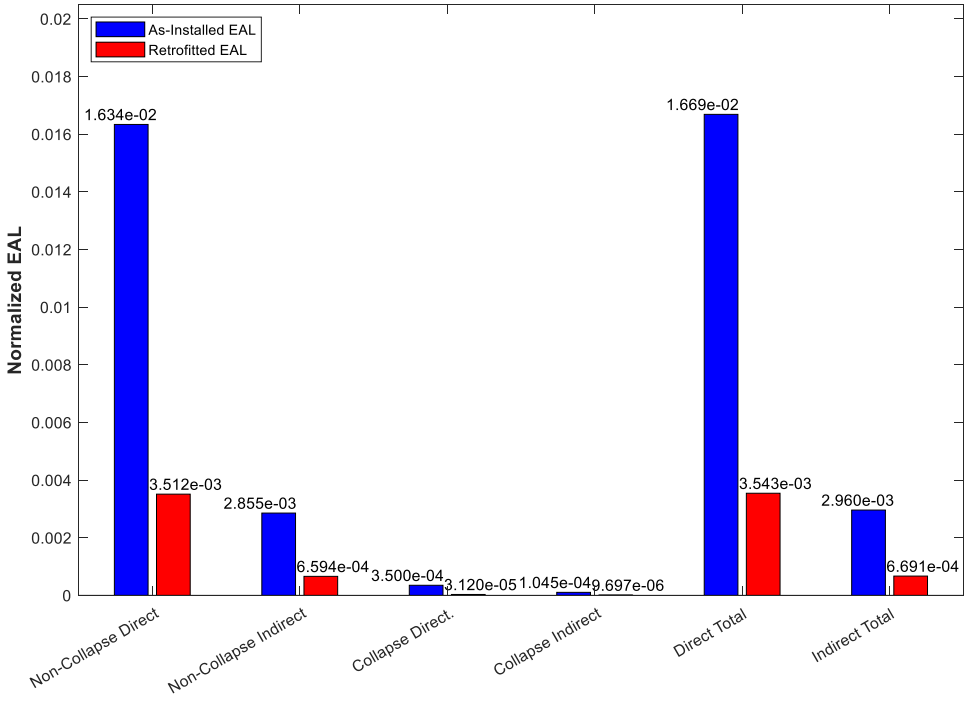

Figure 3.45: 230kV Packard EAL Near-Field Non-Pulse Analysis Results for Northern California

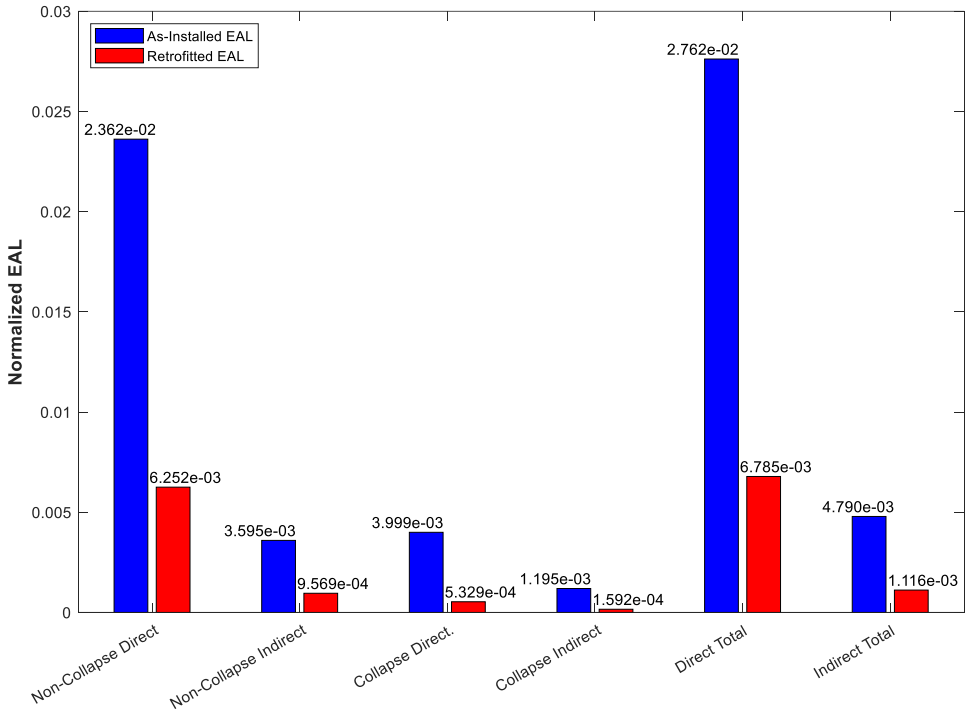

Figure 3.46: 230kV Siemens EAL Far-Field Analysis Results for Southern California

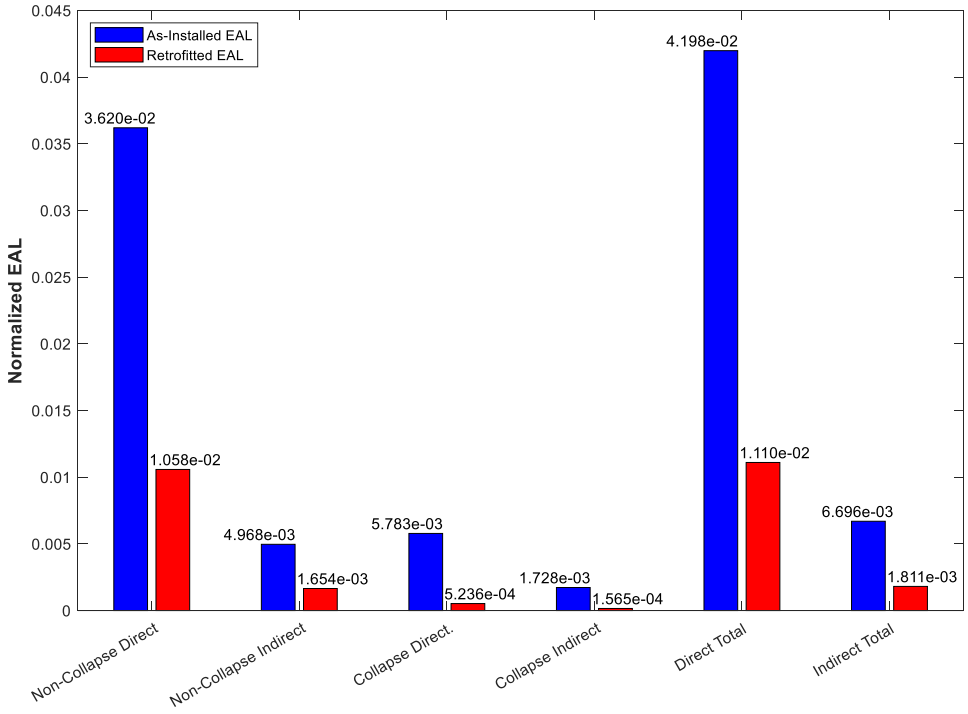

Figure 3.47: 230kV Siemens EAL Far-Field Analysis Results for Northern California

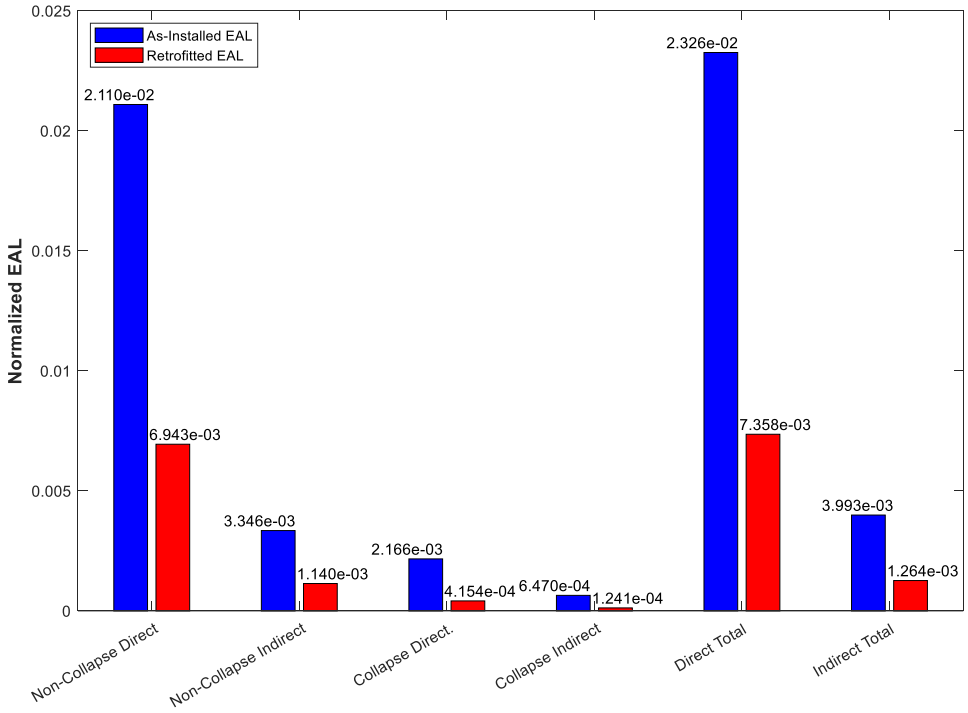

Figure 3.48: 230kV Siemens EAL Near-Field Pulse Analysis Results for Southern California

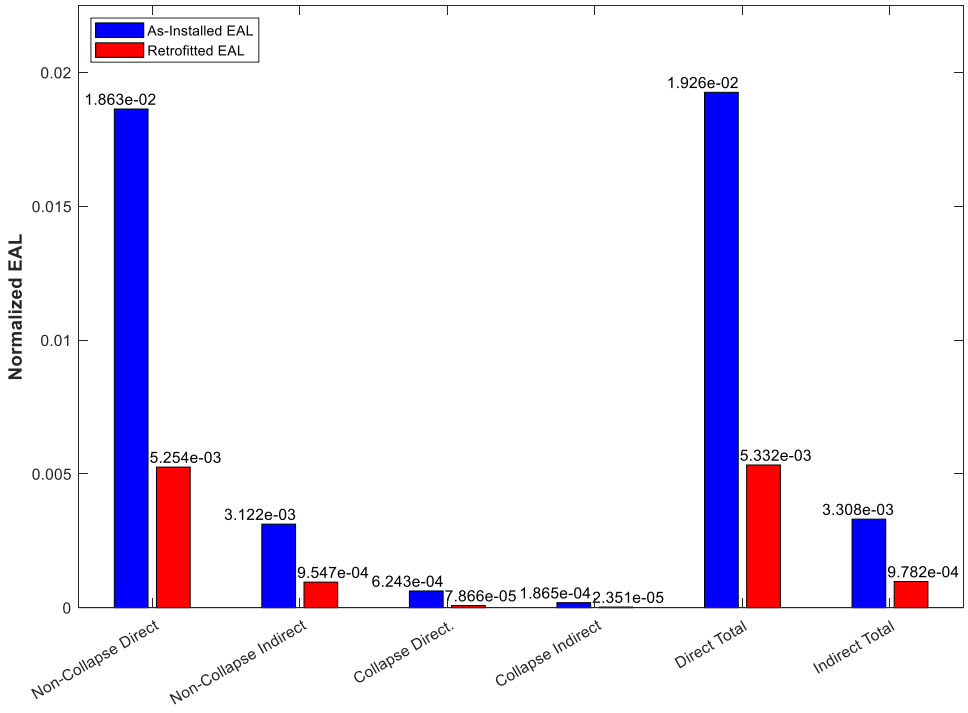

Figure 3.49: 230kV Siemens EAL Near-Field Pulse Analysis Results for Northern California

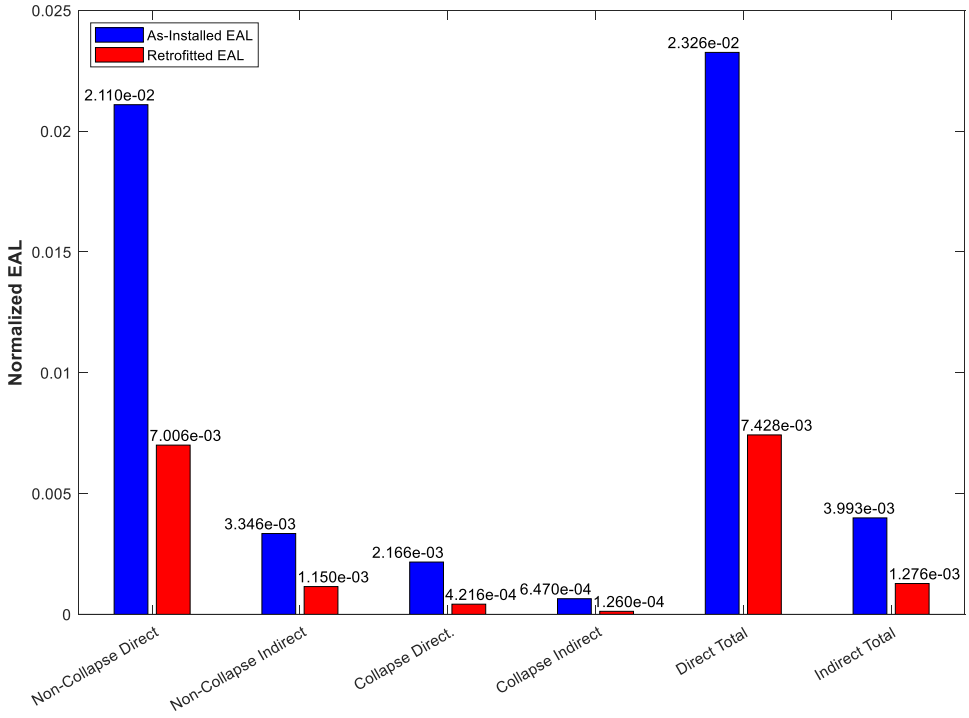

Figure 3.50: 230kV Siemens EAL Near-Field Non-Pulse Analysis Results for Southern California

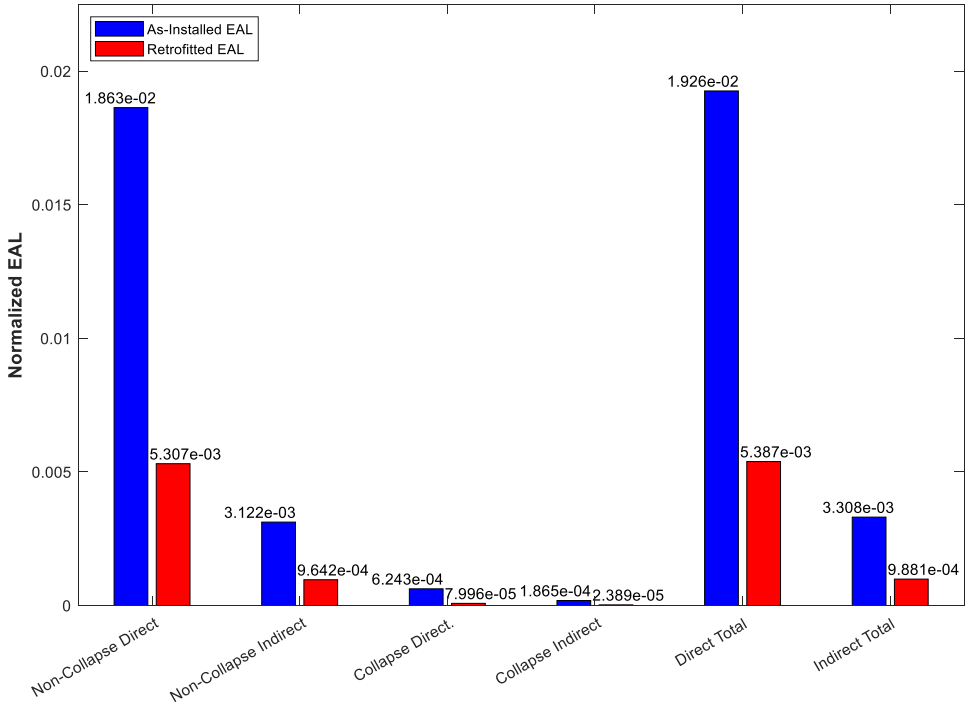

Figure 3.51: 230kV Siemens EAL Near-Field Non-Pulse Analysis Results for Northern California

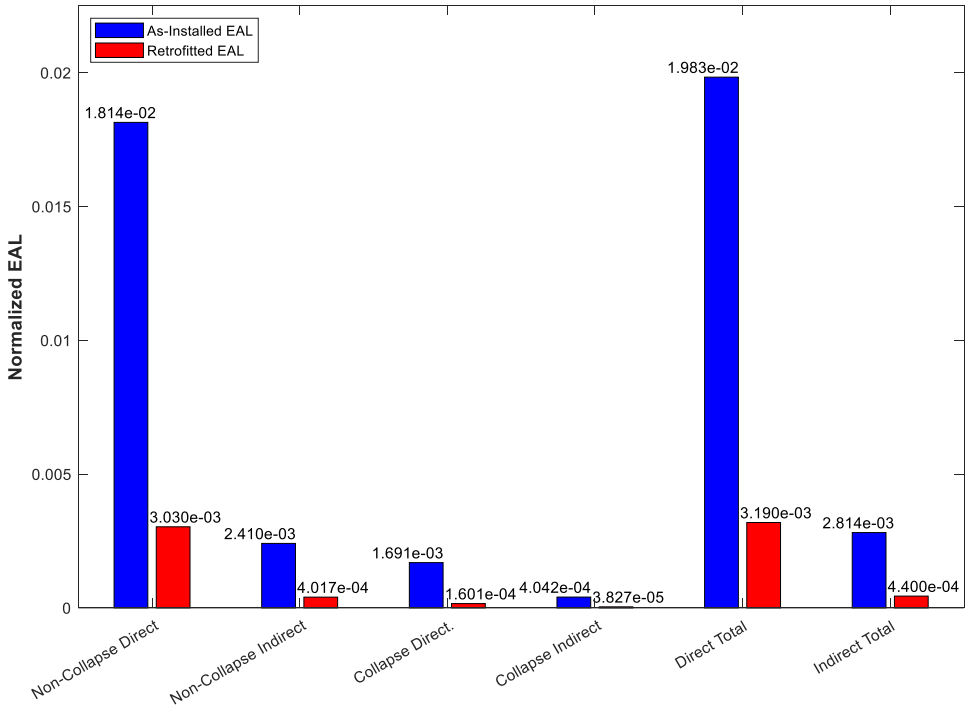

Figure 3.52: 500kV EAL Far-Field Analysis Results for Southern California

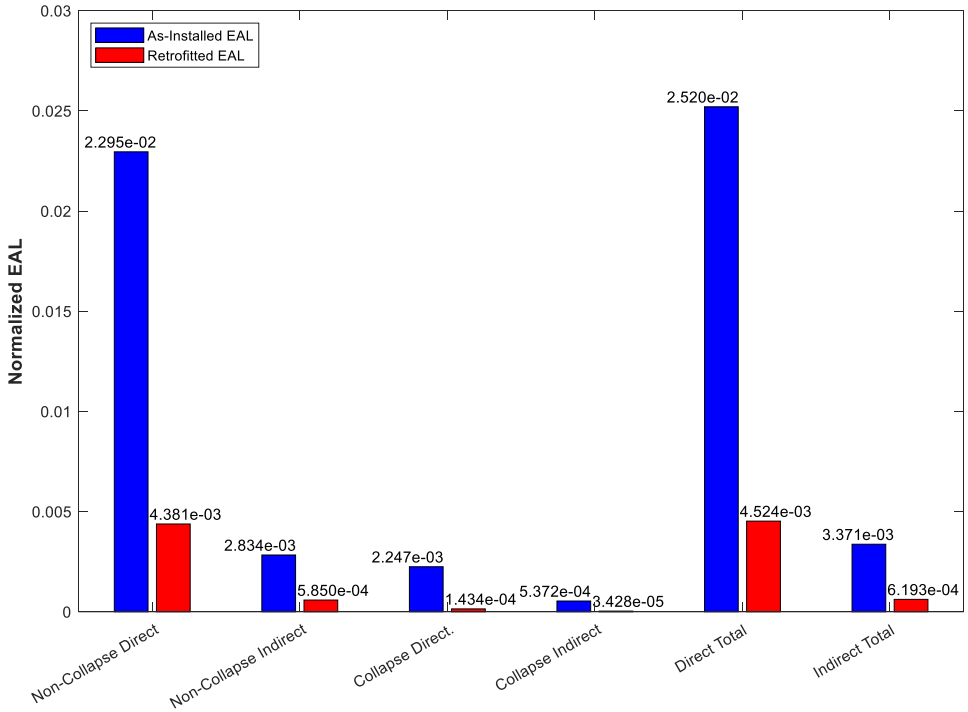

Figure 3.53: 500kV EAL Far-Field Analysis Results for Northern California

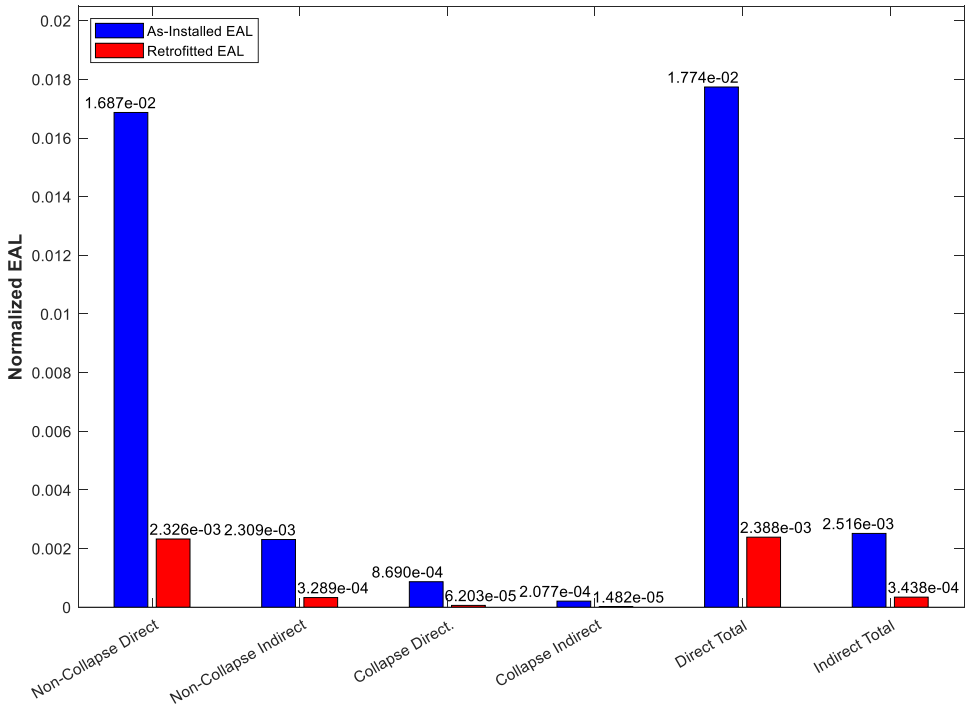

Figure 3.54: 500kV EAL Near-Field Pulse Analysis Results for Southern California

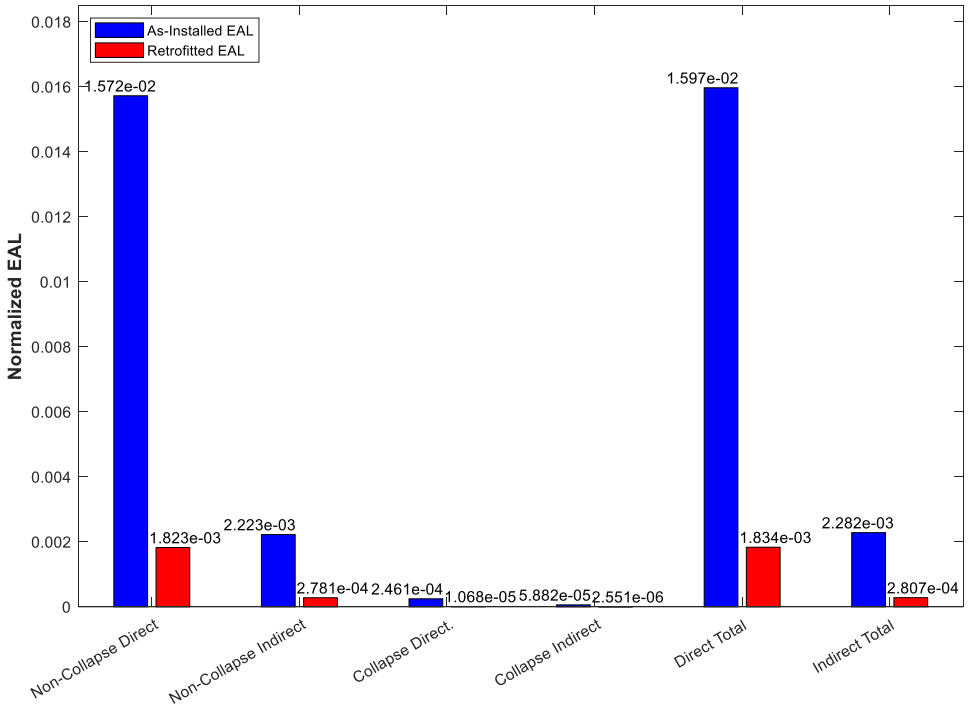

Figure 3.55: 500kV EAL Near-Field Pulse Analysis Results for Northern California

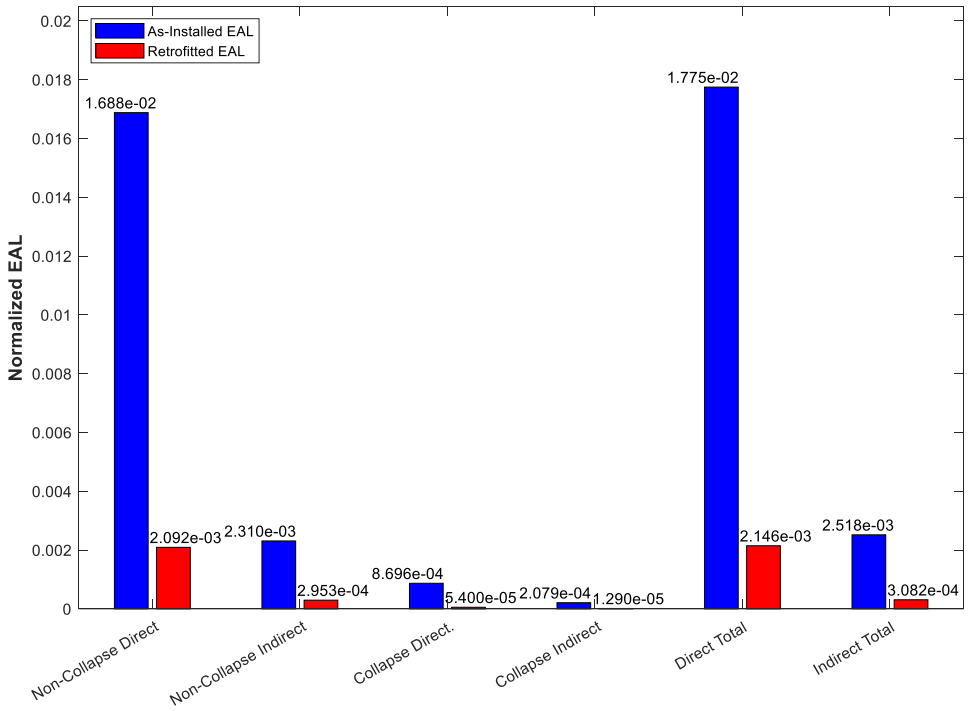

Figure 3.56: 500kV EAL Near-Field Non-Pulse Analysis Results for Southern California

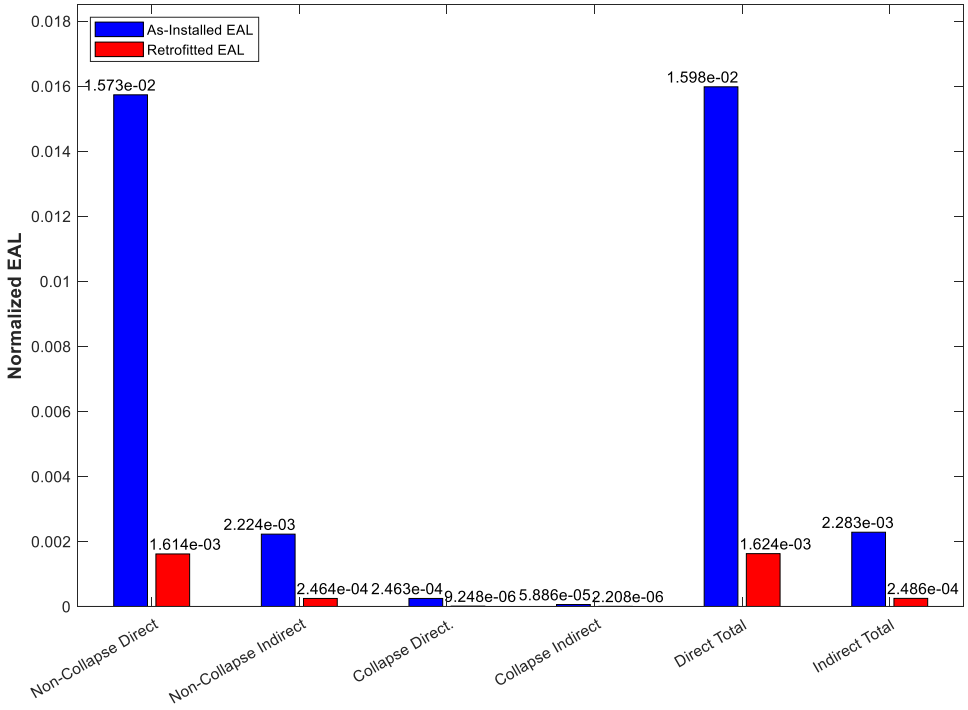

Figure 3.57: 500kV EAL Near-Field Non-Pulse Analysis Results for Northern California

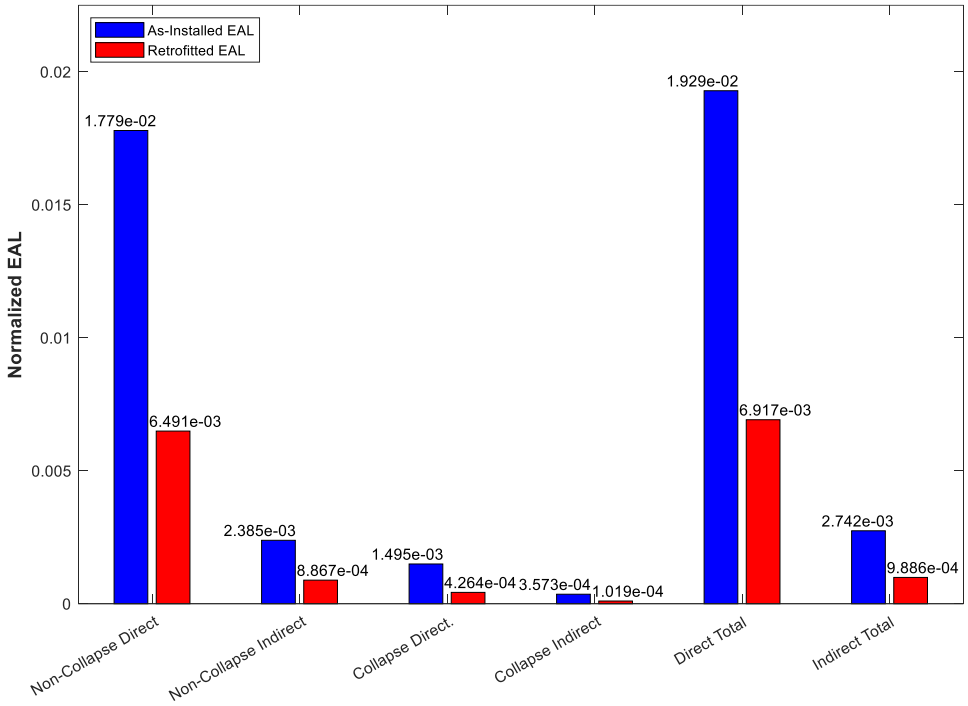

Figure 3.58: 525kV EAL Far-Field Analysis Results for Southern California

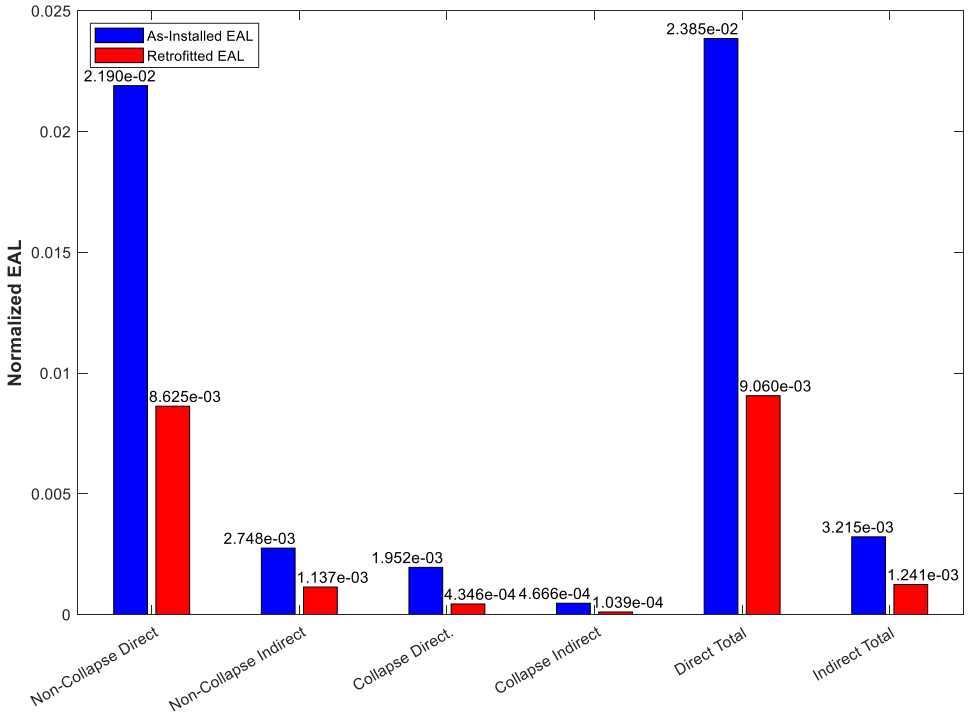

Figure 3.59: 525kV EAL Far-Field Analysis Results for Northern California

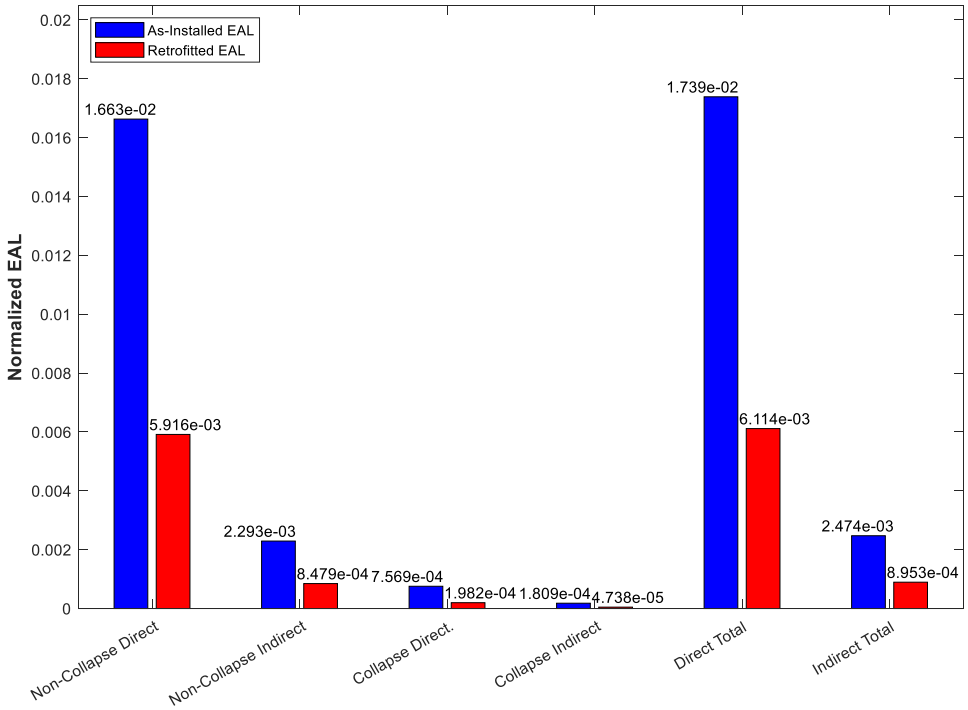

Figure 3.60: 525kV EAL Near-Field Pulse Analysis Results for Southern California

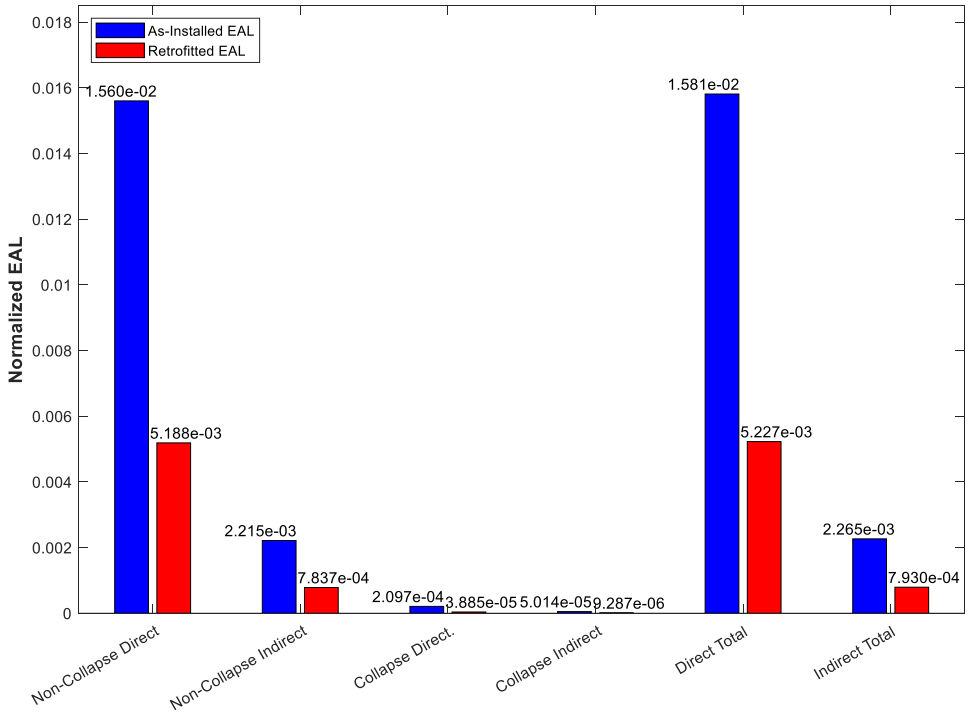

Figure 3.61: 525kV EAL Near-Field Pulse Analysis Results for Northern California

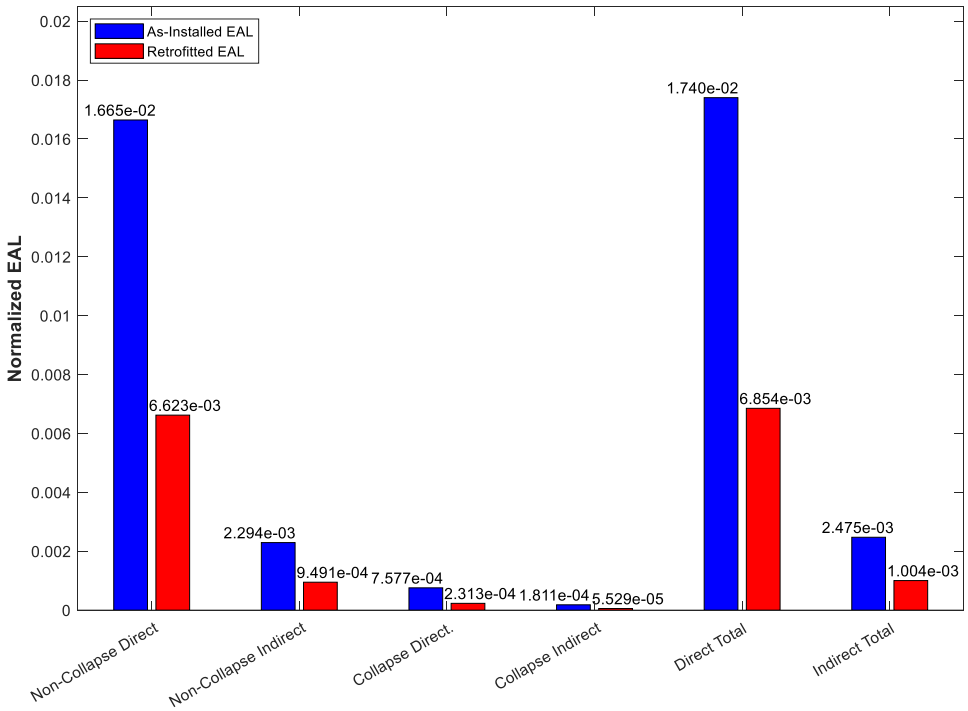

Figure 3.62: 525kV EAL Near-Field Non-Pulse Analysis Results for Southern California

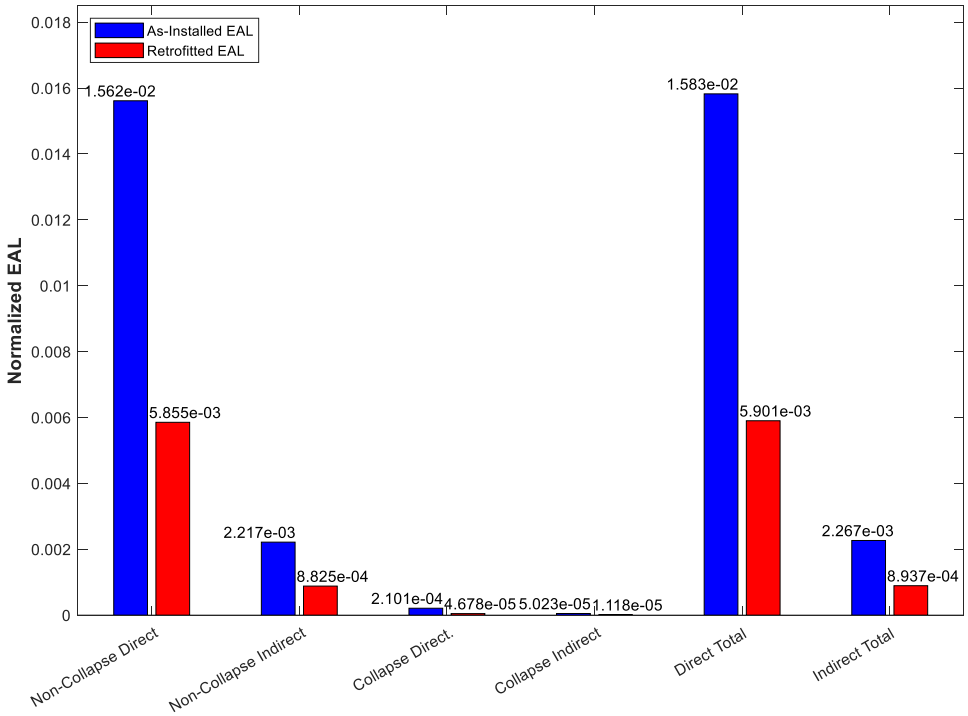

Figure 3.63: 525kV EAL Near-Field Non-Pulse Analysis Results for Northern California

3.5. Discussion of Results

Considering all simulation results presented in section 3.4, the results and implications of such will be discussed herein. The loss curves provided in section 3.4.4.1 were able to properly display the differences between the retrofitted and as-installed models for each case. In most cases the retrofit appeared to result between 33% and 55% of a reduction of total losses in the highest applied spectral acceleration at 2.5g for each variation of losses. There is also a clear indication of the effectiveness of the retrofitting technique by the decreased presence of the collapse-based loss curve values, as the collapse state based curves would typically show reductions between 40% and 75% depending on the transformer model. The one rarity of all the cases is that of the 230kV Packard Near-Field options, which appeared to have an extremely significant decrease of about 67% of the total at 2.5g for the Pulse motions, and a smaller amount of only about 30% for the Non-Pulse motions. This could be due to perhaps something in the nature of the model in question that would react differently to the different ground motion types.

Another point of interest in terms of the loss curves is the impact that the indirect loss analysis appears to have across the steadily increasing spectral acceleration. Due to the nature of the downtime parameters and the drastic difference between a "severe" average downtime of 7 days and a "collapse" average downtime of 30 days, the indirect non-collapse losses seem to be largely overshadowed by their collapse counterpart. Even in all of the retrofitted cases, where the number of collapse damage states achieved is much less than that of the as-installed, it was often that by the time the

indirect non-collapse damage was beginning to form and have a credible loss component, the indirect collapse values were typically equal to (if not greater than) the non-collapse iterations. While this can certainly be contributed to the fact that the time to repair an existing transformer is certainly less than that of complete replacement, it is still an interesting factor of the loss curves.

With that being said, the EAL plots of section 3.4.4.2 better represent the impact of the indirect non-collapse losses. As can be seen by the histograms of the various cases, the non-collapse losses tend to exceed the collapse-based losses by a large margin. Since the value of acceleration needed to achieve a collapse state is much greater than that of only damaging the transformer this fact isn't surprising, but it provides a more realistic representation than that of the loss curves alone. The EAL plots also provide a good representation of the retrofitting technique effectiveness, where in most cases a reduction of 60-80% from the as-installed EAL to the retrofitted EAL is observed. Similar to the loss curves, the 230kV Packard Near-Field cases appear to be the lone outliers, the Pulse configuration having reductions of over 99% in some cases.

The EAL plots also provide some interesting context on the effectiveness of the models in different areas. It appears that each transformer had a trend, where one of the two ground motion types (Far-Field/Near-Field) would have lower loss values in one of the two target areas, while the other ground motion type would be lesser in the second target area. For example, the 525kV transformer showed overall higher EAL values in Southern California for the Near-Field Pulse and Near-Field Non-Pulse plot, however

Northern California would then have a higher EAL value for its Far-Field plot. This same relationship was found across all different transformer configurations.

4. SUMMARY, CONCLUSIONS, AND RECOMMENDATIONS

4.1. Summary

In this study, a risk-based assessment of the performance of medium and high voltage transformer bushing systems under various mounting conditions (as-installed and retrofitted) as well as various seismic excitation inputs was conducted. The retrofit scheme of added flexural stiffeners at the transformer tank top was adopted to more realistically simulate the "rigid-base" format known to cause better survivability in laboratory experimental studies, as can be observed by the durability of the high-voltage porcelain bushings. The purpose of this research was to evaluate the practicality and feasibility of this retrofit solution for electrical transformer bushing systems in terms of decision variables associated with economic losses (dollars) and downtime related to the post-earthquake recovery of electrical substations.

Towards achieving the goal of this research, numerical studies were performed for a variety of transformers, with an equal amount representing medium- and high-voltage transformers namely: (i) the Ferranti Packard 230kV transformer-bushing model, (ii) the Siemens 230kV transformer-bushing model, (iii) the Siemens 500kV transformer-bushing model, and (iv) the Westinghouse 525kV transformer-bushing model. Each transformer was analyzed (linear time history analyses) from two cases, one being as-installed with no applied retrofit, and the other adding flexural stiffeners to enhance seismic resistivity. Each case had three applied ground motion ensembles considered: (i) the FEMA P695 Far-Field ground motion set, (ii) the FEMA P695 Near-

Field Pulse ground motion set, and (iii) the FEMA P695 Near-Field Non-Pulse ground motion set. Each ground motion ensemble was applied to all cases in order to generate fragility curves relating the engineering demand parameter of interest (maximum base bushing moment) to the probability of exceedance of prescribed limit state values for each transformer.

Once the structural analyses were performed for each transformer and respective ground motion ensemble, the principles of the Performance Based Earthquake Engineering (PBEE) framework were applied in order to perform a risk-based performance assessment of the transformer systems. The locations of interest for this study were the Northern and Southern California areas, each location representing that of an active transformer in the state of California fitting the criteria for either Near-Field or Far-Field applicability. These would allow the chance to obtain an expected annual loss value for each location based on the annual frequency of exceedance of ground motions in the specified areas. The total replacement cost distributions for various damage states of the transformer bushing systems were adopted from the HAZUS technical manual, as well as the associated downtime.

With these components, a multi-later Monte Carlo analysis was conducted on all previously mentioned transformer models. The first layer decided the magnitude of the applied intensity measure; the second layer determined the damage state of the transformer in the applied intensity measure; the third and final layer determined the financial losses of the transformer in the simulated damage state. Each transformer configuration went through this analysis with 1,500 iterations per layer, resulting in the

loss curve conditioned on seismic intensity as well as Expected Annual Losses (EAL) plots as presented in Sections 3.4.5 and 3.4.6 of this thesis.

4.2. Conclusions

Considering the results of all the numerical analyses presented for each transformer and ground motion ensemble variation, the primary conclusions are as follows:

- In each ground motion ensemble considered, the applied retrofit scheme displayed a significant improvement in terms of the structural performance of the transformer bushings associated with damage exhibited to the medium- and high-voltage bushings, representing that it is effective across a variety of circumstances.
- Based on the loss analyses, a clear reduction in the collapse damage state influence for all cases was observed, with an overall decrease of at least 20% across the highest considered acceleration for high- and medium-voltage transformers when adopting the retrofit scheme of flexural stiffeners.
- The application of flexural stiffeners as a retrofitting technique provided a significant decrease in the overall losses for every case. The EAL values for the as-installed cases were at least 2.5 times larger than that of the retrofit, and at most nearly 10 times as large as the retrofitted case.
- Across all intensity measures the indirect losses (associated with downtime) appeared to be heavily skewed in terms of the collapse damage state priority over

non-collapse damage states. While this can be expected to a degree as repair time is typically less than the amount of time to replace a full unit, the potential damage of such is better recognized in terms of EAL rather than losses as a function of intensity measure (IM).

- While the individual loss curves may not have shown a significant difference between far-field and near-field ground motion sets, the expected annual loss values overall depicted that near-field cases observed lower expected annual losses when compared to the far-field cases.
- The EAL plots (see Figure 3.40 to Figure 3.63) provide a clear indication of the impact that non-collapse damage states have on the annual losses, with both direct and indirect EALs being exceptionally higher for non-collapse cases than the respective collapse cases. While on one hand this may undervalue the fear of reaching a collapse state, it also exclaims the importance of reducing the achieved damage state (e.g., minor damage rather than severe damage) as much as possible.
- The Northern California selected site for this study appeared to have higher EAL values in comparison to the Southern region of the state in all observed damage types for near-field based earthquakes, while the Southern region displayed higher EAL values for observed far-field ground motions. The percentage reduction was variant among different applied ground motion ensembles, which could play a role in determining which locations may gain a greater benefit out of retrofit application.

4.3. Recommendations for Future Research

From the previously listed conclusions, other topics for future research with regards to the risk-based seismic performance of medium- and high- voltage transformer bushing structures include the following:

- The use of near-field and far-field ground motions provide a good layout for how these ground motions impact different areas of the United States, however another seismic origin of interest would be that of the Cascadia subduction zone (Pacific Northwest). Using a concise and representative ground motion set of such motions, it would be fruitful to confirm the ability of the flexural stiffener retrofit in those conditions and its benefit in terms of structural performance as well as economic losses (direct and indirect impact).
- Although the normalized losses allow for the loss values to be applied to any transformer at a fundamental level, it would be beneficial to have a clearer indication of what transformer components take direct damage after the applied seismic motions for a more intuitive EAL direct loss representation.
- While the applied stiffeners have proven to be an effective local retrofitting technique, it would be beneficial to compare it to a retrofit of a global scale and see the differences in the effectiveness of loss reductions. This would be useful both to see the strength differences and, with EALs, directly compare the difference in EAL reduction and cost of each retrofitting technique.
- The inclusion of other retrofitting techniques, such as base isolation would allow a direct comparison of the applied retrofitting technique to another, while also

providing another subject to apply the adopted risk assessment and observe the results of such.

- Although direct and indirect normalized losses were analyzed for the different transformer configurations, a full life-cycle cost analysis could provide more detailed EAL estimations for the applied PBEE framework.
- A spatial analysis of the retrofit application based on an individual city level could provide a better representation of indirect losses, allowing for direct fiscal representations for both the direct transformer cost based on what voltage rating is used in the area, and allowing for a more direct understanding of what aspects would be impacted by different degrees of downtime of electrical power.

REFERENCES

Ang, A. H.-S., and Tang, W. H. (1984). *Probability Concepts in Engineering Planning and Decision*.

CSI. 2018. SAP 2000 Advanced V19.2.0Computers and Structures Inc.

Fahad, M., and Roh, H. (2013). "Seismic Evaluation and Qualification of Transformer Bushings."

Fahad, M. R., H. , and Oikonomou, K. R., A.M. (2010). "Seismic Evaluation of Transformer Bushings." *Abstract and Presentation at 2010 ASCE/SEI Structures Congress*.

Fallahi, K. (2004). "STUDY OF SEISMIC DAMAGE TO POWER GENERATION AND DISTRIBUTION NETWORK AND REMEDY FOR IMPROVING THE EXISTING SAFETY CRITERIA " *13th World Conference on Earthquake Engineering*(1079).

FEMA (2009). "P695 - Quantification of Building Seismic Performance Factors."

FEMA (2010). "Hazus - MH MR5." *Multi-Hazard Loss Estimation Methodology*, FEMA, ed., Department of Homeland Security, Washington D.C.

FEMA (2012). "Seismic performance assessment of buildings, Volume 1– Methodology." FEMA, ed., Department of Homeland Security, Washington D.C.

Filiatrault, A., and Matt, H. (2006). "Seismic Response of High Voltage Transformer-Bushing Systems." *ASCE Journal of Structural Engineering*, 132(2), 287-295.

Gilani, A. S., Whittaker, A. S., and Fenves, G. L. (2001). "Seismic Evaluation and Retrofit of 230kV Porcelain Transformer Bushings." *Earthquake Spectra*, 17, 597-616.

Gilani, A. S. J., Whittaker, A. S., and Fenves, G. L. (2004). "Earthquake Performance of Porcelain Transformer Bushings." *Earthquake Spectra*, 20(1), 205-223.

Gökçe, T., Orakdöğen, E., and Yüksel, E. (2017). "Seismic Protection of High Voltage Bushings by Using Polyuretan Springs." *16th World Conference on Earthquake Engineering*Santiago, Chile.

Günay, S. M., Khalid M. (2013). "PEER Performance-Based Earthquake Engineering Methodology, Revisited." *Journal of Earthquake Engineering*, 17(6), 829-858.

Hatami, M., Ashtiany, M. G., and Hosseini, M. (2004). "Experimental and Analytical Study of a High Voltage Instrument Transformer." *13th World Conference on Earthquake Engineering*Vancouver, B.C., Canada.

Huang, S.-H., and Lignos, D. G. (2017). "Earthquake-induced loss assessment of steel frame buildings with special moment frames designed in highly seismic regions." *Earthquake Engineering and Structural Dynamics*.

IEEE (2005). "IEEE REcommended Practice for Seismic Design of Substations." IEEE Power Engineering Society.

Jennings, C. W., and Bryant, W. A. (2010). "Fault Activity Map of California (2010)." California Geological Survey, California.

Kitayama, S., Lee, D., Constantinou, M. C., and Kempner, L. (2017). "Probabilistic Seismic Assessment of Seismically Isolated Electrical Transformers Considering Vertical Isolation and Vertical Ground Motion." *Engineering Structures*, 152, 888-900.

Koliou, M., Filiatrault, A., and Reinhorn, A. M. (2013a). "Seismic Response of High-Voltage Transformer-Bushing Systems Incorporating Flexural Stiffeners I: Numerical Study." *Earthquake Spectra*, 29(4), 1335-1352.

Koliou, M., Filiatrault, A., and Reinhorn, A. M. (2013b). "Seismic Response of High-Voltage Transformer-Bushing Systems Incorporating Flexural Stiffeners II: Experimental Study." *Earthquake Spectra*, 29(4), 1353-1367.

Koliou, M., Filiatrault, A. R., Andrei M. , and Oliveto, N. (2012). "Seismic Protection of Electrical Transformer Bushing Systems by Stiffening Techniques." University at Buffalo, State University of New York.

Kong, D. (2010). "Protection of High-Voltage Electrical Equipment Against Severe Shock and Vibrations." Ph.D., University at Buffalo, The State University of New York, Buffalo, NY.

Ma, G. L., and Xie, Q. (2018). "Seismic Analysis of a 500-kV Power Transformer of the Type Damaged in the 2008 Wenchuan Earthquake." *Journal of Performance of Constructed Facilities*.

Mitrani-Reiser, J. (2007). "AN OUNCE OF PREVENTION: PROBABILISTIC LOSS ESTIMATION FOR PERFORMANCE-BASED EARTHQUAKE ENGINEERING " Doctor of Philosophy, California Institute of Technology.

Oikonomou, K. (2010). "Modeling of Electrical Transformers and Seismic Performance." University at Buffalo, The State University of New York.

Oikonomou, K., Constantinou, M. C., Reinhorn, A. M., and Kempner, A. L. (2016). "Seismic Isolation of High Voltage Electrical Power Transformers." *MCEER Techincal Report MCEER-16-0006*.

OSHA "Illustrated Glossery: Substations." <https://www.osha.gov/SLTC/etools/electric_power/illustrated_glossary/substation.html>. (9/1/18, 2018).

Reinhorn, A., Oikonomou, M., Roh, K., and Schiff, H. K., A. L. (2011). "Modeling and Seismic Performance Evaluation of High-Voltage Transformers and Bushings." *MCEER Techincal Report MCEER-11-0006*.

Schiff, A. J. (1998). "Hyogoken Nabu (Kobe) Earthquake of January 17, 1995 Lifeline Performance." *Technical Council on Lifeline Earthquake Engineering (TCLEE), Monograph No. 14*, A. S. o. C. Engineers, ed.

Schiff, A. J. (1999). "Guide to Improved Earthquake Performance of Electric Power Systems." *Manual and Reports on Engineering Practice No.96*, A. S. o. C. Engineers, ed.

Tang, A. K. (2000). "Izmit (Kocaeli), Turkey, Earthquake August 17, 1999 - Including Duzce Earthquake of November 12, 1999 - Lifeline Performance." *Technical Council On Lifeline Earthquake Engineering (TCLEE), Monograph No. 17, ASCE*.

Thong, F. F. (2018). "California Operational Power Plant (Base Map)." Esri, ArcGIS.
USGS (2018). "Unified Hazard Tool." <https://earthquake.usgs.gov/hazards/interactive/>. (02/19/19).

Vamvatsikos, D., and Cornell, A. C. (2002). "Incremental Dynamic Analysis." *Earthquake Engineering and Structural Dynamics*, 31, 491-514.

Villaverde, R., Pardoen, G. C., and Carnalla, S. (2001). "Ground motion amplification at flange level of bushings mounted on electric substation transformers." *Earthquake Engineering and Structural Dynamics*, 30, 621-632.

Zareei, S. A., Hosseini, M., and Ghafory-Ashtiany, M. (2016). "Seismic Failure Probability of a 400kV Power Transformer Using Analytical Fragility Curves." *Engineering Failure Analysis*, 70, 273-289.